JOURNAL OF PETROLOGY | VOLUME 47 | NUMBER 4 | PAGES 705–744 | 2006 | doi:10.1093/petrology/egi091

# Low-pressure Granulites of the Lišov Massif, Southern Bohemia: Viséan Metamorphism of Late Devonian Plutonic Arc Rocks

**VOJTĚCH JANOUŠEK[1,2]*, AXEL GERDES[3], STANISLAV VRÁNA[2], FRITZ FINGER[1], VOJTĚCH ERBAN[2], GERTRUDE FRIEDL[4] AND COLIN J. R. BRAITHWAITE[5]**

[1]DIVISION OF MINERALOGY & MATERIAL SCIENCE, UNIVERSITY OF SALZBURG, HELLBRUNNERSTRASSE 34, A-5020 SALZBURG, AUSTRIA

[2]CZECH GEOLOGICAL SURVEY, KLÁROV 3/131, 118 21 PRAGUE 1, CZECH REPUBLIC

[3]INSTITUTE OF MINERALOGY, J. W. GOETHE-UNIVERSITY, SENCKENBERGANLAGE 28, D-60054 FRANKFURT, GERMANY

[4]DIVISION OF GENERAL GEOLOGY & GEODYNAMICS, UNIVERSITY OF SALZBURG, HELLBRUNNERSTRASSE 34, A-5020 SALZBURG, AUSTRIA

[5]DIVISION OF EARTH SCIENCES, UNIVERSITY OF GLASGOW, GLASGOW G12 8QQ, UK

**RECEIVED DECEMBER 20, 2004; ACCEPTED NOVEMBER 11, 2005; ADVANCE ACCESS PUBLICATION JANUARY 4, 2006**

*The Lišov Granulite Massif differs from neighbouring granulite bodies in the Moldanubian Zone of southern Bohemia (Czech Republic) in including a higher proportion of intermediate–mafic and orthopyroxene-bearing rocks, associated with spinel peridotites but lacking eclogites. In addition to dominantly felsic garnet granulites, other major rock types include quartz dioritic two-pyroxene granulites, tonalitic granulites and charnockites. Minor bodies of high-pressure layered gabbroic garnet granulites and spinel peridotites represent tectonically incorporated foreign elements. The protoliths of the mafic–intermediate granulites (quartz-dioritic and tonalitic) crystallized ~360–370 Ma ago, as indicated by laser ablation inductively coupled plasma mass spectrometry U–Pb ages of abundant zircons with well-preserved magmatic zoning. Strongly metamorphically recrystallized zircons give ages of 330–340 Ma, similar to those of other Moldanubian granulites. For the overwhelming majority of the Lišov granulites peak metamorphic conditions probably did not exceed 800–900°C at 4–5 kbar; the equilibration temperature of the pyroxene granulites was 670–770°C. This is in sharp contrast to conditions of adjacent contemporaneous Moldanubian granulites, which are characterized by a distinct HP–HT signature. The mafic–intermediate Lišov granulites are thought to have originated during Viséan metamorphic overprinting of metaluminous, medium-K calc-alkaline plutonic rocks that formed the mid-crustal root of a Late Devonian magmatic arc. The protolith resembled contemporaneous calc-alkaline intrusions in the European Variscan Belt.*

KEY WORDS: *low-pressure granulites; geothermobarometry; laser-ablation ICP-MS zircon dating; whole-rock geochemistry; Sr–Nd isotopes; Moldanubian Zone*

## INTRODUCTION

Granulite-facies metamorphic rocks provide crucial insights into the conditions and timing of continental collision, crustal thickening and orogenic collapse. Ultimately granulite-facies metamorphism can result in the production of granitic to tonalitic melts, and is, thus, a major process leading to crustal differentiation (e.g. Arculus & Ruff, 1990; Clemens, 1990). Hence careful and comprehensive study of these rocks provides a key to understanding the nature and development of ancient orogens, including the Variscan collisional belt in Central Europe (Pin & Vielzeuf, 1983; O'Brien & Rötzler, 2003).

The Variscan granulites of the Bohemian Massif have received much attention because many display a clear

*Corresponding author. Present address: Czech Geological Survey, Klárov 3/131, 118 21 Prague 1, Czech Republic. Telephone: +420 251085308. Fax: +420 251818748. E-mail: janousek@cgu.cz

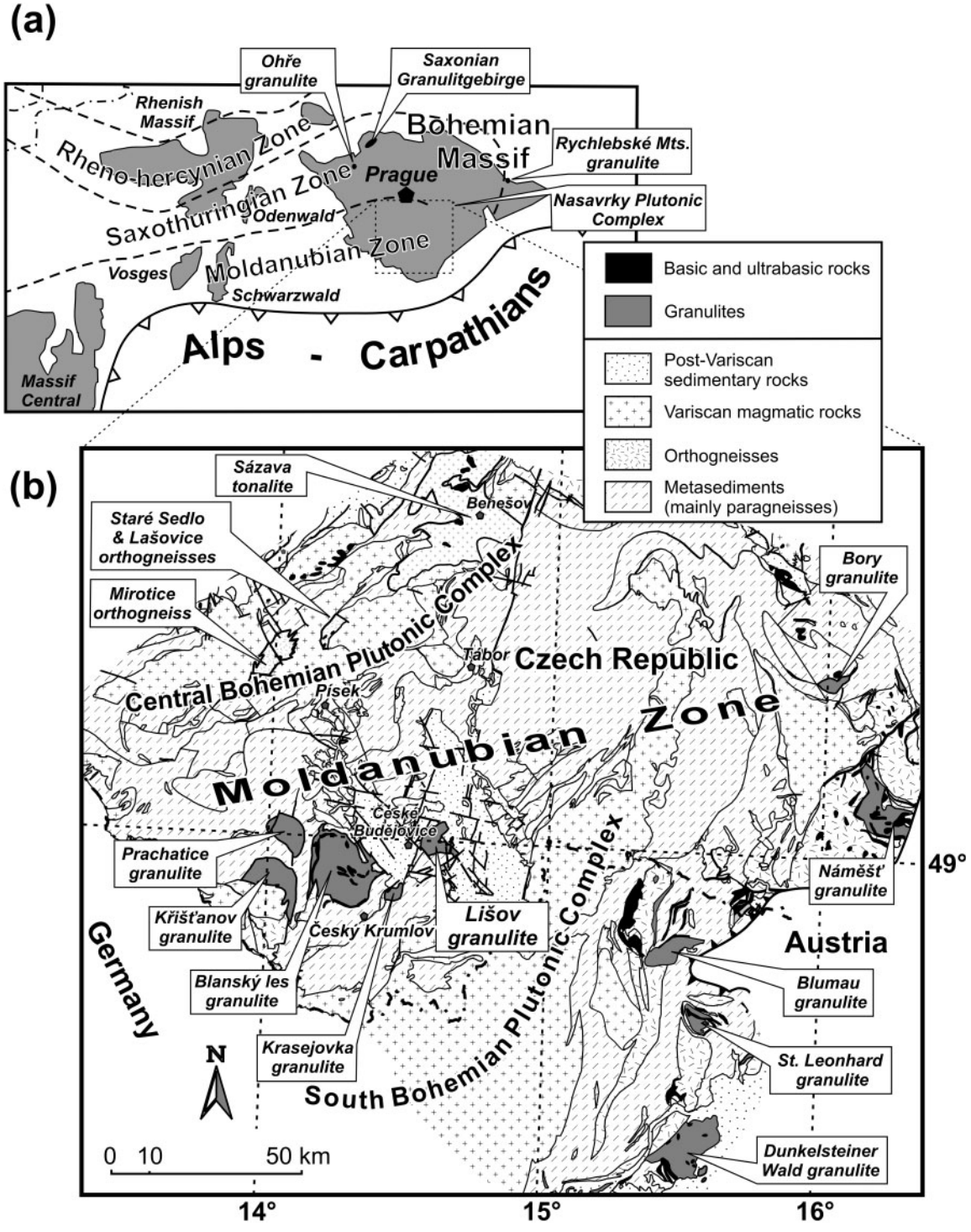


**Fig. 1.** (a) Location of the studied area in the context of the Central European Variscides. (b) Geological sketch of the Moldanubian Zone in southern Bohemia (modified from the Czech Geological Survey map, 1:500 000).

high-$P$–high-$T$ metamorphic signature [see O'Brien & Rötzler (2003) and O'Brien (2006) for reviews]. The high pressures have commonly been attributed to subduction at an active Variscan continental margin; the reasons for the high temperatures are still a matter of debate. In particular, the Gföhl Assemblage of the Moldanubian Zone (Lower Austria, SW Moravia and southern Bohemia: Fig. 1), following what was probably

the very first scientific account of granulites (von Justi, 1754), has become a classic and much investigated granulite-bearing terrain (e.g. Fiala *et al.*, 1987*b*; Vellmer, 1992; O'Brien & Carswell, 1993; Wendt *et al.*, 1994; Cooke, 2000; Kröner *et al.*, 2000; O'Brien, 2000).

A distinctive feature of the Moldanubian granulites is the dominance of felsic types with igneous (leucogranitic) protoliths (Fiala *et al.*, 1987*b*; Vellmer, 1992; Janoušek *et al.*, 2004*b*); by contrast, intermediate–mafic igneous and metasedimentary granulites are relatively rare. The reasons for this distinction are not yet fully understood [see review by Janoušek *et al.* (2004*b*)]. Unlike several larger granulite outcrops in southern Bohemia and Lower Austria (especially Blanský les, St. Leonhard and Dunkelsteiner Wald) that have been the subject of numerous detailed studies (Carswell & O'Brien, 1993; Fiala *et al.*, 1995; Vrána *et al.*, 1995; Petrakakis, 1997; O'Brien & Rötzler, 2003; O'Brien, 2006, and references therein), the Lišov Granulite Massif (LGM, Fig. 1b) has so far received little attention. This is unfortunate, as both petrological and geochemical data set it apart from other Moldanubian occurrences (see also Vrána & Šrámek, 1999).

The most striking features of the LGM are:

(1) a predominantly low-pressure, medium- to high-temperature metamorphic record;

(2) an abundance of orthopyroxene-bearing rock types (mafic granulites–felsic charnockites);

(3) an absence of $Al_2SiO_5$ phases, corundum and cordierite in felsic granulites;

(4) a presence of spinel peridotites (ultramafic rocks in other Moldanubian granulite terranes are mostly garnet-bearing);

(5) an absence of eclogites.

The aim of this study is to characterize the granulites of the Lišov Massif in terms of petrology and metamorphic evolution, together with the age, nature and petrogenesis of their igneous protoliths. The mechanism of LP granulite-facies metamorphism, following soon (~20 Ma) after the formation of the protoliths, and the incorporation of the resulting LP granulites into HP–HT crustal units at the climactic stage of the Viséan continental collision, is of particular significance. Thus, the Lišov granulites have important geotectonic implications for the interpretation of the development of the European Variscides, as most low-pressure granulite rocks documented so far formed much later in the orogen's history (at ~300 Ma, Pin & Vielzeuf, 1983).

Here we also provide an explanation for the relative abundance of mafic to intermediate granulite types at Lišov in comparison with other Moldanubian granulite massifs, and examine the sources and characteristics of the continental-arc magmatism that seems to have been responsible for the generation of their protoliths.

An additional general point is the ability of zircon to preserve growth zoning through subsequent high-grade metamorphism. The mechanism of metamorphic recrystallization of the zircon, ultimately leading to resetting of the U–Pb system, is critically assessed. The discussion demonstrates the utility of laser-ablation inductively coupled plasma mass spectrometry (LA–ICP–MS), in conjunction with optical cathodoluminescence (CL) and back-scattered electron (BSE) imaging, in resolving igneous and metamorphic ages separated by intervals of only a few tens of millions of years.

## GEOLOGICAL SETTING

### South Bohemian granulites

The Moldanubian Zone of the Bohemian Massif (Fig. 1) is a tectonic assemblage of medium- to high-grade metamorphic rocks, intruded by numerous granitoid masses. It comprises several crustal segments of contrasting age, ranging from ~2·1 Ga to Palaeozoic, but overall relationships are obscured by a complex polyphase deformational history (Dallmeyer *et al.*, 1995, and references therein). The Moldanubian Zone has been subdivided into a structurally lower and mainly metasedimentary Drosendorf Assemblage and above this, the higher grade allochthonous Gföhl Assemblage (Fuchs & Matura, 1976; Franke, 2000).

The lower part of the Drosendorf Assemblage is referred to as the Monotonous Unit (Ostrong Unit) and consists mainly of partly migmatitic garnet–biotite–sillimanite paragneisses with minor orthogneisses and amphibolites. The upper part, the Variegated Unit (the Drosendorf Unit *sensu stricto*), comprises paragneisses with intercalations of amphibolite, calc-silicate gneiss, marble, quartzite and graphite schist. The Gföhl Assemblage includes abundant granulite- and eclogite-facies metamorphic rocks: anatectic gneisses with granulites, garnet and spinel peridotites, pyroxenites, dunites and eclogites (Fuchs & Matura, 1976; Fiala *et al.*, 1995).

### Lišov Granulite Massif

A number of granulite bodies are present in southern Bohemia. The Blanský les Massif is the largest, followed by the Křišťanov, Prachatice, Lišov and Krasejovka masses and bodies too small to be shown in Fig. 1b. The Lišov Massif (*c.* 40 $km^2$) lies *c.* 5 km east of České Budějovice. Much of its western part consists of felsic granulites (Suk *et al.*, 1978, 1981), but two small intermediate–mafic granulite masses crop out near Zvíkov to the east (Vajner, 1964) and there are also several spinel peridotite bodies, up to 0·7 km long (Fig. 2).

The Lišov Granulite Massif (LGM) is bordered to the south and west by migmatitic biotite (± sillimanite and cordierite) paragneisses of the Monotonous and

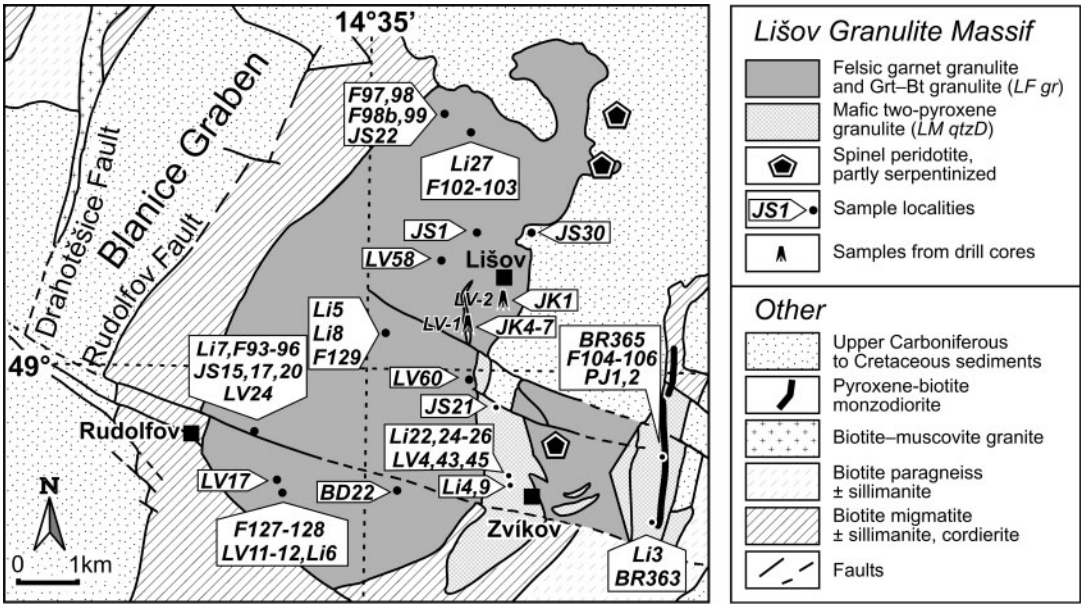


**Fig. 2.** Schematic map of the Lišov Massif (after Suk *et al.*, 1981; Suk 1982), showing the locations of whole-rock samples collected in the course of this study (with prefixes BR, LV and Li) and previously published data (prefixes: PJ, Jakeš, 1967; JS, Slabý, 1983; F, Fiala *et al.*, 1987*a*; JK, Kotková, 1998*b*).

Variegated units. The southern limits of the massif are modified by faulting but the eastern and northeastern boundaries are covered by Upper Cretaceous sediments. The structural setting has been described by Vrána & Šrámek (1999).

A single multigrain U–Pb zircon age of 345 ± 5 Ma is available for the rocks of the LGM (from a quartz dioritic two-pyroxene granulite at Rudolfov; van Breemen *et al.*, 1982). This age corresponds well to the best age estimate for the granulite-facies metamorphism in the Gföhl Assemblage [see Kröner *et al.* (2000) and O'Brien & Rötzler (2003) for reviews].

## ANALYTICAL TECHNIQUES

### Cathodoluminescence

The petrographic studies have benefited from optical CL observations (Marshall, 1988; Pagel *et al.*, 2000) using a CITL Technosyn 8200 Mk 4 apparatus at the University of Glasgow. Typical operating conditions were 26 kV, with a gun current of 210 μA, and a vacuum of ~1·2 mbar. Images were recorded on a Nikon DN100 digital camera.

Selected zircon grains were mounted in epoxy and polished prior to imaging and ICP-MS analysis. The CL investigations of the zircons were carried out on a LEICA Stereoscan 430 scanning electron microscope, equipped with an OXFORD MiniCL detector, at the Division of General Geology and Geodynamics, University of Salzburg (operating conditions: 15 kV, 500 pA probe current).

### Electron microprobe

Preliminary mineral analyses were carried out using an ARL-SEMQ microprobe and CamScan 4-90DV microprobe equipped with Link-ISIS Oxford Instruments EDX, both at the Czech Geological Survey (CGS).

Final analyses included in this study were obtained with a Cameca SX-100 electron microprobe at the Joint Laboratory of Electron Microscopy and Microanalysis, Masaryk University, Brno (analysts P. Sulovský and R. Čopjaková). The accelerating voltage was 15 kV, the probe current 10 and 20 nA, beam diameter 1 μm (5 and 15 μm for feldspars), and counting times were 10–20 s for major elements and 30–60 s for minor elements. The following standards were used: sanidine for Si, Al and K; albite and jadeite for Na; almandine for Fe; olivine for Mg; andradite for Ca; rhodonite for Mn; hornblende for Ti; chromite for Cr; topaz for F; apatite for P; barite for Ba; a modified set of standards was used for spinels and ilmenite. Data were reduced using the X–Φ routine.

### Whole-rock geochemistry

Most of the major-element whole-rock analyses were performed by wet chemistry in the CGS. The relative 2σ uncertainties for the given concentrations were better than 1% ($SiO_2$), 2% (FeO), 5% ($Al_2O_3$, $K_2O$, $Na_2O$), 7% ($TiO_2$, MnO, CaO), 10% ($Fe_2O_3$) and 15% (but mainly <6%) MgO. A few of the major-element analyses and most trace elements were determined by X-ray fluorescence (XRF; Bruker AXS) at the Division of Mineralogy and Material Science, University of Salzburg, on lithium

tetraborate glass beads and pressed pellets, respectively. The tube conditions were 4 kW and 60 kV; counting time was optimized automatically up to 400 s to obtain a detection limit of *c.* 1 ppm. Typical errors from the counting statistics were ±1 ppm at low concentrations (<10 ppm) and better than ±5% (relative) for the rest.

The rare earth elements (REE) were obtained mainly by ICP using an OES Perkin-Elmer Plasma II in the CGS. Some Co and Zn data were determined by atomic absorption spectroscopy (AAS) in the same laboratory.

Several samples were analysed in the Acme Analytical Laboratories, Vancouver, Canada. The majority of the trace elements were determined by $LiBO_2$ fusion and ICP-MS/OES, except for precious and base metals analysed by aqua regia digestion followed by ICP-MS.

Data management, recalculation, plotting and statistical evaluation of the geochemical data were facilitated using the R software package *GCDkit* (Janoušek *et al.*, 2003).

## Laser-ablation ICP-MS dating of zircon

The U–Pb isotopic analyses were performed using a Thermo-Finnigan Element II sector field ICP-MS system coupled to a Merkantek/New Wave 213 nm UV laser system at Frankfurt University. The masses of $^{202}$Hg, $^{204}$Hg + Pb, $^{206}$Pb, $^{207}$Pb, $^{208}$Pb, $^{232}$Th, $^{235}$U and $^{238}$U were measured in peak jumping mode during 30–90 s sample ablation. A spot size of 25–30 μm was used as the best compromise between spatial resolution and acceptable internal precision of the $^{207}$Pb/$^{206}$Pb and $^{206}$Pb/$^{238}$U ratios. At this spot size a typical mean $^{238}$U signal of 5 to $9 \times 10^5$ counts per seconds (c.p.s.) on the GJ-1 reference zircon (~240 ppm U) was achieved using 44% laser power and 10 Hz repetition rate. During the 90 s ablation the laser drilled ~40–50 μm deep and the signal dropped to about 1·5 to $2{\cdot}5 \times 10^5$ c.p.s. Data were collected at four points per peak by integrating 35 mass scans in 2·5 s. A teardrop-shaped, low-volume laser cell (NIGL, Nottingham) with a washout time below 1 s (Horstwood *et al.*, 2003) allowed precise time-resolved data acquisition; this was important when the laser drilled more than one growth zone during analysis.

Raw data were processed offline in an Excel spreadsheet. The inter-element fractionation was corrected by linear regression, whereby the intercept gives the 'true' ratio at the initial stage of ablation. The typical internal precision of $^{206}$Pb/$^{238}$U was 0·6% (1 standard error, SE). The ratio obtained was normalized to the reference zircon GJ-1 by multiplying by the difference between the inter-element fractionation corrected ratio of GJ-1 and its reference value (obtained by isotope dilution thermal ionization mass spectrometry; ID-TIMS). Frequent analyses of zircon with known (GJ-1, 91500, Temora, SL13 and AS3) and unknown U–Pb ages in the Frankfurt laboratory, using 91500 or GJ-1 zircon as references, show that an external precision and an accuracy of about 1% can be achieved routinely for crack-free grains with a homogeneous U–Pb composition (Gerdes, 2005). All errors (1σ confidence level on ratios, 2σ on ages) are propagated with the reproducibility (standard deviation, SD) of the standard over the session or day taken into account. For the U/Pb and Th/Pb ratios this is usually twice the internal precision of the single analyses. For the calculations of concordia ages and weighted averages, as well as plotting of concordia diagrams, we used Isoplot/Ex 2.49 (Ludwig, 2001).

The typical background, measured for 30 s prior to each analysis, was below 50 and 5 c.p.s. for Pb and U isotopes, respectively. During the two analytical sessions the mean $^{204}$Hg gas blanks, calculated from the measured $^{202}$Hg signal, were below 300 and 200 c.p.s., respectively. A common lead correction was applied based on the interference-corrected $^{204}$Pb and the two-stage model of Stacey & Kramers (1975). However, the $^{204}$Pb signal was commonly low or below the limit of detection. Nevertheless, in cases of relatively low radiogenic Pb signals the applied correction caused a scatter in $^{207}$Pb/$^{206}$Pb ratios and significantly increased the $^{207}$Pb/$^{206}$Pb errors. For some analyses there was a noticeable tendency to overcorrect the common-Pb contribution (see, e.g. Table 6). The interpretations in this paper are mainly based on the $^{206}$Pb/$^{238}$U age as this is the more precise and accurate, because of better counting statistics and general robustness against a common-Pb correction. The $^{206}$Pb/$^{238}$U analyses usually gave the most stable time-resolved isotope ratio (1 SE = 0·5–1·3%), indicating ablation of only homogeneous material. The $^{207}$Pb/$^{206}$Pb ages suffer from a low $^{207}$Pb signal resulting from the small laser spot size used and the uncertainty arising from the detection of common Pb. Within-run precision of the common-Pb corrected ratio (1 SE = 1·2–7·7%) is generally worse than the external reproducibility of the GJ-1 standard, as precision and reproducibility depend mainly on counting statistics. Because of the low $^{207}$Pb abundance and the dependence of the $^{207}$Pb/$^{206}$Pb error on the slope of the concordia, the $^{207}$Pb/$^{206}$Pb ages of Palaeozoic grains are generally less accurate than U–Pb ages. The signal intensity of $^{208}$Pb in the sample grains was similar to that of the $^{207}$Pb. Thus the $^{208}$Pb/$^{232}$Th ratio is very sensitive to common Pb corrections and to errors derived from it. With $^{208}$Pb signals of less than 1000 c.p.s. the $^{208}$Pb/$^{232}$Th has the poorest reproducibility (*c.* 6·2%, 2σ) of all isotope ratios determined on the GJ-1 standard.

## Radiogenic isotopes

For the isotopic study, samples were dissolved using a HF–HCl–$HNO_3$ mixture. Strontium and bulk REE were

isolated by cation-exchange chromatography on quartz columns with BioRad AG-W X8 resin; Nd was further separated on quartz columns with Biobeads S-X8 coated with HDEHP (Richard *et al.*, 1976). Isotopic analyses were performed using a Finnigan MAT 262 TIMS system in static mode with a double Re filament assembly (at CGS). The $^{143}Nd/^{144}Nd$ ratios were corrected for mass fractionation to $^{146}Nd/^{144}Nd = 0{\cdot}7219$, and $^{87}Sr/^{86}Sr$ ratios assuming $^{86}Sr/^{88}Sr = 0{\cdot}1194$. External reproducibility is given by the results of repeat analyses of the La Jolla [$^{143}Nd/^{144}Nd = 0{\cdot}511858 \pm 20$ ($2\sigma$) $n = 74$] and NBS 987 ($^{87}Sr/^{86}Sr = 0{\cdot}710262 \pm 86$, $n = 136$) isotopic standards.

The Rb and Sr concentrations, and Rb/Sr ratios, were determined by an approach similar to that of Harvey & Atkin (1981, and references therein) using the XRF devices in the CGS and at the University of Salzburg. The Sm and Nd determinations were carried out on ICP-OES Perkin-Elmer Plasma II system (at CGS) or by isotope dilution on a Thermo-Finnigan Neptune multi-collector ICP-MS system (at the University of Frankfurt).

The decay constants are from Steiger & Jäger (1977: Sr) and Lugmair & Marti (1978: Nd). The $\varepsilon^{i}_{Nd}$ values and single-stage CHUR Nd model ages were obtained using the Bulk Earth parameters of Jacobsen & Wasserburg (1980); the two-stage Depleted Mantle Nd model ages ($T^{DM}_{Nd}$) were calculated after Liew & Hofmann (1988).

## PETROLOGY AND MINERAL CHEMISTRY

### The main rock types and their field relations

Throughout this paper the Lišov granulites are classified into two main suites: (1) LF ('felsic'): garnet–orthopyroxene charnockites (*LF ch*) and leucocratic garnet granulites (*LF gr*); (2) LM ('mafic'): two-pyroxene quartz dioritic granulites (*LM qtzD*) enclosing pyroxenite xenoliths and cut by picritic dykes, and two-pyroxene tonalitic (*LM to*) granulites.

As noted, the LGM includes a significantly higher proportion of intermediate and mafic rocks than other granulite massifs in the Moldanubian Zone; felsic garnet (± biotite) granulites (*LF gr*) nevertheless predominate. In Lišov, locally preserved, unfoliated and pristine garnet-bearing hypersolvus leucogranulites are considered to be the protolith to widespread foliated and mylonitic felsic granulites that are characterized by the disintegration of mesoperthite to fine-grained mosaics of K-feldspar, sodic plagioclase and platy quartz (Vrána & Jakeš, 1982). In the northern part of the LGM, felsic garnet–biotite granulite gneisses contain what may be relics of a migmatitic texture.

Two-pyroxene, garnet-free quartz dioritic granulites (*LM qtzD*) form two larger (*c.* 4 km$^2$) bodies near Zvíkov (Fig. 2). These contain small enclaves of pyroxenites, <0·5 m across, with either high-Ca clinopyroxene or enstatite predominating. Fine-grained basic dykes several centimetres wide cut the foliation of the quartz dioritic granulite (Fig. 3a) and also bear the imprint of granulite-facies metamorphism.

There are no units of clinopyroxene (± biotite) tonalitic granulites (*LF to*) large enough to be shown in Fig. 2, but sporadic outcrops occur at several places in the LGM (e.g. at Vlkovice and in borehole LV-2, south of Lišov; Kotková, 1998*b*; Fig. 2). In the quarry near Rudolfov, alternating layers 0·1–2 m thick range from quartz diorite through tonalite to minor charnockite. The original relationships of the juxtaposed rock types have been obscured by tectonic transposition, which has obliterated many of the primary contacts.

Garnet–orthopyroxene charnockites, including fine-grained, relatively massive and foliated types, are known from four localities (*LF ch*). They form tabular and podiform bodies, up to 300 m long, and also *c.* 0·2 m thick layers in banded sequences of quartz dioritic and tonalitic granulites (at Rudolfov).

#### *'Mafic' suite (LM)*

*Two-pyroxene quartz dioritic granulites (LM qtzD).* Two-pyroxene granulites (± biotite, hornblende) are fine-grained, foliated rocks with orthopyroxene + clinopyroxene + biotite + plagioclase + quartz (± K-feldspar, hornblende) and accessory minerals, mostly ilmenite, apatite and zircon (Table 1). Pyroxenes with plagioclase (± biotite, K-feldspar and quartz) form an equilibrated granular mosaic (Figs 3b and c, and 4a and b). Exceptionally, sample Li-26 contains scattered rare garnet porphyroblasts ~10 mm across.

A dark green–grey massive dyke intruding the granulites *LM qtzD* (Li-25) has a granular structure with a grain size of 0·1–0·6 mm. The rock is dominated by brown pargasitic amphibole. Minor orthopyroxene occurs scattered in an equilibrium amphibole–plagioclase mosaic. Another dyke, sample BR-462 shown in Fig. 3a, has a mineral assemblage and mineral composition closely comparable with the surrounding granulite *LM qtzD*.

*Clinopyroxene tonalitic granulites (LM to).* Foliated fine-grained pyroxene–biotite granulites are characterized by a mineral assemblage including clinopyroxene + biotite + plagioclase + quartz (± K-feldspar, hornblende). In sample Li-3, CL studies revealed large bright greenish-yellow (more calcic) subhedral centres of plagioclase augen, surrounded by dull violet-brown plagioclase rims resting in a recrystallized plagioclase–K-feldspar matrix (Fig. 4c and d). Accessory minerals are ilmenite,

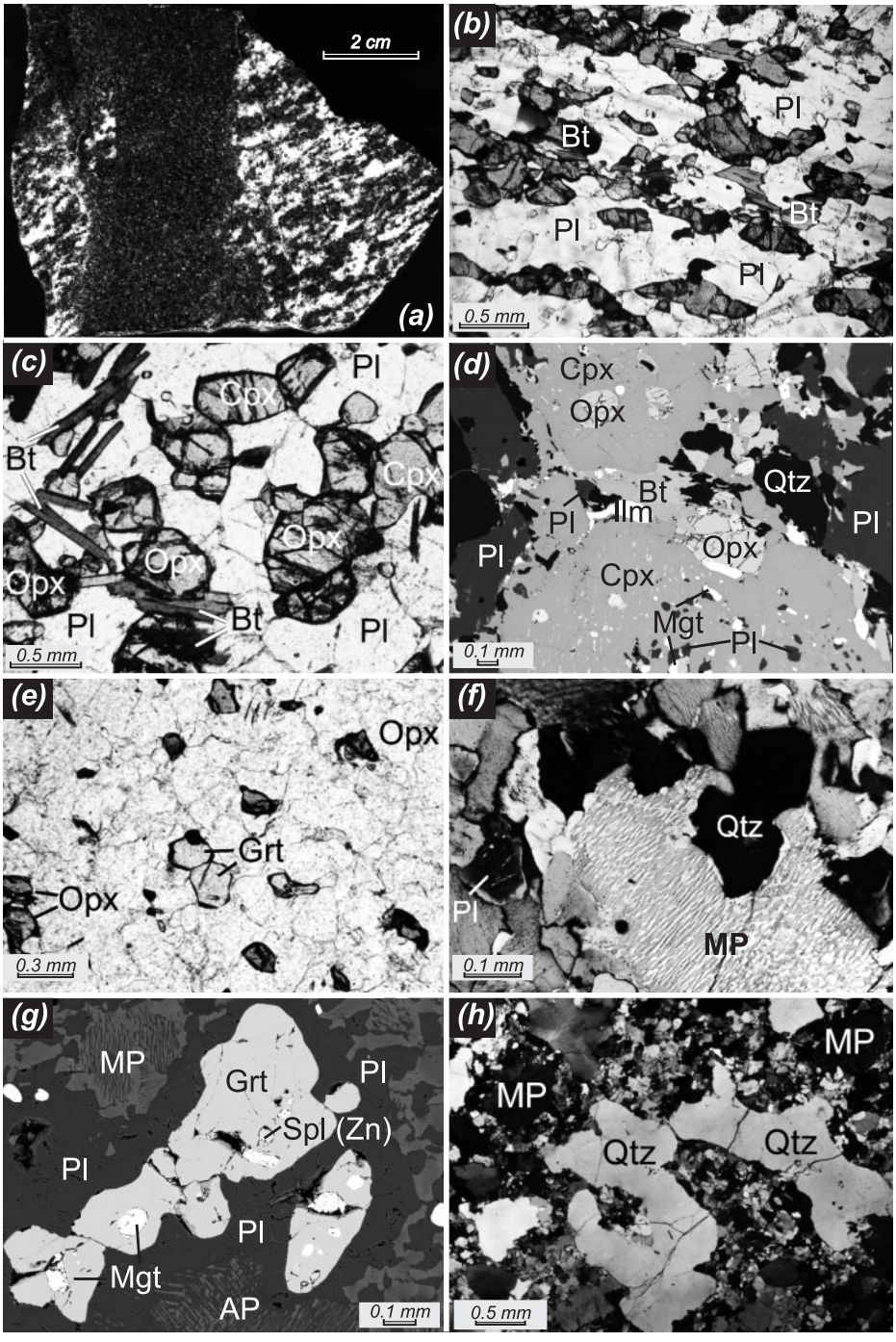


**Fig. 3.** (a) Common two-pyroxene quartz dioritic granulite (*LM qtzD*) cut by a thin dyke of fine-grained mafic granulite BR-462; Zvíkov, at the dam of the pond. (b) Strong parallel fabric and (c) equilibrium granular mosaic in mafic two-pyroxene granulite LV-60 (*LM qtzD*), 2 km NW of Zvíkov. Both: plane-polarized light. (d) Below centre—poikilitic crystal of high-Ca clinopyroxene (augite) with inclusions of plagioclase, magnetite, hornblende, and unmixed lamellae of orthopyroxene. The crystal is interpreted as a probable magmatic pyroxene relic. BSE image of the sample Li-4, *LM qtzD*; Zvíkov. (e) Structure of garnet–orthopyroxene charnockite Li-5 (*LF ch*), disused quarry 2 km WSW of Lišov. Plane-polarized light. (f) Mesoperthite (MP), primary plagioclase (Pl) and quartz (Qtz) in felsic garnet granulite (*LF gr*) V-127 (archive sample of Vajner, 1964), Hlincova Hora. Crossed polars. (g) Cluster of anhedral garnet crystals with numerous inclusions of magnetite and rare zincian spinel [Spl (Zn)], rimmed by sodic oligoclase. Mesoperthite (MP) at top left, antiperthite (AP) at centre bottom. BSE image of the felsic garnet granulite *LF gr* Li-6, Hlincova Hora. (h) Relict primary shapes of quartz grains, unmodified by deformation, in felsic garnet granulite V-127 (*LF gr*), Hlincova Hora. Mesoperthite (MP) is largely recrystallized to fine-grained mosaic of oligoclase and K-feldspar. Crossed polars. The mineral abbreviations are after Kretz (1983) apart from mesoperthite (MP) and antiperthite (AP).

*Table 1: Localization and estimated modal mineralogy (vol. %) of the studied rock samples*

| Sample | Rock type | Locality | Pl® | Cpx® | Pl | | Cpx | Opx | Grt | Hbl | Bt | Qtz | Kfs | MP | Ilm | Mgt | Ap | Zrn | Rt |
|---|---|---|---|---|---|---|---|---|---|---|---|---|---|---|---|---|---|---|---|
| Li-25 | Mafic dyke | 1 | | | 40 | | | 2 | | 56 | | | | | | 2 | | | |
| Li-22 | Pyroxenite | 2 | | + | 3 | $An_{82}$ | 50 | 34 | | 6 | 7 | | | | | | | | |
| LV-4 | Pyroxenite | 2 | | + | | | 50 | 45 | | | 5 | | | | | | | | |
| Li-26 | Quartz dioritic granulite | 1 | | | 64 | $An_{47}$ | 10 | 12 | <5 | | 6 | 2 | 1 | | 1 | + | + | + | |
| BR-363 | Quartz dioritic granulite | 3 | | | 60 | $An_{48}$ | 12 | 10 | | 5 | 10 | 2 | | | 1 | | + | + | |
| BR-365 | Quartz dioritic granulite | 4 | $An_{48-51}$ | + | 66 | $An_{45}$ | 10 | 7 | | 1 | 8 | 4 | 3 | | 1 | | + | + | |
| Li-4 | Quartz dioritic granulite | 5 | | + | 68 | $An_{46}$ | 12 | 9 | | | 8 | 1 | | | 1 | + | + | + | |
| LV-60 | Quartz dioritic granulite | 6 | | | 67 | | 12 | 12 | | | 7 | 1 | | | 1 | | + | + | |
| Li-3 | Bt–Cpx tonalitic granulite | 3 | $An_{47-51}$ | | 68 | | 7 | | | | 12 | 12 | | | + | | | | |
| Li-7 | Retrogressed tonalitic Bt–Hbl granulite | 7 | | | 60 | | | | | 12 | 10 | 18 | | | + | | + | | |
| Li-5 | Charnockite | 8 | | | 32 | $An_{25-27}$ | | 5 | 4 | | | 35 | + | 24 | + | | + | + | |
| BD-22 | Charnockite | 9 | | | 40 | $An_{23}$ | | 3 | 2 | | + | 32 | 12 | 10 | + | | | | |
| LV-58 | Charnockite | 10 | | | 35 | $An_{27}$ | | 4 | 2 | | 1 | 33 | 15 | 10 | + | | | | |
| LV-24 | Charnockite | 7 | | | 18 | $An_{18}$ | | 3 | 1 | | | 36 | 30 | 12 | | + | | | |
| Li-6 | Felsic Grt granulite | 11 | | | 7 | | | | 4 | | | 39 | | 50 | | + | + | + | + |
| LV-11 | Felsic Grt granulite | 11 | | | 6 | | | | 5 | | + | 32 | + | 56 | + | + | + | + | |
| LV-17 | Felsic Grt granulite | 12 | | | 10 | | | | 4 | | + | 34 | 6 | 45 | + | + | + | + | |

Sample localities: 1, Li-25, Li-26: Zvíkov; boulders *c*. 0·5 km north of the village, at a hill close to a farm. 2, Li-22, LV-4: Zvíkov; rock outcrops at the pond in western part of Zvíkov. 3, BR 363, Li-3: Vlkovice; loose blocks at disused quarry, 400 m east of Vlkovice. 4, BR 365: Skalice; disused quarry 20 m east of the Vlkovice–Štepánovice road. 5, Li-4: Zvíkov; borehole at the pond in western part of Zvíkov. 6, LV-60: rock outcrop at the pond 2 km NNW of Zvíkov. 7, Li-7, LV-24: Rudolfov; disused quarry in a valley 500 m east of Rudolfov. 8, Li-5: Lišov; disused quarry in forest at elevation 565 m, 1·5 km SW of Lišov. 9, BD-22: blocks at elevation, 1·5 km west of Zvíkov. 10, LV-58: disused quarry 1 km NW of Lišov. 11, Li-6, LV-11, LV-12; Hlincova Hora: disused quarry in forest SW of the village. LV-17: loose blocks 0·7 km WNW of Hlincova Hora. Pl® and Cpx® are relict magmatic plagioclase and clinopyroxene (see text for explanation). Symbols of rock-forming minerals are after Kretz (1983), apart from MP (mesoperthite + antiperthite).

apatite and zircon. A few of the mafic granulites *LM to* are mylonitic and are retrogressed to foliated fine-grained hornblende–biotite gneiss (Li-7). In these rocks, the hornblende is newly formed after pyroxene, whereas biotite and quartz are recrystallized; some plagioclase grains remain from the granulite stage.

### *'Felsic' suite (LF)*

*Garnet–orthopyroxene charnockites (LF ch)*. The fine-grained garnet–orthopyroxene charnockites consist of quartz, plagioclase, mesoperthite, orthopyroxene and garnet. Accessory minerals are apatite, zircon and ilmenite. The granulites *LF ch* appear massive in hand specimen, but under the microscope they reveal a foliation defined by elongated quartz grains, with aggregates of orthopyroxene and feldspars (Figs 3e, and 4e and f). The granular mosaic texture indicates an equilibrated assemblage (Fig. 4f).

Feldspars are typically perthitic K-feldspar, with mesoperthite in some samples, but calcic oligoclase is also relatively abundant. Quartz typically forms nearly equant grains, although they are sometimes elongated in the foliation planes (e.g. Fig. 4e and f).

*Leucocratic garnet granulites (LF gr)*. These fine-grained massive rocks were described as 'hypersolvus garnet leucogranites' by Vrána & Jakeš (1982) (e.g. samples Li-6, LV-11, 12, 17). Information on their early history is derived from relict domains, accounting for less than 5 vol. % of the outcrops, that are weakly foliated and preserve their primary high-temperature mineralogy (Figs 3f and g, and 4g and h). However, typically, the rocks are largely mylonitized, recrystallized and foliated with platy quartz and fine-grained feldspar mosaic (Fig. 3h). Accessory minerals are magnetite, apatite, zircon and fine-grained acicular rutile.

### *Garnet-bearing two-pyroxene granulites of gabbroic composition (LGb)*

A modally layered sequence of gabbroic garnet–two-pyroxene (± hornblende, biotite) granulites is confined to a small area 0·5 km SW of Lišov (borehole LV-1: Kotková, 1998*b*) (Fig. 2). They are fine-grained, foliated rocks with compositional banding on a millimetre to

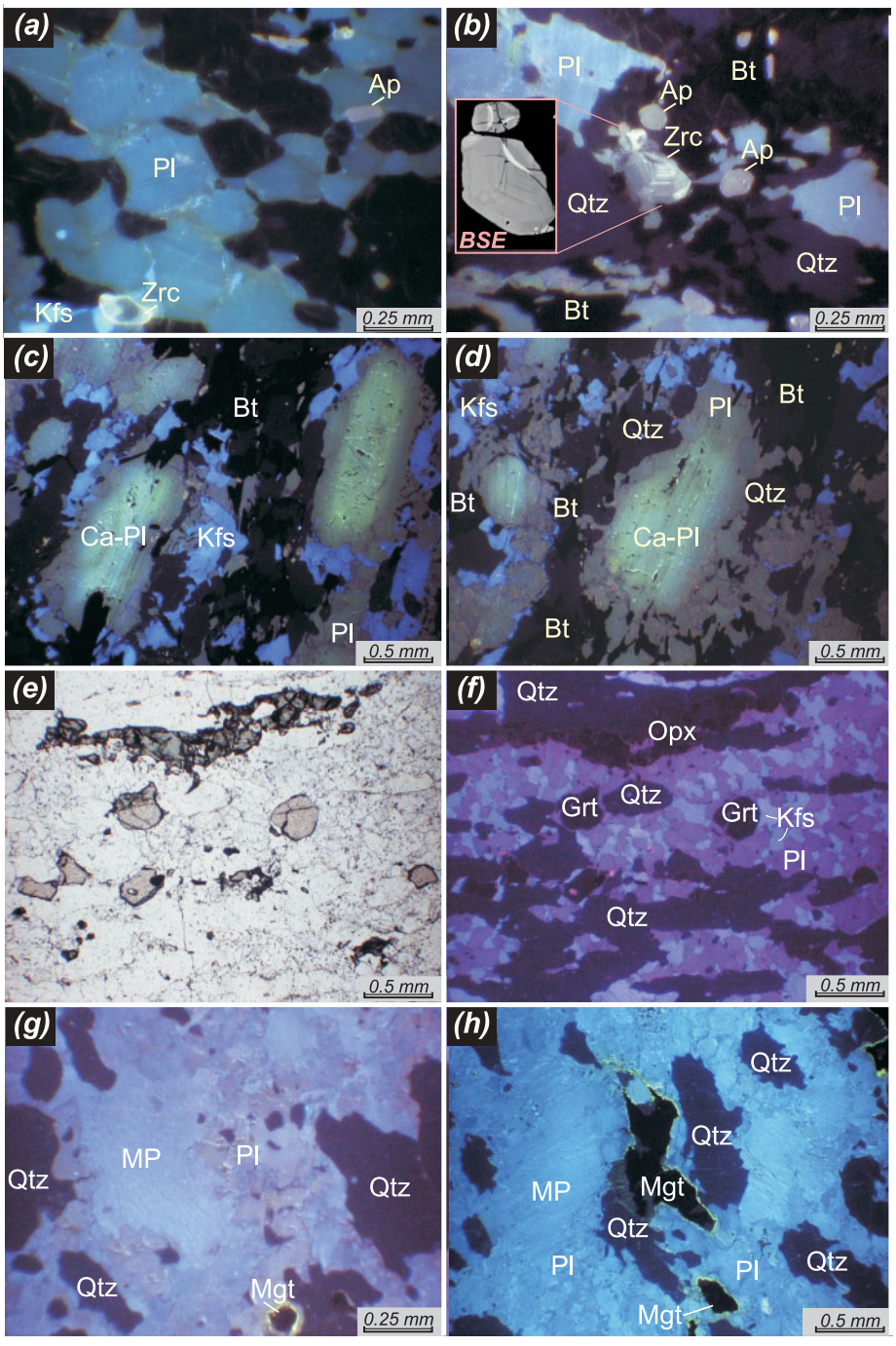


**Fig. 4.** Cathodoluminescence photomicrographs from the Lišov granulites (except for e). (a, b) Plagioclase-rich (dull grey–blue luminescence) mafic granulites (*LM qtzD*) Li-26 (a) and Li-4 (b) from the Zvíkov area. Minor K-feldspar has a bright blue luminescence; stubby apatite is pink. Note the bright yellow–green zircon, showing in (b) a strong oscillatory and sector zoning; this is less apparent in the BSE image (inset). The non-luminescent phases are biotite, pyroxenes and quartz. (c, d) Relict calcic plagioclase augen (Ca-Pl) surrounded by pale violet–brown metamorphic plagioclase (Pl) in tonalitic granulite (*LM to*) Li-3 from Vlkovice. The matrix is formed by mylonitic bright blue K-feldspar and non-luminescent phases, mainly quartz and biotite. The latter encloses numerous minute pink apatite crystals. (e, f) Photomicrographs showing the same area in plane-polarized light (e) and under CL (f) of garnet–orthopyroxene charnockite (*LF ch*) Li-5. The non-luminescent grains of garnet and orthopyroxene are enclosed within an equilibrated mosaic of K-feldspar and plagioclase (blue–violet). Common quartz in lenticular aggregates is non-luminescent. (g, h) Felsic hypersolvus granulite (*LF gr*) Li-6 showing well-preserved mesoperthite (MP), recrystallized only at the margins into a fine-grained mosaic of two feldspars. Non-luminescent quartz occurs in elongated grains with irregular margins. In (h), the other non-luminescent mineral, magnetite, is surrounded by thin films of a yellow alteration (?) product. The mineral abbreviations are after Kretz (1983) apart from mesoperthite (MP).

decimetre scale. Dark bands are enriched in ferromagnesian minerals (orthopyroxene, hornblende, clinopyroxene, garnet and biotite), whereas light bands contain dominantly plagioclase.

According to Kotková (1998*b*), garnet porphyroblasts up to 5 mm diameter are surrounded by, or completely transformed to, radiating coronas consisting of symplectites of plagioclase + orthopyroxene ± hornblende (± spinel). Early high-Ca clinopyroxene, which originally coexisted with garnet, is sometimes preserved in these relics. Within a short distance from the symplectite, the texture changes to become an equilibrated granular mosaic. Planar fabrics commonly reflect mylonitic banding, overprinted by high-$T$ recrystallization. This rock type, with an early high-pressure imprint is, like the spinel peridotite bodies, considered to be a foreign component in the massif.

## MINERAL CHEMISTRY

Selected mineral analyses for individual minerals are given in Table 2. The complete dataset can be downloaded from the *Journal of Petrology* website at http://www.petrology.oxfordjournals.org.

### Orthopyroxene

Orthopyroxene in the quartz dioritic granulites forms an equilibrium mosaic with plagioclase, high-Ca clinopyroxene and biotite. The composition is $Fs_{46–50}Wo_{1·4–1·6}$ (Table 2). High-magnification BSE images demonstrate that it is free of lamellar unmixed phases. The mineral is pleochroic (X, light red-brown; Y, beige; Z, light grey-green). In a few samples it is altered to a low-temperature assemblage of actinolite + anthophyllite/cummingtonite (Leake *et al.*, 1997) and chlorite. The composition of orthopyroxene in the pyroxenites is $Fs_{24}Wo_{1}$. Orthopyroxene in charnockites is ferrosilite ($Fs_{65–71}Wo_{0·7–1·1}$; Morimoto, 1988) but the more magnesian sample LV-24 contains Mg-rich ferrosilite $Fs_{54}Wo_{0·3}$. The mineral is strongly pleochroic (X, red brown; Y, beige; Z, bluish green).

### Clinopyroxene

In the quartz dioritic and tonalitic granulites clinopyroxene occurs as equant grains in equilibrated mosaics of other major minerals. It is light grey green and Ca-rich ($Fs_{14–20}Wo_{44–45}$), whereas in pyroxenites its composition is $Fs_{8}Wo_{47–48}$. A few samples contain relict grains up to 1·5 mm across of primary magmatic pyroxene, with inclusions of plagioclase, magnetite and ilmenite, together with minute (<1·5 μm) lamellae of unmixed orthopyroxene, forming <3–5 vol. % of the host grain (Fig. 3d). Thin orthopyroxene lamellae also occur in some relatively large grains of recrystallized clinopyroxene in the granulites *LM qtzD*. In the pyroxenites, the unmixed lamellae are considerably thicker.

### Amphibole

Amphiboles occur as an accessory or minor phase in the primary granulite assemblages. In the quartz dioritic samples they are Ti-rich pargasites (~2 wt % $TiO_2$) with a greenish-brown pleochroism. Both fluorine and chlorine are below detection limits. The amphibole in the pyroxenite (Li-22) is a bright light brown magnesiohornblende. Secondary, green amphibole in tonalitic sample Li-7 falls at the boundary between magnesiohornblende and ferrohornblende, with 0·3–0·4 wt % $TiO_2$.

### Garnet

Garnet forms anhedral grains <1 mm across but scattered euhedral crystals are also present, particularly in mesoperthite. Garnet $Alm_{75–78}Prp_{10–13}Grs_{6–8}$ is confined to garnet–orthopyroxene charnockites; the relatively magnesium-rich sample LV-24 contains garnet $Alm_{71–72}Prp_{22–23}Grs_{3}$. Garnets in leucocratic garnet granulites have the composition $Alm_{68–77}Prp_{18–26}Grs_{1–3}$. Although there is some compositional variation among samples with rather similar whole-rock compositions, individual garnet crystals do not vary by more than 2 mol % of end-members. An insignificant decline in Ca towards crystal rims is compensated by minor increases in Fe and Mg. The spessartine content is uniformly low, 2·6–3·5 mol %. It is notable that crystals lack reaction rims, and plagioclase moats in particular, probably indicating a negligible loss of calcium during the evolution of these rocks.

The yttrium content is high (0·1–0·2 wt % $Y_2O_3$) in leucocratic garnet granulites and higher still (0·2–0·7 wt % $Y_2O_3$) in charnockite garnet. It seems that in the charnockites the garnet Y concentrations are inversely proportional to the modal proportion of garnet in any given sample, reaching the highest value in LV-24 with <1 vol. % garnet. By contrast, the garnets from leucocratic Moldanubian granulites in western Moravia contain three- to five-fold lower yttrium abundances (Čopjaková *et al.*, 2005).

Exceptionally, garnet also occurs in quartz dioritic granulite (Li-26). In this sample, characterized by the presence of magnetite, the garnet contains 3·5–7·4 mol % andradite that may reflect stabilization by a locally increased oxygen fugacity.

### Biotite

The biotite in quartz dioritic granulites is rich in $TiO_2$ (5·3–6·1 wt %), with an Mg/Fe ratio near unity. It shows equilibrium relationships to pyroxenes in the metamorphic assemblage. The dark mica in the pyroxenite is phlogopite with 4·4 wt % $TiO_2$ and 0·4 wt % F.

*Table 2: Representative analyses of rock-forming minerals from Lišov granulites—LM and LF*

| | Lišov granulites—LM | | | | | | | | |
|---|---|---|---|---|---|---|---|---|---|
| Rock type: | Pyroxenite | | | | | *LM qtzD* | | | |
| Mineral: | Cpx | Opx | Phl | Hbl | Pl | Cpx | Opx | Bt | Hbl |
| Sample: | Li-22 | Li-22 | Li-22 | Li-22 | Li-22 | Li-4 | Li-4 | Li-4 | Li-4 |
| Analysis no.: | 3 | 5 | 6 | 8 | 10 | 35 | 31 | 32 | 14 |
| *wt %* | | | | | | | | | |
| $SiO_2$ | 53·32 | 55·43 | 39·32 | 51·64 | 47·67 | 52·51 | 51·39 | 36·23 | 42·30 |
| $TiO_2$ | 0·27 | 0·11 | 4·38 | 0·81 | | 0·19 | 0·13 | 5·67 | 2·06 |
| $Al_2O_3$ | 1·79 | 1·62 | 14·47 | 6·98 | 33·74 | 1·76 | 1·41 | 14·16 | 11·48 |
| $Cr_2O_3$ | 0·26 | 0·16 | 0·45 | 0·21 | | 0·09 | | 0·04 | 0·04 |
| $V_2O_3$ | | | | | | | | | |
| FeO* | 4·81 | 15·67 | 8·25 | 6·00 | 0·08 | 11·46 | 28·97 | 19·79 | 17·86 |
| MnO | 0·15 | 0·33 | 0·04 | 0·08 | | 0·38 | 0·96 | 0·12 | 0·19 |
| MgO | 15·72 | 27·57 | 18·89 | 18·89 | 0·03 | 12·36 | 17·40 | 10·96 | 9·84 |
| CaO | 24·03 | 0·52 | | 12·51 | 17·22 | 22·04 | 0·74 | | 11·52 |
| $Na_2O$ | 0·29 | | 0·41 | 1·07 | 2·08 | 0·41 | | 0·08 | 1·35 |
| $K_2O$ | | | 9·34 | 0·51 | 0·07 | | 0·00 | 9·28 | 1·68 |
| $P_2O_5$ | | | | | | | | | |
| SrO | | | | | 0·12 | | | | |
| BaO | | | | | | | | | |
| F | | | 0·41 | | | | | | |
| Cl | | | 0·07 | | | | | 0·16 | |
| ZnO | | | | | | | | | |
| $Y_2O_3$ | | | | | | | | | |
| $Nb_2O_3$ | | | | | | | | | |
| Total | 100·64 | 101·41 | 96·03 | 98·70 | 101·01 | 101·20 | 101·00 | 96·49 | 98·32 |
| *Number of atoms (p.f.u.)* | | | | | | | | | |
| Si | 1·944 | 1·969 | 5·610 | 7·172 | 8·683 | 1·953 | 1·958 | 5·484 | 6·342 |
| Ti | 0·007 | 0·003 | 0·470 | 0·085 | | 0·005 | 0·004 | 0·646 | 0·232 |
| Al | 0·077 | 0·068 | 2·433 | 1·143 | 7·243 | 0·077 | 0·063 | 2·525 | 2·029 |
| Cr | 0·007 | 0·004 | 0·051 | 0·023 | | 0·003 | | 0·005 | 0·005 |
| V | | | | | | | | | |
| $Fe^{3+}$ | 0·034 | | | 0·139 | | 0·033 | 0·014 | | 0·261 |
| $Fe^{2+}$ | 0·113 | 0·466 | 0·984 | 0·558 | 0·012 | 0·324 | 0·910 | 2·504 | 1·978 |
| Mn | 0·005 | 0·010 | 0·005 | 0·009 | | 0·012 | 0·031 | 0·015 | 0·024 |
| Mg | 0·854 | 1·460 | 4·017 | 3·911 | 0·008 | 0·685 | 0·989 | 2·472 | 2·199 |
| Ca | 0·939 | 0·020 | | 1·862 | 3·361 | 0·878 | 0·030 | | 1·851 |
| Na | 0·020 | | 0·113 | 0·288 | 0·735 | 0·030 | | 0·023 | 0·392 |
| K | | | 1·700 | 0·090 | 0·016 | | 0·001 | 1·791 | 0.321 |
| P | | | | | | | | | |
| Sr | | | | | 0·013 | | | | |
| Ba | | | | | | | | | |
| Zn | | | | | | | | | |
| Y | | | | | | | | | |
| Nb | | | | | | | | | |
| Total | 4·000 | 4·000 | 15·383 | 15·279 | 20·071 | 4·000 | 4·000 | 15·471 | 15·635 |

*Table 2: Continued*

| | Lišov granulites—LM | | | | | | |
|---|---|---|---|---|---|---|---|
| Rock type: | *LM qtzD* | | | *LM to* | | | |
| Mineral: | Pl | Mt | Ilm | Cpx | Bt | Pl | Kfs |
| Sample: | Li-4 | Li-4 | Li-4 | Li-3 | Li-3 | Li-3 | Li-3 |
| Analysis no.: | 33 | 27 | 26 | 55 | 57 | 60 | 59 |
| *wt %* | | | | | | | |
| $SiO_2$ | 57·61 | 0·07 | | 52·93 | 37·56 | 60·19 | 65·16 |
| $TiO_2$ | | 5·97 | 47·70 | 0·12 | 3·89 | | |
| $Al_2O_3$ | 27·30 | 1·40 | 0·02 | 1·34 | 14·28 | 25·82 | 18·82 |
| $Cr_2O_3$ | | 1·44 | 0·05 | 0·04 | 0·08 | | |
| $V_2O_3$ | | 0·75 | 0·22 | | | | |
| FeO* | 0·17 | 82·45 | 42·12 | 10·81 | 17·58 | 0·13 | |
| MnO | | 0·84 | 0·87 | 0·63 | 0·18 | | |
| MgO | | 0·02 | 0·11 | 12·56 | 13·02 | | |
| CaO | 9·56 | 0·21 | | 21·70 | | 7·47 | 0·07 |
| $Na_2O$ | 6·01 | | | 0·38 | 0·11 | 7·22 | 1·34 |
| $K_2O$ | 0·43 | | | | 9·67 | 0·38 | 14·45 |
| $P_2O_5$ | | | | | | | 0·15 |
| SrO | 0·12 | | | | | | 0·86 |
| BaO | | | | | | | 0·86 |
| F | | | | | | | |
| Cl | | | | | 0·18 | | |
| ZnO | | 0·24 | | | | | |
| $Y_2O_3$ | | | | | | | |
| $Nb_2O_3$ | | | 0·05 | | | | |
| Total | 101·20 | 93·39 | 99·95 | 100·72 | 96·55 | 101·21 | 100·87 |
| *Number of atoms (p.f.u.)* | | | | | | | |
| Si | 10·240 | 0·003 | | 1·977 | 5·615 | 10·619 | 11·939 |
| Ti | | 0·174 | 0·900 | 0·003 | 0·438 | | |
| Al | 5·719 | 0·064 | 0·000 | 0·059 | 2·516 | 5·369 | 4·064 |
| Cr | | 0·044 | 0·000 | 0·001 | 0·009 | | |
| V | | 0·022 | 0·000 | | | | |
| $Fe^{3+}$ | 0·025 | 1·538 | 0·880 | 0·338 | 2·198 | 0·019 | |
| $Fe^{2+}$ | | 1·140 | 0·180 | 0·007 | | | |
| Mn | | 0·027 | 0·020 | 0·020 | 0·023 | | |
| Mg | | 0·001 | 0·000 | 0·699 | 2·902 | | |
| Ca | 1·821 | 0·009 | | 0·868 | | 1·412 | 0·014 |
| Na | 2·071 | | | 0·028 | 0·032 | 2·470 | 0·476 |
| K | 0·098 | | | | 1·844 | 0·086 | 3·378 |
| P | | | | | | | 0·003 |
| Sr | 0·012 | | | | | | 0·016 |
| Ba | | | | | | | 0·062 |
| Zn | | 0·007 | | | | | |
| Y | | | | | | | |
| Nb | | | 0·000 | | | | |
| Total | 19·985 | 3·029 | 2·000 | 4·000 | 15·577 | 19·974 | 19·951 |

*Table 2: Continued*

| | Lišov granulites—LF | | | | | | | | | |
|---|---|---|---|---|---|---|---|---|---|---|
| Rock type: | *LF ch* | | | | | | *LF gr* | | | |
| Mineral: | Opx | Grt core | Grt rim | Pl | Kfs | Ilm | Grt core | Grt rim | MP | Mt |
| Sample: | Li-5 | Li-5 | Li-5 | Li-5 | Li-5 | Li-5 | Li-6 | Li-6 | Li-6 | Li-6 |
| Analysis no.: | 69 | 71 | 68 | 75 | 76 | 77 | 82 | 85 | av·88–92 | 94 |
| *wt %* | | | | | | | | | | |
| $SiO_2$ | 49·09 | 37·75 | 37·48 | 62·98 | 65·53 | 0·03 | 37·80 | 37·81 | 66·09 | 0·08 |
| $TiO_2$ | 0·11 | 0·02 | | | | 49·57 | 0·04 | 0·02 | | 2·93 |
| $Al_2O_3$ | 1·15 | 20·59 | 20·59 | 24·03 | 18·80 | | 20·98 | 21·04 | 19·65 | 2·24 |
| $Cr_2O_3$ | | 0·04 | 0·05 | | | 0·05 | | | | |
| $V_2O_3$ | | | | | | 0·07 | | | | 0·07 |
| FeO* | 38·24 | 32·85 | 33·53 | 0·12 | | 49·11 | 36·05 | 34·78 | 0·01 | 88·16 |
| MnO | 0·46 | 1·29 | 1·40 | | | 0·30 | 1·42 | 1·40 | | 0·09 |
| MgO | 11·02 | 3·09 | 2·84 | | | 0·22 | 4·47 | 4·44 | | 0·07 |
| CaO | 0·35 | 3·67 | 3·28 | 5·65 | 0·10 | | 1·26 | 1·02 | 0·87 | |
| $Na_2O$ | | | | 8·53 | 1·76 | | 0·03 | | 4·51 | |
| $K_2O$ | | | | 0·21 | 14·05 | | | | 9·70 | |
| $P_2O_5$ | | 0·03 | 0·03 | | | | 0·04 | 0·02 | 0·03 | |
| SrO | | | | | 0·07 | | | | | |
| BaO | | | | | 0·43 | | | | 0·03 | |
| $Y_2O_3$ | | 0·17 | 0·24 | | | | 0·13 | 0·14 | | |
| $Nb_2O_3$ | | | | | | 0·12 | | | | |
| Total | 100·57 | 100·21 | 99·94 | 101·52 | 100·74 | 99·47 | 101·23 | 100·67 | 100·89 | 93·64 |
| *Number of atoms (p.f.u.)* | | | | | | | | | | |
| Si | 1·967 | 6·033 | 6·026 | 11·013 | 11·963 | 0·001 | 5·976 | 6·005 | 11·848 | 0·003 |
| Ti | 0·003 | 0·002 | | | | 0·943 | 0·005 | 0·002 | | 0·084 |
| Al | 0·054 | 3·878 | 3·902 | 4·952 | 4·045 | | 3·909 | 3·938 | 4·152 | 0·101 |
| Cr | | 0·005 | 0·006 | | | 0·001 | 0·000 | 0·000 | | |
| V | | | | | | | | | | 0·002 |
| $Fe^{3+}$ | 1·281 | 4·390 | 4·508 | 0·018 | | 0·931 | 4·543 | 4·574 | 0·001 | 1·726 |
| $Fe^{2+}$ | 0·005 | 0·096 | 0·067 | | | 0·108 | 0·093 | 0·045 | | 1·080 |
| Mn | 0·016 | 0·175 | 0·191 | | | 0·006 | 0·190 | 0·188 | | 0·003 |
| Mg | 0·658 | 0·736 | 0·681 | | | 0·008 | 1·054 | 1·051 | | 0·004 |
| Ca | 0·015 | 0·628 | 0·565 | 1·059 | 0·020 | | 0·213 | 0·174 | 0·167 | |
| Na | | | | 2·892 | 0·623 | | | | 1·568 | |
| K | | | | 0·047 | 3·272 | | | | 2·219 | |
| P | | 0·004 | 0·004 | | | | 0·005 | 0·003 | 0·005 | |
| Sr | | | | | 0·007 | | | | | |
| Ba | | | | | 0·031 | | | | 0·002 | |
| Y | | 0·014 | 0·021 | | | | 0·011 | 0·012 | | |
| Nb | | | | | | 0·002 | | | | |
| Total | 4·000 | 15·962 | 15·970 | 19·980 | 19·962 | 2·000 | 16·000 | 15·992 | 19·962 | 3·003 |

*All Fe as FeO.

The mineral abbreviations are after Kretz (1983), apart from MP (mesoperthite). The mineral formulae were calculated and the $Fe^{3+}$ concentrations estimated using an unpublished R program *GCDkit-Mineral* of the present authors, except for magnetite recalculated by *MinCalc* (Melín & Kunst, 1992). The $Fe^{3+}$ estimations in ilmenite, pyroxene and spinel were carried out using the algorithm of Droop (1987), in amphibole averaging the maximum and minimum ferric iron contents (see Leake *et al.*, 1997, Appendix 2), in garnet iteratively assuming a fixed sum of cations in the Y site (Al, Ti, Cr, Y, P, $Fe^{3+}$). Recalculation options: feldspars 32 O, amphiboles 23 O, biotite and phlogopite 22 (O, F, Cl), garnet 4 cations in the Y site, ilmenite total 2 cations, pyroxene total 4 cations, spinel total 3 cations. The complete dataset can be downloaded from http://www.petrology.oxfordjournals.org.

### Feldspars

The compositions of plagioclases in the main granulite groups are shown in Table 2. Subhedral tabular plagioclase crystals with more calcic cores occur in a few quartz dioritic and tonalitic granulites (e.g. BR-365: core $An_{48–51}$, rim $An_{45}$; Li-3: core $An_{47–51}$, rim $An_{35–37}$). On textural grounds (Fig. 4c and d), and with regard to comparison with the recrystallized plagioclase in the matrix, the tabular crystals are interpreted as relics from the plutonic protolith. Potassic feldspars and sodic plagioclases in leucocratic garnet granulites occur predominantly as mesoperthite and antiperthite intergrowths, owing to unmixing of the original ternary feldspars. The pristine leucogranulite samples containing nearly equant quartz grains were little affected by mylonitization and the related disintegration of mesoperthite to fine-grained mosaics of secondary feldspars. They preserve a simple assemblage of quartz + unmixed ternary feldspars (Fig. 3g) (mesoperthite Ab/Or ~ 1 and $An_{4–6}$, locally also antiperthite) with a small amount of primary plagioclase (<5 vol. %). Estimates of the temperature required to form the original ternary compositions are typically above 900°C (Fuhrman & Lindsley, 1988; O'Brien & Rötzler, 2003). However, a more specialized study is required to rigorously apply feldspar thermometry to both ternary feldspar types.

## THERMOBAROMETRY

Two-pyroxene thermometry (Brey & Köhler, 1990) on five quartz dioritic granulite samples gave $T = 710–720$°C and on two pyroxenite samples $T = 770–840$°C (Table 3). The equilibration conditions of four charnockites have been constrained by garnet–orthopyroxene–plagioclase–quartz geothermobarometry (Lal, 1993; implemented by Reche & Martinez, 1996) to $P = 3·5–5·0$ kbar and $T = 625–745$°C (Table 3). Core compositions were used in all calculations. However, the differences in *Grs* and *Prp* content between cores and rims of garnet crystals are typically <2 mol %, *Fs* in orthopyroxene varies by <1 mol %, and *An* in plagioclase varies by 1–3 mol %. This fact points, in agreement with textural relations of the phases, to a prolonged annealing and equilibration of the mineral assemblages. Samples selected for thermobarometry were devoid of amphibolite-facies retrogressive imprint.

The somewhat higher temperatures calculated for pyroxenites can be interpreted as reflecting metamorphic modification of relict magmatic clino- and orthopyroxene. Some large clinopyroxene crystals in pyroxenites and several quartz dioritic granulites (e.g. Li-4, BR-365) contain thin unmixed lamellae of orthopyroxene, accounting for <3–5 vol. % of the host clinopyroxene. Numerical simulation, adding 3 % of orthopyroxene back to clinopyroxene composition, showed that the temperatures obtained by the two-pyroxene thermometry (Table 3) may be underestimated by up to *c.* 40°C for quartz dioritic granulites (Li-4) or *c.* 100°C for pyroxenites (Li-22).

The samples contain no evidence for a previous higher grade metamorphic history, such as mineral inclusions indicative of an older HP stage. On the contrary, several samples still preserve large (Fig. 4c and d) subhedral plagioclases (*LM qtzD*) and poikilitic clinopyroxenes (Fig. 3d), both of which are interpreted as having survived from the original magmatic protolith (see Table 1 and previous section)

## WHOLE-ROCK GEOCHEMISTRY

### Major elements

The whole-rock geochemical variations in the LGM have been studied using over 20 new analyses (Tables 4 and 5) supplemented by data from the literature (Jakeš, 1967; Slabý, 1983; Fiala *et al.*, 1987*a*; Kotková, 1998*b*). Major-element based cluster analysis was employed to classify a few samples from the literature for which accurate petrographic descriptions were lacking.

The granulites are subalkaline (Fig. 5a), defining a calc-alkaline trend in the AFM plot (Fig. 5b). In the multicationic P–Q diagram of Debon & Le Fort (1983) (Fig. 5c) many of the felsic Lišov granulites (*LF gr*) fall into adamellite–granite domains, close to the frequency maximum for most other Moldanubian granulite massifs (see Janoušek *et al.*, 2004*b*, fig. 4). In contrast, the charnockitic types (*LF ch*) correspond to granodiorite–adamellite and the more mafic varieties fall mainly into the fields of gabbro–quartz diorite–tonalite, albeit with small overlaps into adjacent monzonitic domains.

The mafic Lišov granulites are exclusively metaluminous, as shown by the mean values of Shand's index A/CNK [molar $Al_2O_3/(CaO + Na_2O + K_2O)$, Fig. 6]: *LM qtzD* = 0·80 (0·73–0·89) and *LM to* = 0·89 (0·78–0·98). The granitic granulites *LF gr* and the charnockites (*LF ch*) are mostly slightly peraluminous, A/CNK = 0·95–1·20 (mean 1·07) and A/CNK = 0·95–1·10 (1·05), respectively. Most of the Lišov granulites can be characterized as medium-K to high-K calc-alkaline rocks on the basis of the $SiO_2$–$K_2O$ diagram (Peccerillo & Taylor, 1976) (Fig. 6).

There are strong negative correlations between whole-rock $SiO_2$ and $TiO_2$, $Al_2O_3$, $FeO_t$, MgO and CaO for most of the petrographic groups (Fig. 6). The graphs with $K_2O$ and mg number [mg number = molar $Mg/(Mg + Fe_t)$] are characterized by inflections or discontinuities at $SiO_2$ ~60 and/or ~70 wt %. The pyroxenites with relatively low $Al_2O_3$, $TiO_2$ and alkalis, coupled with high MgO, CaO and mg number, show trends that are commonly oblique to those defined by the *LM qtzD* granulites.

*Table 3: Thermobarometry for Lišov granulite samples*

| Sample | Opx | | | Cpx | | | $T$ (°C) | $P$ (kbar) |
|---|---|---|---|---|---|---|---|---|
| | $X_{Fe}$ | Ca | Na | $X_{Fe}$ | Ca | Na | | |
| *Pyroxenites* | | | | | | | | |
| Li-22 | 0·233 | 0·018 | — | 0·141 | 0·903 | 0·026 | 770[a] | |
| LV-4 | 0·319 | 0·017 | — | 0·196 | 0·858 | 0·025 | 840 | |
| *Mafic granulites, quartz dioritic* | | | | | | | | |
| BR-363 | 0·481 | 0·029 | — | 0·327 | 0·876 | 0·023 | 720[a] | |
| Li-4 | 0·479 | 0·030 | — | 0·321 | 0·878 | 0·029 | 715 | |
| BR-365 | 0·489 | 0·028 | — | 0·339 | 0·872 | 0·036 | 710 | |
| LV-60 | 0·465 | 0·031 | — | 0·262 | 0·883 | 0·030 | 710 | |
| Li-26 | 0·476 | 0·023 | — | 0·303 | 0·880 | 0·034 | 700 | |

| | Grt | | | | | Opx | | | | | | | | | Pl | | | | |
|---|---|---|---|---|---|---|---|---|---|---|---|---|---|---|---|---|---|---|---|
| | $Fe^{2+}$ | $Fe^{3+}$ | Mg | Mn | Ca | Si | $Al^{t}$ | Ti | $Fe^{3+}$ | $Fe^{2+}$ | Mg | Mn | Na | Ca | Ca | Na | K | | |
| *Charnockites* | | | | | | | | | | | | | | | | | | | |
| Li-5 | 2·163 | 0·068 | 0·366 | 0·087 | 0·313 | 1·967 | 0·054 | 0·003 | 0·005 | 1·281 | 0·658 | 0·015 | — | 0·015 | 0·265 | 0·724 | 0·011 | 672[b] | 4·5[b] |
| BD-22 | 2·263 | 0·060 | 0·287 | 0·111 | 0·304 | 1·967 | 0·042 | 0·004 | 0·019 | 1·351 | 0·561 | 0·023 | 0·007 | 0·021 | 0·235 | 0·762 | 0·010 | 673 | 4·5 |
| LV-58 | 2·309 | 0·042 | 0·323 | 0·092 | 0·276 | 1·958 | 0·059 | 0·005 | 0·014 | 1·314 | 0·618 | 0·015 | — | 0·015 | 0·267 | 0·714 | 0·017 | 625 | 3·5 |
| LV-24 | 2·103 | 0·046 | 0·678 | 0·083 | 0·121 | 1·932 | 0·111 | 0·003 | 0·017 | 1·029 | 0·885 | 0·015 | — | 0·006 | 0·176 | 0·792 | 0·021 | 745 | 5·0 |

| | Grt | | | | Mesoperthite | | | | |
|---|---|---|---|---|---|---|---|---|---|
| | $X_{Ca}$ | $X_{Mg}$ | $X_{Fe}$ | $X_{Mn}$ | $X_{Or}$ | $X_{Ab}$ | $X_{An}$ | | |
| *Felsic garnet granulite* | | | | | | | | | |
| LV-11 | 0·038 | 0·214 | 0·722 | 0·026 | 0·516 | 0·421 | 0·063 | 900–1000[c] | |
| *Garnet two-pyroxene granulite (Kotková 1998a, 1998b)* | | | | | | | | 910 | 14·6 |

Calibrations after: [a]Brey & Köhler (1990); [b]Lal (1993) in Reche & Martinez (1996); [c]Fuhrman & Lindsley (1988).

## Trace elements

The Lišov samples resemble other Moldanubian granulites in being practically undepleted in large ion lithophile elements (LILE) (Fiala *et al.*, 1987*a*). However, binary plots of $SiO_2$ vs trace elements (Fig. 7) display conspicuous differences for the various granulite groups. Two types of trace-element distribution can be discerned: (1) elements whose concentrations generally increase or decrease in the succession *LM qtzD–LM to–LF ch–LF gr* (Rb, Y), and (2) those forming highly scattered convex-upward trends, with an inflection or discontinuity at $SiO_2$ ~60–65% (La, Zr). The pyroxenites again have a special position (characterized by low La coupled with high Ni).

The compositions of the granulites *LM qtzD* were normalized to average normal mid-ocean ridge basalt (N-MORB; Sun & McDonough, 1989) (Fig. 8a). The patterns are all enriched in LILE, starting at >40 × N-MORB (Cs, Rb) and falling to slightly less than 0·8 × N-MORB (heavy REE; HREE). All show superimposed troughs in Nb and peaks in Ba and Pb; P and Zr are depleted in most samples. Interestingly, the pattern of the picritic dyke (Li-25) reveals contents of high field strength elements (HFSE) and REE only slightly higher than those of MORB (Fig. 8b). Elements mobile in hydrous fluids (Cs, Rb, Ba, Th, U, K, Pb and Sr) are, however, strongly enriched. Similar LILE/HFSE enrichments are typical

*Table 4: Selected whole-rock major-element data (wt %) for the granulites of the Lišov Massif*

| Sample: | Li-25[a] | Li22A[a] | LV-4[a] | BR-363 | Li-26[a] | BR-365 | Li-4 | Li-3 | Li-7 | Li-5 | Li-6 | LV-17 | LV-11 | LV-12 |
|---|---|---|---|---|---|---|---|---|---|---|---|---|---|---|
| Locality: | Zvíkov | Zvíkov | Zvíkov | Vlkovice | Zvíkov | Skalice | Zvíkov | Vlkovice | Rudolfov | Lišov | H.Hora | H.Hora | H.Hora | H.Hora |
| Rock group: | *dyke* | *Pxte* | *Pxte* | *LM qtzD* | *LM qtzD* | *LM qtzD* | *LM qtzD* | *LM to* | *LM to* | *LF ch* | *LF gr* | *LF gr* | *LF gr* | *LF gr* |
| $SiO_2$ | 43·50 | 51·01 | 51·62 | 52·04 | 53·03 | 53·63 | 55·34 | 60·48 | 65·22 | 73·04 | 77·21 | 77·50 | 77·54 | 77·89 |
| $TiO_2$ | 1·93 | 0·60 | 0·34 | 1·02 | 0·97 | 0·93 | 0·97 | 0·77 | 0·58 | 0·41 | 0·11 | 0·05 | 0·08 | 0·03 |
| $Al_2O_3$ | 19·81 | 6·08 | 3·72 | 17·64 | 18·14 | 17·70 | 17·73 | 15·52 | 14·49 | 13·40 | 12·50 | 12·35 | 12·37 | 12·36 |
| $Fe_2O_3$ | — | — | — | 0·94 | — | 0·93 | 1·37 | 0·27 | 1·00 | 0·25 | 0·11 | 0·04 | 0·31 | 0·01 |
| FeO | 9·64 | 8·78 | 10·36 | 7·97 | 8·58 | 7·16 | 6·19 | 4·95 | 4·54 | 2·88 | 1·19 | 0·86 | 0·79 | 0·88 |
| MnO | 0·15 | 0·16 | 0·24 | 0·17 | 0·16 | 0·15 | 0·14 | 0·10 | 0·11 | 0·06 | 0·04 | 0·03 | 0·03 | 0·02 |
| MgO | 8·84 | 18·86 | 15·07 | 5·39 | 4·73 | 4·40 | 3·89 | 3·73 | 2·99 | 0·60 | 0·13 | 0·16 | 0·13 | 0·05 |
| CaO | 12·04 | 11·91 | 16·67 | 8·36 | 8·47 | 7·82 | 7·92 | 4·78 | 5·76 | 2·01 | 0·67 | 0·69 | 0·82 | 0·65 |
| $Na_2O$ | 1·38 | 0·53 | 0·51 | 3·02 | 3·38 | 3·28 | 3·18 | 2·87 | 2·78 | 3·19 | 3·13 | 3·06 | 3·28 | 3·17 |
| $K_2O$ | 0·85 | 0·68 | 0·15 | 1·50 | 1·51 | 1·98 | 1·70 | 3·62 | 1·35 | 3·46 | 4·40 | 4·82 | 4·20 | 4·60 |
| $P_2O_5$ | 0·03 | 0·01 | 0·03 | 0·26 | 0·28 | 0·22 | 0·25 | 0·31 | 0·08 | 0·07 | b.d. | 0·03 | 0·02 | 0·02 |
| $CO_2$ | — | — | — | 0·02 | — | 0·12 | 0·06 | 0·05 | 0·03 | 0·02 | 0·02 | — | 0·01 | 0·01 |
| $Cr_2O_3$ | 0·01 | 0·28 | 0·28 | 0·01 | 0·01 | 0·01 | 0·01 | 0·02 | 0·01 | 0·01 | 0·00 | 0·00 | 0·00 | 0·00 |
| BaO | 0·05 | 0·05 | 0·01 | 0·11 | 0·15 | 0·16 | 0·12 | 0·12 | 0·12 | 0·10 | 0·03 | 0·03 | 0·04 | 0·01 |
| $H_2O^+$ | 1·70[b] | 1·40[b] | 0·37[b] | 1·30 | — | 0·89 | 1·07 | 1·20 | 1·06 | 0·19 | 0·10 | — | 0·06 | 0·07 |
| F | — | — | — | 0·05 | 0·03 | 0·09 | 0·089 | 0·129 | 0·075 | 0·044 | 0·035 | — | 0·03 | 0·09 |
| S | 0·06 | 0·15 | 0·01 | 0·06 | 0·06 | 0·06 | 0·05 | 0·07 | 0·08 | 0·02 | 0·01 | 0·03 | 0·03 | 0·04 |
| $H_2O^-$ | — | — | — | 0·09 | — | 0·07 | 0·13 | 0·22 | 0·14 | 0·13 | 0·13 | — | 0·10 | 0·16 |
| Total | 99·99 | 100·35 | 99·38 | 99·95 | 99·50 | 99·60 | 100·21 | 99·20 | 100·41 | 99·88 | 99·81 | 99·65 | 99·84 | 100·06 |
| A/CNK | 0·79 | 0·26 | 0·12 | 0·81 | 0·80 | 0·81 | 0·83 | 0·90 | 0·88 | 1·06 | 1·12 | 1·07 | 1·08 | 1·09 |
| K (%) | 0·71 | 0·56 | 0·13 | 1·25 | 1·25 | 1·64 | 1·41 | 3·01 | 1·12 | 2·87 | 3·65 | 4·00 | 3·49 | 3·82 |
| $K_2O/Na_2O$ | 0·62 | 1·28 | 0·29 | 0·50 | 0·45 | 0·60 | 0·53 | 1·26 | 0·49 | 1·08 | 1·41 | 1·58 | 1·28 | 1·45 |
| mg no. | 62·06 | 79·29 | 72·19 | 52·15 | 49·58 | 49·51 | 48·30 | 56·15 | 49·49 | 25·62 | 15·24 | 24·14 | 17·82 | 9·11 |

[a]Samples analysed by XRF at Institut für Mineralogie, Universität Salzburg. The remaining major elements were obtained by wet chemistry in the Czech Geological Survey, Prague–Barrandov.
[b]Loss on ignition.
Pxte, pyroxenite.

of K-rich basalts from continental margin arc settings (e.g. Saunders *et al.*, 1991; Pearce & Parkinson, 1993; Tatsumi & Eggins, 1995).

The quartz dioritic granulites (the shaded fields in Fig. 8a–d) differ from other Moldanubian massifs in having elevated divalent LILE concentrations (Sr, Pb ± Ba), whereas K and HREE tend to be somewhat lower (Fig. 8c). These differences can be accounted for by a higher degree of fractionation in the mafic–intermediate granulites from bodies other than that at Lišov, which nearly all have fairly high silica contents and mg number <60.

The dyke Li-25 is geochemically rather primitive, as shown by the flat, slightly convex-upward REE pattern ($Ce_N/Yb_N$ = 1·2: Table 5) at *c.* 15–20 × chondrite and lack of any Eu anomaly (Eu/Eu* = 1·04) (Fig. 9a). The pyroxenite Li-22A is somewhat more fractionated, as indicated by a weak LREE/HREE enrichment ($Ce_N/Yb_N$ = 3·1) and a distinct negative Eu anomaly (Eu/Eu* = 0·60) (Fig. 9a). The *LM qtzD* granulites are characterized by moderately light REE (LREE)-enriched patterns ($Ce_N/Yb_N$ = 5·8–6·4) with slightly negative Eu anomalies (Eu/Eu* = 0·80–0·86) (Fig. 9a). The tonalitic granulites (*LM to*) contain the highest $\sum$REE in the dataset (Fig. 9b and c), with moderately LREE-enriched patterns ($Ce_N/Yb_N$ = 3·7–7·9) and pronounced negative Eu anomalies (Eu/Eu* = 0·50–0·62). A similar pattern is also seen in sample JK-1 of Kotková (1998*b*), which has the highest total, and in particular HREE content.

The charnockite (*LF ch*) has a relatively flat REE pattern ($Ce_N/Yb_N$ = 2·9) with a strong negative Eu anomaly (Eu/Eu* = 0·39) (Fig. 9c). The leucogranulite (*LF gr*) has the lowest LREE/HREE ratio ($Ce_N/Yb_N$ = 2·1) and a deep Eu anomaly (Eu/Eu* <0·16, with the Eu below the detection limit of 0·18 ppm).

*Table 5: Selected whole-rock trace-element analyses for the Lišov granulites (ppm)*[a]

| Sample: | Li-25[b] | Li-22A[b] | LV-4[c] | BR-363[c] | Li-26[c] | BR-365[c] | Li-4[c] | Li-3[c] | Li-7[c] | Li-5[c] | Li-6[c] | LV-17[c] | LV-11[c] | LV-12[c] |
|---|---|---|---|---|---|---|---|---|---|---|---|---|---|---|
| Locality: | Zvíkov | Zvíkov | Zvíkov | Vlkovice | Zvíkov | Skalice | Zvíkov | Vlkovice | Rudolfov | Lišov | H.Hora | H.Hora | H.Hora | H.Hora |
| Rock group: | dyke | Pxte | Pxte | LM qtzD | LM qtzD | LM qtzD | LM qtzD | LM to | LM to | LF ch | LF gr | LF gr | LF gr | LF gr |
| Ba | 448.4 | 431.3 | 124 | 920 | 1338 | 1427 | 1066 | 1083 | 457 | 925 | 267 | 253 | 363 | 106 |
| Rb | 16.2 | 27.9 | 6 | 27 | 21 | 53 | 51 | 166 | 29 | 81 | 166 | 177 | 111 | 207 |
| Sr | 439.2 | 112.6 | 71 | 648 | 643 | 580 | 565 | 375 | 135 | 84 | 21 | 25 | 47 | 21 |
| Zr | 26.5 | 37.5 | 87 | 61 | 99 | 140 | 119 | 156 | 127 | 164 | 56 | 40 | 60 | 50 |
| Y | 32.1 | 22.8 | 56 | 22 | 27 | 28 | 24 | 26 | 30 | 42 | 33 | 65 | 61 | 45 |
| Ni | 7.0 | 122.4 | 105 | 18 | 19 | 16 | 17 | 28 | b.d. | b.d. | b.d. | 2 | 3 | 2 |
| Co | 37.6 | 62.4 | 42 | 24 | 23 | 21 | *21* | *19* | *16* | *4* | *2* | 1 | 1 | 1 |
| Cr | 68 | 1934 | 1902 | 68 | 52 | 59 | 71 | 138 | 95 | 36 | 19 | 9 | 13 | 10 |
| Zn | 28 | 13 | *115* | *90* | 93 | 91 | *88* | *74* | *86* | *32* | *23* | 12 | 12 | 8 |
| Ga | 18.8 | 9.5 | 7.1 | 19.1 | 22.2 | 19.0 | 20.3 | 17.8 | 18.1 | 16.8 | 16.6 | 15.3 | 15.3 | 16.7 |
| Hf | 1.3 | 1.7 | 1.9 | 0.6 | 2.5 | 3.6 | 2.4 | 4.3 | 4.6 | 4.9 | 1.8 | 0.9 | 1.2 | 2.1 |
| Nb | 2.5 | 1.1 | 5.2 | 7.3 | 7.3 | 9.0 | 8.3 | 12.7 | 8.1 | 7.0 | 3.2 | 1.6 | 1.4 | 1.7 |
| U | 0.1 | 0.2 | 2.5 | 0.6 | b.d. | b.d. | 0.5 | 1.0 | 3.1 | 2.7 | 2.6 | 9.6 | 7.5 | 3.5 |
| K/Rb | 441 | 205 | 208 | 461 | 597 | 310 | 277 | 181 | 386 | 355 | 220 | 226 | 314 | 184 |
| Rb/Sr | 0.04 | 0.25 | 0.08 | 0.04 | 0.03 | 0.09 | 0.09 | 0.44 | 0.21 | 0.96 | 7.90 | 7.08 | 2.36 | 9.89 |
| Ba/Sr | 1.02 | 3.83 | 1.75 | 1.42 | 2.08 | 2.46 | 1.89 | 2.89 | 3.39 | 11.01 | 12.71 | 10.12 | 7.72 | 5.05 |
| *REE*[c] | | | | | | | | | | | | | | |
| La | 4.8 | 7.8 | — | *26.6* | — | *30.8* | *27.5* | *39.5* | *39.5* | *32.4* | *19.1* | — | — | — |
| Ce | 14.2 | 25.5 | — | *53.9* | — | *61.4* | *60.8* | *88.1* | *74.9* | *61.2* | *36.8* | — | — | — |
| Pr | 2.19 | 3.8 | — | *6.2* | — | *7.0* | *8.3* | *12.1* | *11.9* | *7.7* | *5.1* | — | — | — |
| Nd | 12.0 | 18.2 | — | *26.3* | — | *30.9* | *33.4* | *43.4* | *37.7* | *27.3* | *13.5* | — | — | — |
| Sm | 4.1 | 4.6 | — | *6.4* | — | *7.1* | *6.4* | *8.9* | *7.9* | *5.6* | *2.4* | — | — | — |
| Eu | 1.56 | 0.89 | — | *1.63* | — | *1.64* | *1.71* | *1.37* | *1.75* | *0.81* | *<0.18* | — | — | — |
| Gd | 5.17 | 4.42 | — | *5.3* | — | *5.5* | *7.0* | *8.0* | *9.3* | *7.2* | *5.0* | — | — | — |
| Tb | 0.93 | 0.69 | — | *<0.90* | — | *<0.90* | *<0.90* | *<0.90* | *1.00* | *0.94* | *<0.90* | — | — | — |
| Dy | 5.66 | 4.26 | — | *4.3* | — | *4.9* | *4.6* | *5.6* | *8.3* | *8.2* | *7.4* | — | — | — |
| Ho | 1.26 | 0.83 | — | *0.90* | — | *1.00* | *0.82* | *1.01* | *1.60* | *1.69* | *1.52* | — | — | — |
| Er | 3.45 | 2.32 | — | *2.5* | — | *2.6* | *2.6* | *2.6* | *4.6* | *5.4* | *4.8* | — | — | — |
| Tm | 0.48 | 0.34 | — | *0.40* | — | *<0.40* | *<0.40* | *<0.40* | *0.57* | *0.65* | *0.48* | — | — | — |
| Yb | 3.04 | 2.15 | — | *2.27* | — | *2.48* | *2.73* | *2.90* | *5.24* | *5.37* | *4.57* | — | — | — |
| Lu | 0.43 | 0.35 | — | *0.35* | — | *0.40* | *0.34* | *0.39* | *0.75* | *0.76* | *0.66* | — | — | — |
| Eu/Eu* | 1.04 | 0.60 | | *0.86* | | *0.80* | *0.78* | *0.50* | *0.62* | *0.39* | *<0.16* | | | |
| $Ce_N/Yb_N$ | 1.21 | 3.07 | | *6.14* | | *6.40* | *5.76* | *7.86* | *3.70* | 2.95 | 2.08 | | | |

[a]REE contents in ppm and normalized (N) by chondrite (Boynton, 1984).
[b]Samples Li-25 and Li22A were analysed by ICP-MS in the Acme Analytical Laboratories, Vancouver, Canada. Most of the trace elements were determined following $LiBO_2$ fusion; only for Ni and Zn were they dissolved in aqua regia.
[c]The data were obtained by XRF at Institut für Mineralogie, Universität Salzburg, except for those in italics, which were determined by AAS (Co and Zn) and ICP-OES (the remaining elements) in the laboratories of the Czech Geological Survey, Prague–Barrandov. (See the text for analytical details.)
b.d., below detection limit.

## U–Pb zircon geochronology

A combined study of internal zoning (CL, BSE) and LA–ICP–MS dating of zircons in quartz dioritic (Li-4, Zvíkov) and tonalitic (Li-3, Vlkovice) granulites aimed to constrain the nature and age of the protolith to the 'mafic' suite from Lišov. Representative CL images of zircons are presented in Figs 10 and 12, analytical data in Table 6, and concordia diagrams in Fig. 11. The majority of the LA–ICP–MS spot analyses yielded concordant Late Devonian to Early Carboniferous ages.

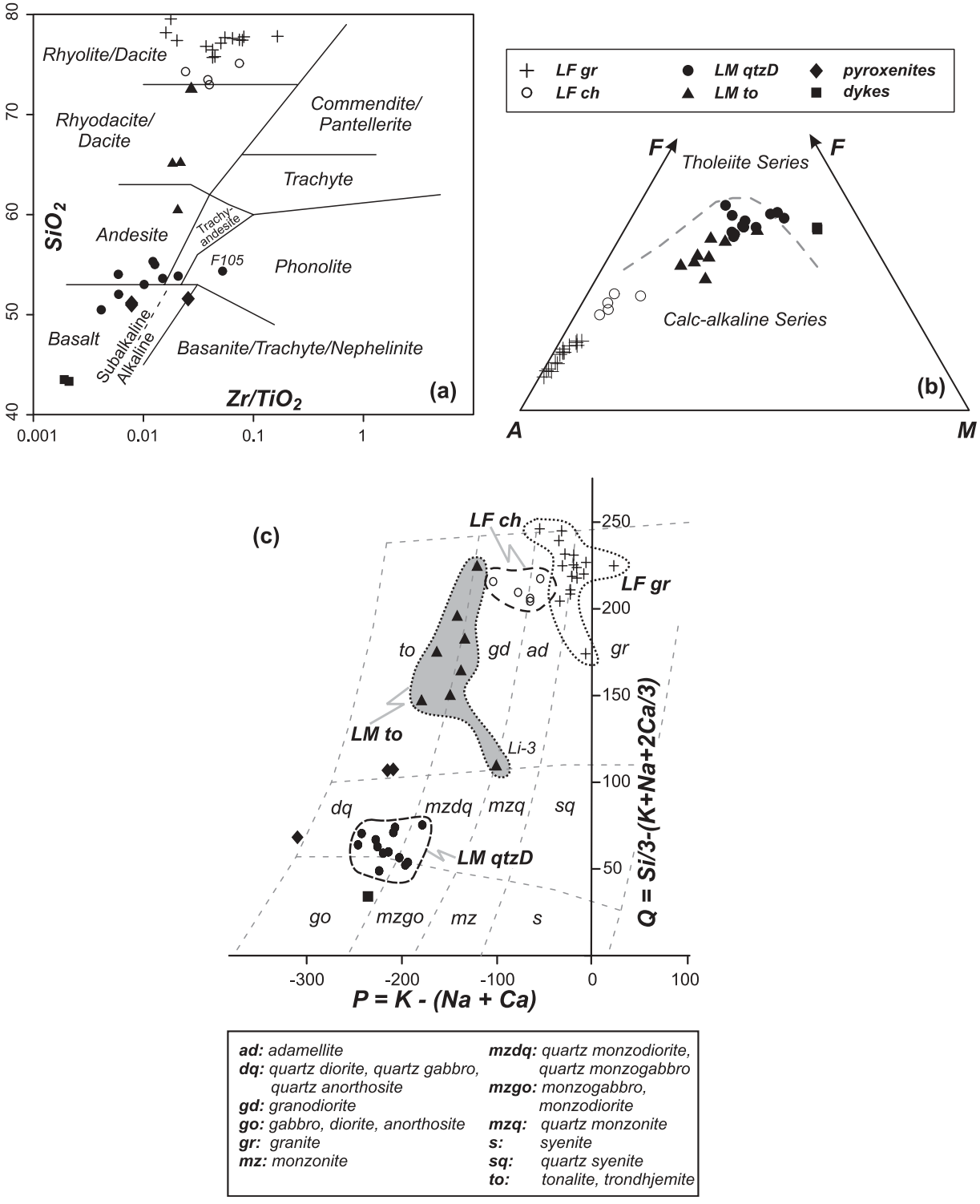


**Fig. 5.** (a) Classification of the Lišov granulites in the $Zr/TiO_2$–$SiO_2$ plot (Winchester & Floyd, 1977). (b) AFM diagram (A = $Na_2O$ + $K_2O$, F = $FeO_t$, M = MgO: Irvine & Baragar, 1971) showing a calc-alkaline trend. The analyses obtained in the course of the current study were supplemented by literature data (see caption to Fig. 2 for details). *LF*, felsic granulites; *ch*, charnockites; *gr*, granitic granulites; *LM*, mafic granulites; *qtzD*, quartz dioritic, essentially garnet-free granulites; *to*, tonalitic granulites. (c) Multicationic P–Q plot (Debon & Le Fort, 1983); P represents the proportion of K-feldspar to plagioclase and Q the quartz content.

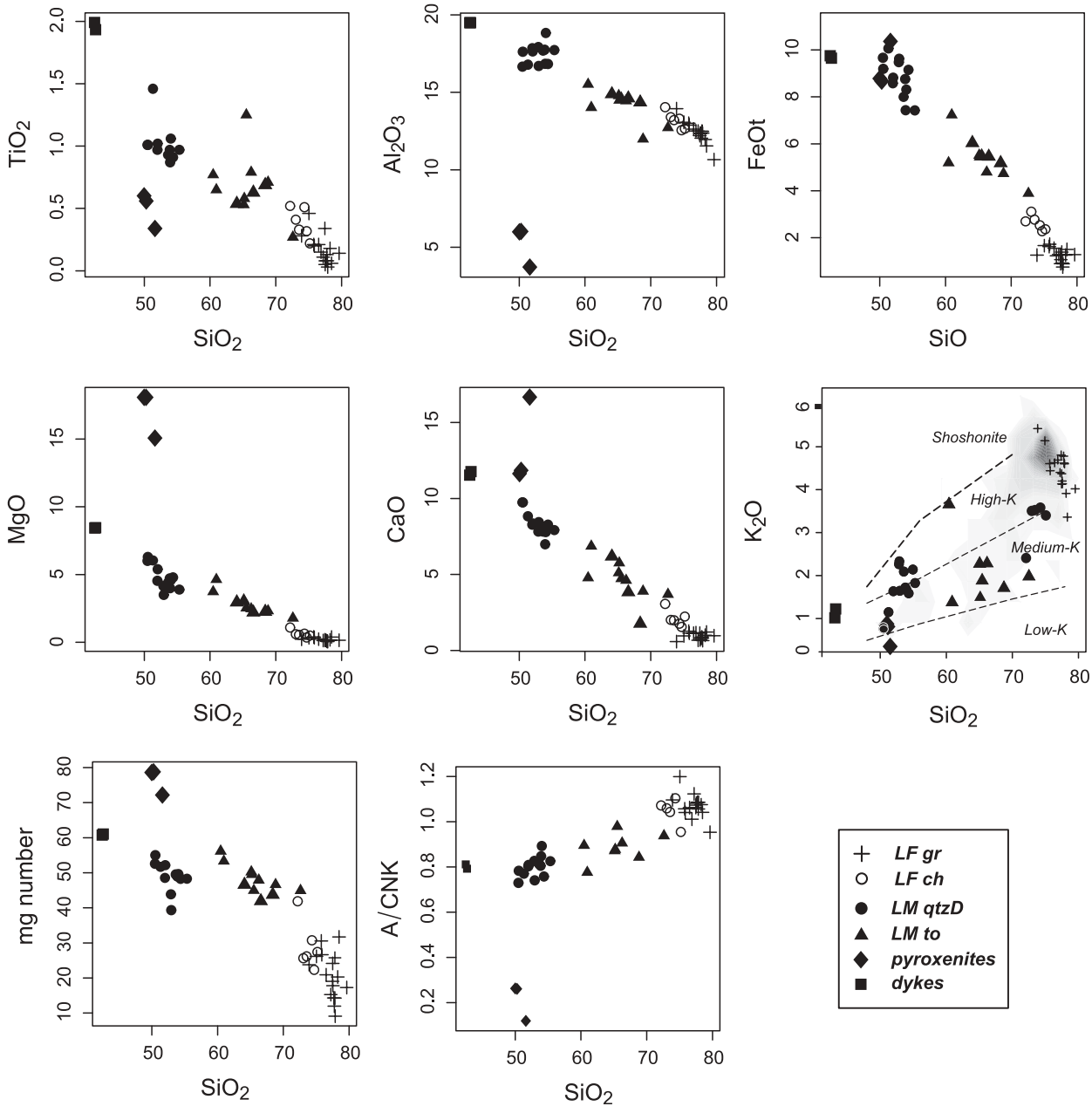


**Fig. 6.** Variation diagrams of $SiO_2$ (wt %) vs major-element oxides (wt %) and Shand's index (A/CNK) for the Lišov granulites. The discrimination boundaries between the tholeiitic, calc-alkaline, high-K calc-alkaline and shoshonitic rocks in the $SiO_2$–$K_2O$ plot are those of Peccerillo & Taylor (1976). The frequency of all Moldanubian samples in the same diagram is expressed by various shades of grey (Janoušek *et al.*, 2004*b*).

*Quartz diorite Li-4 (LM qtzD)*

This sample contains numerous small prismatic zircons, typically slightly rounded (Fig. 10a, b and e). Although many grains preserve an oscillatory zoning, suggesting a magmatic origin (Fig. 10a), others commonly seem to be recrystallized with the primary zones blurred and thickened (Pidgeon, 1992; Pidgeon *et al.*, 1998; Corfu *et al.*, 2003) (Fig. 10c). The complex texture of some grains is illustrated in Fig. 10e. A rounded, xenocrystic core in the centre is surrounded by a mantle that exhibits an original oscillatory zoning. However, this is progressively blurred by recrystallization and is obliterated, most markedly to the left and upper side of the outer zone of the grain.

At a more advanced stage of the solid-state recrystallization, a convoluted zoning appears, which is usually interpreted as a result of a complex elemental diffusion

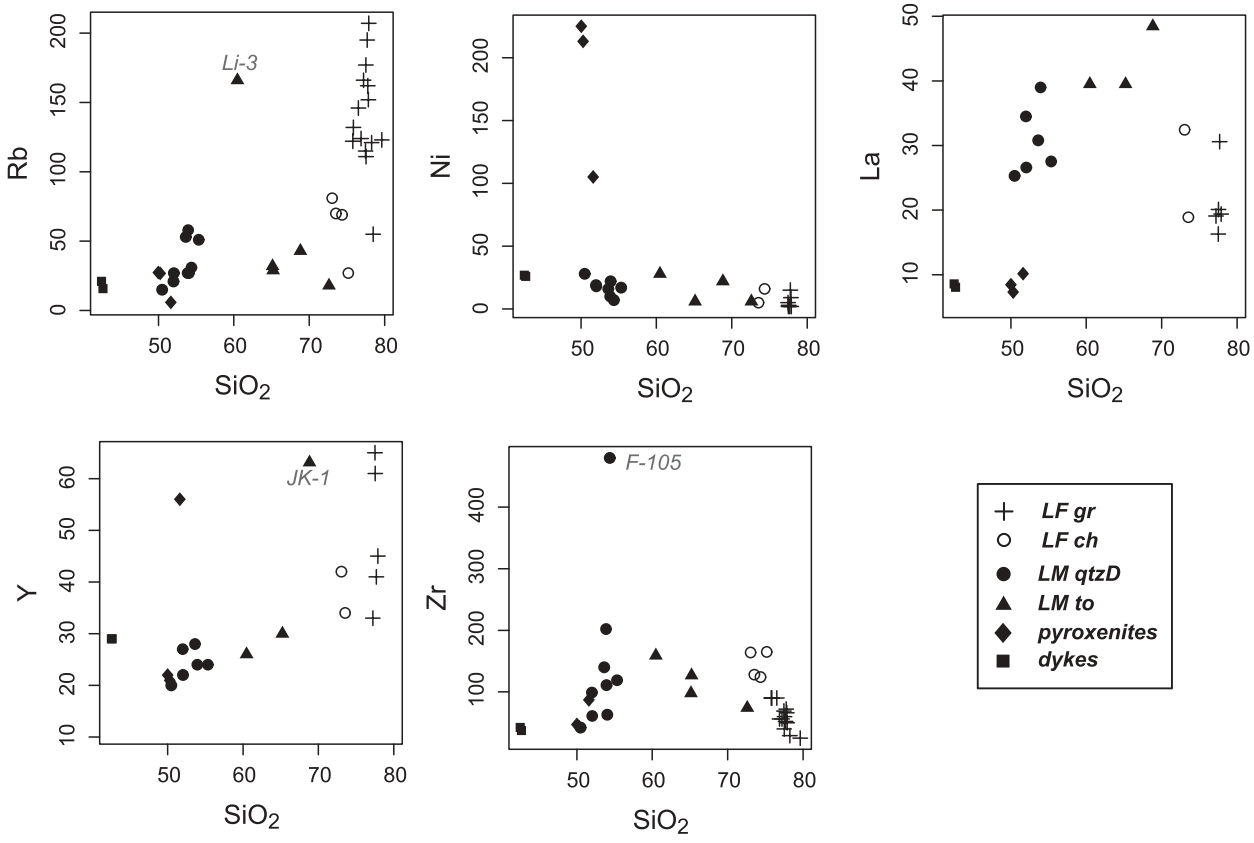


**Fig. 7.** Variation diagrams of $SiO_2$ (wt %) vs selected trace elements (ppm) for the studied granulites.

(Hoskin & Black, 2000; Hoskin & Schaltegger, 2003). The process can result in almost complete obliteration of the magmatic zoning, with only rare relics preserved (Fig. 10c). About 15 % of the grains, mostly prismatic and small (120 μm × 60 μm), show well-preserved oscillatory zoning, but this is usually truncated by a relatively small nearly featureless metamorphic rim (Fig. 10a and b). Figure 10f shows an example with a larger overgrowth around a small residual prismatic core.

In addition to small and generally unbroken prismatic zircons, the mineral concentrates contain numerous larger angular fragments. A BSE study of the thin section reveals that these are crushed interstitial grains (Fig. 10d), whose shape is mostly determined by adjacent existing phases. Similar morphologies with only partly developed crystal faces are typical of zircons in many basic rocks, where they commonly reflect relatively late crystallization (Corfu *et al.*, 2003, and references therein). Delayed nucleation is due to the low original Zr content of the magma, when compared with the typically high Zr solubility in basic melts (Watson & Harrison, 1983). Indeed, the parental magma of the protolith of the granulites *LM qtzD* may initially have been zircon-undersaturated, as indicated by a positive trend in the silica-poor part of the $SiO_2$–Zr plot (Fig. 7) (Hoskin *et al.*, 2000) and the calculated zircon saturation temperatures (*c.* 600–800°C; Li-4: 700°C), too low for a magma of comparable $SiO_2$ content.

The interstitial grains show a continuous spectrum of variously modified primary zoning, starting from oscillatory, through more complex (convoluted or fir-tree sector zoning: Fig. 10d) to nearly unzoned grains or fragments thereof.

Thus, based on textural observations we can distinguish at least three domains of different ages in zircons in this sample: (a) rounded xenocrystic cores; (b) oscillatory-zoned domains of probably magmatic origin; (c) recrystallized and blurred zones and outer rims. The xenocrystic cores in the centres of the grains were not visible in optical CL images, except for grain 11 (Fig. 10e). However, in the course of five analyses the laser drilled into older cores that were detected because of the short response time of the system (Fig. 11c). Analysis A1 (Fig. 11d) penetrated the same core as analysed in A3 (Fig. 10e, central spot). Five of the six analyses of the cores yielded $^{206}Pb/^{238}U$ ages of 469 ± 19 to 524 ± 50 Ma with a weighted average of 486 ± 20 Ma (2σ; MSWD = 1·5). These appear to be concordant or only slightly discordant, having a concordia age of 487 ± 11 Ma (2σ; MSWD = 1·7). The core of grain 11 yielded clearly

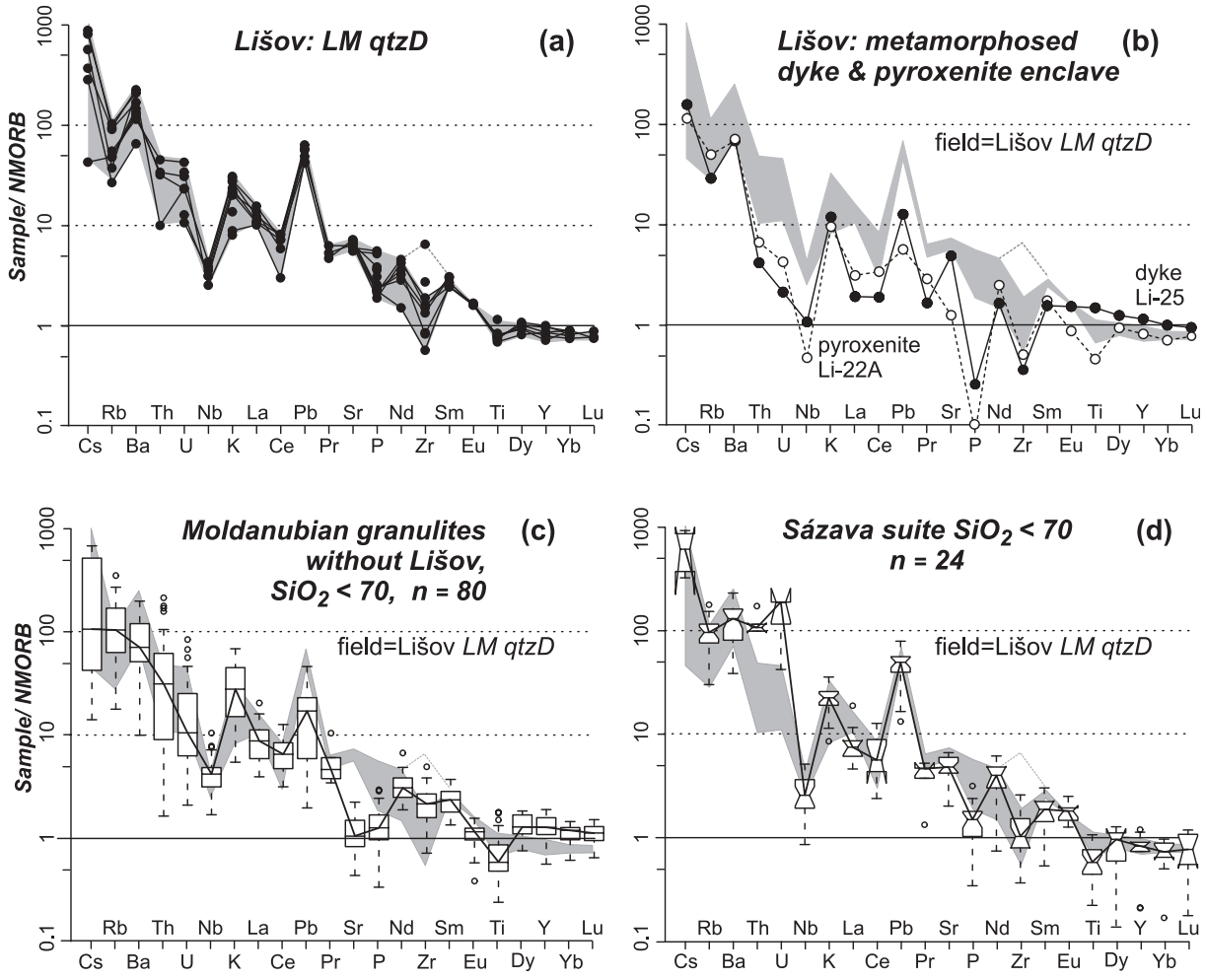


**Fig. 8.** N-MORB-normalized (Sun & McDonough, 1989) spider plots for the Lišov *LM qtzD* granulites (a), as well as the associated dyke Li-25 and pyroxenite LI-22A (b). (c) Spider boxplot (Janoušek *et al.*, 2004*b*) for the Moldanubian granulites, omitting the Lišov data and analyses with $SiO_2$ >70%. For each element, the box represents 50% of the population (limited by two quartiles); the horizontal line inside is the median, the vertical dashed lines show the total range without outliers (denoted by small circles). (d) Spider boxplot for magmatic rocks of the Sázava suite, Central Bohemian Plutonic Complex, with $SiO_2$ <70% (Janoušek *et al.*, 2000, 2004*a*). A grey field for *LM qtzD* is shown in all diagrams.

discordant analyses with $^{206}Pb/^{238}U$ and $^{207}Pb/^{206}Pb$ ages of 389 ± 13 and 574 ± 85 Ma, respectively. In general, the elevated $^{207}Pb/^{206}Pb$ errors do not allow a single crystallization age for these zircon cores to be postulated without independent evidence for their common origin. In addition, we cannot rule out some mixing between inherited cores and the surrounding zircon as a result of the limited spatial resolution of the laser and the effects of pit wall ablation (Griffin *et al.*, 2002), which could also account for the large analytical errors. Thus the $^{206}Pb/^{238}U$ ages should be interpreted as a minimum constraint and an interval of 470–600 Ma taken as the best age estimate for the crystallization of the xenocrystic cores (Fig. 11c).

The oscillatory-zoned domains were usually analysed in grains where only a small secondary rim was developed (Fig. 10a and b). They showed a relatively homogeneous $^{206}Pb/^{238}U$ age distribution (Fig. 11b). Only three examples of grains with partially recrystallized domains have been analysed (grain 11: analyses A1 and A2; grain 13: analysis A8). Analyses A1 and A2 yielded $^{206}Pb/^{238}U$ ages that only just overlap within the 2σ error (352 ± 10 and 371 ± 10 Ma; Fig. 10e). Thus the younger age of A1 could be interpreted in terms of Pb loss and/or partial resetting, as this part of the grain seems to have been more affected by recrystallization. However, both $^{206}Pb/^{238}U$ ages fall, together with that of A8, within the range for the other eight analyses from oscillatory-zoned domains. All 11 analyses give a concordia age of 360 ± 3 Ma (2σ; MSWD = 0·9: Fig. 11b), which is identical to the mean age of 361 ± 3 Ma if A1 and A8 are excluded. It is, nevertheless, likely that even some of

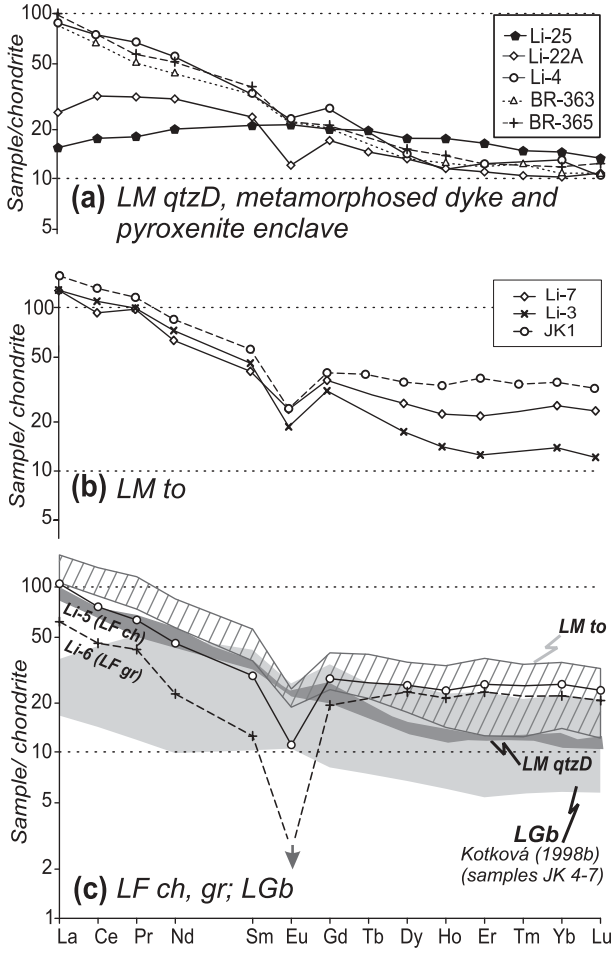


**Fig. 9.** Chondrite-normalized (Boynton, 1984) REE patterns of the Lišov granulites. (a) Mafic quartz dioritic granulites (*LM qtzD*), together with the associated dyke Li-25 and pyroxenite LI-22A; (b) tonalitic granulites (*LM to*); (c) felsic granulites (*LF gr* and *LF ch*). In (c), the dark grey field for *LM qtzD*, diagonally shaded field for *LM to* and the light grey field for the garnet-bearing gabbroic granulites (*LGb*) are shown for comparison. Data from this work and Kotková [1998*b*: sample JK1 in (b) and light grey field in (c)].

the grains with well-preserved oscillatory zoning were affected by small degrees of Pb loss and the U–Pb ages give only minimum constraints.

In examples of the third zircon domain, only grains showing complete or almost complete recrystallization (Fig. 10c) have been analysed, to avoid mixed ages. The only exception might have been grain 14 (Fig. 10d). However, the two analyses of grain 14 are indistinguishable from those in the other six grains. All eight analyses show a very homogeneous $^{206}Pb/^{238}U$ age distribution with a concordia age of 339 ± 3 Ma (2σ; MSWD = 0·8; Fig. 11a). The <10 μm wide rims of the oscillatory-zoned grains could not be dated because of the limited spatial resolution. However, an age similar to that of the recrystallized domains is assumed.

Thus, based on the U–Pb analyses it is clear that the oscillatory-zoned domains and the recrystallized, blurred and unzoned domains and rims reflect two independent events. These relate to crystallization of the igneous protolith and to a subsequent strong granulite-facies overprint. However, these events cannot be distinguished on the basis of $^{207}Pb/^{206}Pb$ (345 ± 22 Ma vs 318 ± 41 Ma) and $^{208}Pb/^{232}Th$ (~320–400 Ma) ages (Table 6), because of the limited precision of these methods. Nevertheless, in general they support a Late Devonian–Carboniferous age of crystallization for both of these zircon generations.

However, complex scenarios involving incomplete resetting of the U–Pb system, partial Pb loss or even perhaps an earlier onset of the metamorphic overprint, closer to the Devonian protolith age, cannot be resolved using the LA–ICP–MS method. There is a similar problem in the case of analyses where the two age components (~360 Ma igneous and ~340 Ma metamorphic) might have accidentally mixed during ablation. Thus the age of 360 Ma remains likely to be a minimum estimate for the protolith formation, although the real age cannot differ substantially (<10 Ma difference). If the protolith were much older, the reasonable precision and low MSWD value for the whole population would necessitate binary mixing in practically identical proportions for all grains, and this is considered unlikely. Based on the bimodal distribution of $^{206}Pb/^{238}U$ ages of zircons with distinct types of internal zoning we infer a Late Devonian (Famennian) age for the igneous protolith and a strong granulite-facies overprint at *c.* 340 Ma.

### *Tonalite Li-3 (LM to)*

The zircon population contains a large proportion of subhedral to nearly euhedral stubby (Fig. 12a, b and f) to needle-like (Fig. 12d) crystals. Growth zoning is little modified, with only slightly blurred and thickened primary zones close to the grain margins. The most common grains have large, nearly uniform, central zones, succeeded by closely spaced oscillatory-zoned bands (Fig. 12a and b); sector zoning (Fig. 12e and h) is rare.

Other grains have slightly rounded prismatic or needle-like shapes but show blurred and thickened zoning (Fig. 12i), locally with relict domains preserving features of magmatic origin (Fig. 12c and e–g). In the final stage of alteration crystals appear rounded and their original internal structures have been almost erased and replaced by convoluted zoning (Fig. 12g and i). Slightly resorbed grains with regularly zoned inner domains and generally featureless irregular overgrowths (Fig. 12c) are relatively common in this sample.

The absence of irregular interstitial zircons like those abundant in sample Li-4 can be explained by the fact that the magma was likely to have been saturated in zircon close to the liquidus. Sample Li-3 plots beyond

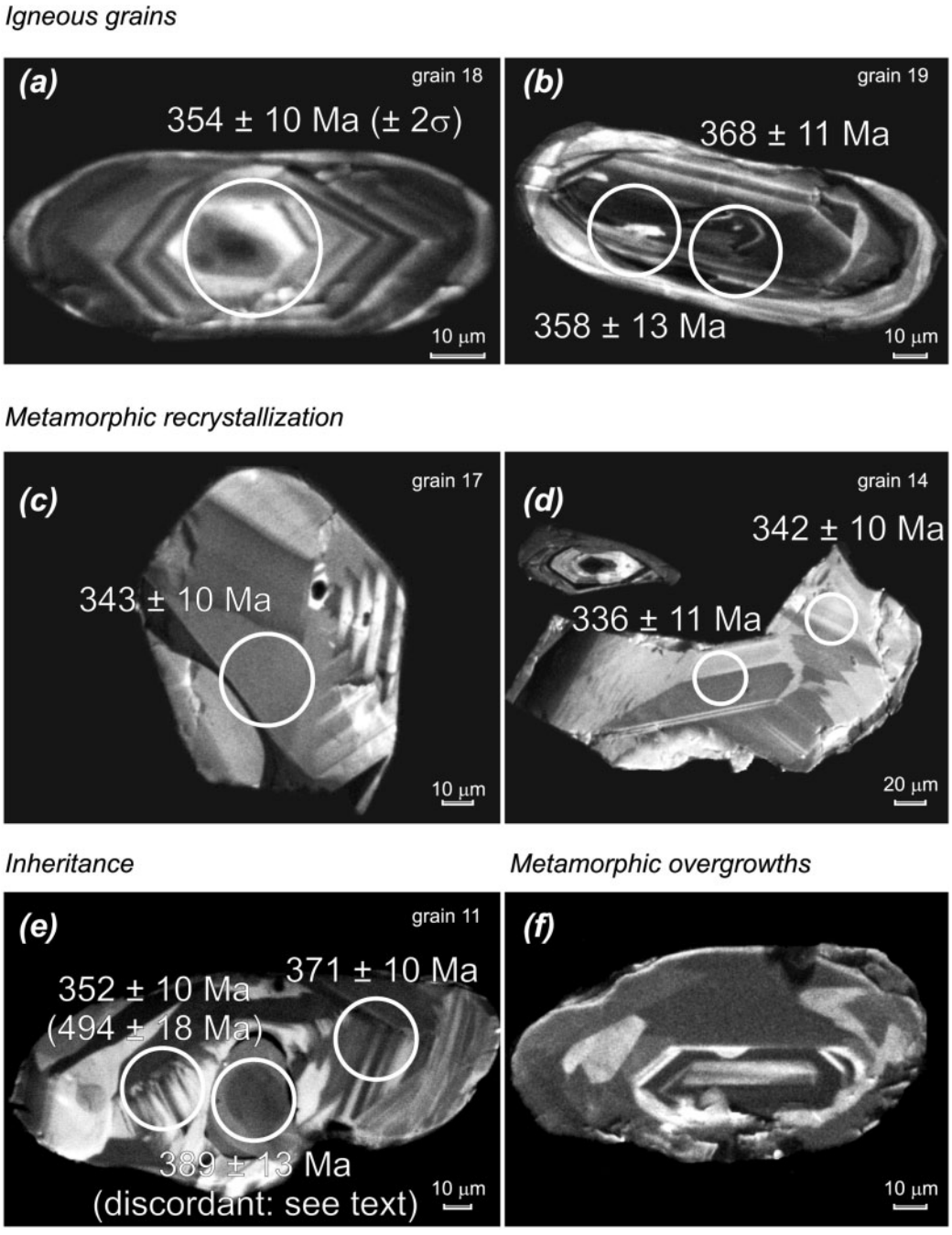


**Fig. 10.** Representative CL images of zircons from the quartz dioritic granulite Li-4. Approximate locations of the laser-ablation pits and corresponding $^{206}Pb/^{238}U$ ages are shown for the grains analysed; numbers of analyses refer to those in Table 6.

the inflection point in the $SiO_2$–Zr diagram (Fig. 7) and the zircon saturation temperatures (Watson & Harrison, 1983) are higher than in many of the *LM qtzD* granulites (~720–750°C; the highest value is that for Li-3).

Analogous to that of the quartz dioritic granulite sample, we interpret the original texture of the grains in the tonalitic granulite Li-3 as having formed during crystallization of the magmatic protolith. The zoning has been variously affected by later overgrowth and recrystallization, reflecting the granulite-facies overprint. However, magmatic growth zones seem to be less well preserved than in grains from Li-4 and it is commonly difficult to distinguish domains in CL images. No xenocrystic cores were identified under the CL but

*Table 6: U–Pb LA–ICP–MS data for quartz dioritic granulite Li-4 and tonalitic granulite Li-3*

| Grain | Spot | $^{207}Pb^{a}$ (c.p.s.) | Concentrations | | Th/U | Atomic ratios | | | | | Ages (Ma) | | | |
|---|---|---|---|---|---|---|---|---|---|---|---|---|---|---|
| | | | $U^{b}$ (ppm) | $Pb^{b}$ (ppm) | | $^{206}Pb^{c}/^{238}U \pm 1\sigma\%^{e}$ | $^{207}Pb^{c}/^{235}U \pm 1\sigma\%^{e}$ | rho$^{d}$ | $^{208}Pb^{c}/^{232}U \pm 1\sigma\%^{e}$ | $^{207}Pb^{f}/^{206}Pb \pm 1\sigma\%^{e}$ | $^{207}Pb/^{235}U \pm 2\sigma\%$ | $^{206}Pb/^{238}U \pm 2\sigma$ | $^{208}Pb/^{232}Th$ | $^{207}Pb/^{206}Pb$ |
| *Quartz dioritic granulite Li-4* | | | | | | | | | | | | | | |
| Zr11 | A1 | 1253 | 194 | 11·7 | 0·60 | 0·0561 ± 1·4 | 0·4104 ± 2·6 | 0·53 | 0·0185 ± 5·5 | 0·0528 ± 2·2 | 348 ± 18 | 352 ± 10 | 371 | 319 |
| Zr11 | A2 | 1226 | 165 | 10·5 | 0·63 | 0·0593 ± 1·4 | 0·4402 ± 3·4 | 0·41 | 0·0195 ± 5·7 | 0·0535 ± 3·1 | 371 ± 25 | 371 ± 10 | 385 | 352 |
| Zr5 | A5 | 2057 | 262 | 15·6 | 0·48 | 0·0575 ± 1·3 | 0·4256 ± 3·1 | 0·42 | 0·0188 ± 5·6 | 0·0534 ± 2·8 | 360 ± 22 | 360 ± 10 | 370 | 344 |
| Zr18 | A6 | 4123 | 607 | 34·9 | 0·44 | 0·0565 ± 1·4 | 0·4190 ± 2·5 | 0·56 | 0·0174 ± 3·3 | 0·0535 ± 2·1 | 355 ± 18 | 354 ± 10 | 345 | 350 |
| Zr20 | A10 | 2818 | 331 | 19·8 | 0·45 | 0·0582 ± 1·5 | 0·4260 ± 2·8 | 0·52 | 0·0181 ± 4·0 | 0·0528 ± 2·4 | 359 ± 20 | 365 ± 11 | 358 | 311 |
| Zr19 | A12 | 4736 | 401 | 24·1 | 0·48 | 0·0587 ± 1·5 | 0·4401 ± 3·2 | 0·47 | 0·0192 ± 3·8 | 0·0541 ± 2·8 | 371 ± 24 | 368 ± 11 | 380 | 374 |
| Zr19 | A11 | 4199 | 563 | 31·2 | 0·22 | 0·0571 ± 1·9 | 0·4240 ± 2·8 | 0·66 | 0·0194 ± 7·8 | 0·0535 ± 2·1 | 359 ± 20 | 358 ± 13 | 389 | 352 |
| Zr23 | A13 | 1560 | 239 | 14·3 | 0·59 | 0·0571 ± 1·4 | 0·4324 ± 3·0 | 0·47 | 0·0174 ± 3·2 | 0·0546 ± 2·6 | 365 ± 22 | 358 ± 10 | 344 | 395 |
| Zr22 | A20 | 2542 | 355 | 21·7 | 0·68 | 0·0566 ± 1·5 | 0·4266 ± 2·7 | 0·56 | 0·0188 ± 3·7 | 0·0543 ± 2·2 | 361 ± 20 | 355 ± 11 | 371 | 383 |
| Zr21 | A9 | 3061 | 432 | 24·4 | 0·42 | 0·0564 ± 1·5 | 0·4147 ± 2·8 | 0·52 | 0·0186 ± 4·0 | 0·0530 ± 2·4 | 347 ± 20 | 354 ± 11 | 368 | 285 |
| Zr13 | A8 | 1694 | 251 | 15·2 | 0·62 | 0·0573 ± 1·4 | 0·4255 ± 2·6 | 0·52 | 0·0198 ± 3·5 | 0·0535 ± 2·2 | 360 ± 19 | 359 ± 10 | 390 | 348 |
| Zr6 | A4 | 2124 | 287 | 16·0 | 0·53 | 0·0527 ± 1·3 | 0·3963 ± 2·7 | 0·50 | 0·0166 ± 3·7 | 0·0546 ± 2·1 | 339 ± 18 | 331 ± 10 | 327 | 394 |
| Zr10 | A19 | 1476 | 232 | 12·7 | 0·39 | 0·0541 ± 1·6 | 0·4038 ± 4·1 | 0·38 | 0·0192 ± 3·6 | 0·0541 ± 2·6 | 344 ± 28 | 340 ± 11 | 378 | 374 |
| Zr12 | A18 | 3995 | 605 | 33·7 | 0·44 | 0·0548 ± 1·4 | 0·3922 ± 2·9 | 0·48 | 0·0181 ± 3·3 | 0·0519 ± 2·4 | 336 ± 20 | 344 ± 10 | 358 | 280 |
| Zr17 | A7 | 1976 | 284 | 16·5 | 0·54 | 0·0547 ± 1·4 | 0·3961 ± 2·8 | 0·48 | 0·0205 ± 3·9 | 0·0525 ± 2·2 | 339 ± 19 | 343 ± 10 | 404 | 306 |
| Zr14 | A14 | 1010 | 164 | 9·0 | 0·44 | 0·0536 ± 1·6 | 0·3921 ± 3·5 | 0·45 | 0·0173 ± 4·3 | 0·0531 ± 3·1 | 336 ± 24 | 336 ± 11 | 343 | 333 |
| Zr14 | A15 | 1215 | 188 | 10·3 | 0·38 | 0·0545 ± 1·4 | 0·3813 ± 3·9 | 0·37 | 0·0178 ± 4·0 | 0·0508 ± 2·8 | 328 ± 25 | 342 ± 10 | 352 | 229 |
| Zr9 | A16 | 2730 | 547 | 30·9 | 0·40 | 0·0543 ± 1·4 | 0·3940 ± 3·7 | 0·38 | 0·0191 ± 5·8 | 0·0519 ± 3·4 | 334 ± 25 | 341 ± 10 | 382 | 281 |
| Zr7 | A17 | 2696 | 430 | 23·6 | 0·44 | 0·0538 ± 1·6 | 0·3846 ± 2·9 | 0·54 | 0·0196 ± 4·6 | 0·0519 ± 2·9 | 331 ± 19 | 338 ± 11 | 387 | 281 |
| Zr11 | A3 | 1847 | 216 | 13·9 | 0·44 | 0·0622 ± 1·7 | 0·5105 ± 3·4 | 0·49 | 0·0217 ± 3·6 | 0·0592 ± 2·9 | 419 ± 28 | 389 ± 13 | 427 | 574 |
| Zr11 | A1_2 | 1313 | 92 | 8·6 | 0·60 | 0·0797 ± 1·8 | 0·6597 ± 2·8 | 0·64 | 0·0302 ± 6·3 | 0·0597 ± 2·4 | 515 ± 29 | 494 ± 18 | 602 | 592 |
| Zr23 | A21 | 1560 | 239 | 19·1 | 0·59 | 0·0790 ± 2·8 | 0·6323 ± 4·1 | 0·70 | 0·0267 ± 4·8 | 0·0575 ± 3·8 | 498 ± 40 | 490 ± 28 | 525 | 512 |
| Zr9 | A16_2 | 959 | 86 | 7·1 | 0·65 | 0·0770 ± 3·3 | 0·6934 ± 11 | 0·31 | 0·0246 ± 4·7 | 0·0652 ± 2·4 | 535 ± 117 | 478 ± 32 | 485 | 782 |
| Zr12 | A18_2 | 3027 | 413 | 34·7 | 0·45 | 0·0847 ± 4·8 | 0·6525 ± 6·1 | 0·78 | 0·0270 ± 4·3 | 0·0558 ± 2·6 | 510 ± 62 | 524 ± 50 | 530 | 445 |
| Zr7 | A17_2 | 2387 | 347 | 26·2 | 0·46 | 0·0754 ± 2·1 | 0·5953 ± 9·0 | 0·23 | 0·0243 ± 5·1 | 0·0572 ± 6·3 | 474 ± 85 | 469 ± 19 | 478 | 500 |
| GJ-1$^{g}$ | $n = 10$ | 2694 | 240 | 20·4 | 0·03 | 0·0917 ± 1·2 | 0·7667 ± 2·1 | 0·58 | 0·0396 ± 3·0 | 0·0606 ± 1·8 | 576 ± 25 | 563 ± 14 | 796 | 626 |

| Grain | Spot | $^{207}Pb$[a] (c.p.s.) | Concentrations | | Th/U | Atomic ratios | | | | | Ages (Ma) | | | |
|---|---|---|---|---|---|---|---|---|---|---|---|---|---|---|
| | | | U[b] (ppm) | Pb[b] (ppm) | | $^{206}Pb^{c}/^{238}U \pm 1\sigma\%^{e}$ | $^{207}Pb^{c}/^{235}U \pm 1\sigma\%^{e}$ | rho[d] | $^{208}Pb^{c}/^{232}U \pm 1\sigma\%^{e}$ | $^{207}Pb^{f}/^{206}Pb \pm 1\sigma\%^{e}$ | $^{207}Pb/^{235}U \pm 2\sigma\%$ | $^{206}Pb/^{238}U \pm 2\sigma$ | $^{208}Pb/^{232}Th$ | $^{207}Pb/^{206}Pb$ |
| *Tonalitic granulite Li-3* | | | | | | | | | | | | | | |
| T14 | A2 | 1869 | 479 | 29·6 | 0·53 | 0·0537 ± 1·4 | 0·4065 ± 3·5 | 0·41 | 0·0147 ± 4·8 | 0·0549 ± 3·2 | 346 ± 24 | 337 ± 10 | 295 | 408 |
| T33 | A3 | 1302 | 343 | 19·1 | 0·34 | 0·0521 ± 1·5 | 0·3805 ± 4·2 | 0·35 | 0·0146 ± 3·8 | 0·0530 ± 3·9 | 326 ± 23 | 327 ± 10 | 293 | 329 |
| T12 | A7 | 1742 | 406 | 24·0 | 0·46 | 0·0524 ± 1·8 | 0·3788 ± 4·0 | 0·45 | 0·0158 ± 4·3 | 0·0524 ± 3·5 | 326 ± 26 | 329 ± 12 | 317 | 303 |
| T36 | A19 | 1007 | 236 | 14·1 | 0·39 | 0·0537 ± 1·6 | 0·3804 ± 7·9 | 0·20 | 0·0142 ± 4·0 | 0·0513 ± 7·7 | 327 ± 52 | 337 ± 11 | 284 | 256 |
| T42 | A20 | 839 | 170 | 10·3 | 0·31 | 0·0531 ± 1·8 | 0·3626 ± 5·4 | 0·34 | 0·0126 ± 5·5 | 0·0495 ± 5·1 | 314 ± 34 | 333 ± 12 | 252 | 173 |
| T2core | A1 | 862 | 155 | 11·3 | 0·48 | 0·0689 ± 1·1 | 0·5547 ± 4·3 | 0·26 | 0·0151 ± 4·7 | 0·0584 ± 4·2 | 448 ± 39 | 429 ± 10 | 303 | 546 |
| T2 | A26 | 1079 | 259 | 14·9 | 0·45 | 0·0545 ± 1·7 | 0·4034 ± 4·1 | 0·40 | 0·0155 ± 3·8 | 0·0536 ± 3·8 | 344 ± 28 | 342 ± 11 | 311 | 356 |
| T26 | A15 | 1145 | 295 | 16·9 | 0·38 | 0·0526 ± 1·6 | 0·3815 ± 3·2 | 0·49 | 0·0161 ± 4·3 | 0·0526 ± 2·8 | 328 ± 21 | 330 ± 10 | 323 | 314 |
| T21 | A10 | 1227 | 241 | 14·0 | 0·54 | 0·0559 ± 1·7 | 0·4069 ± 2·9 | 0·59 | 0·0183 ± 3·7 | 0·0528 ± 2·1 | 347 ± 20 | 351 ± 12 | 367 | 318 |
| T19 | A11 | 971 | 187 | 11·1 | 0·36 | 0·0564 ± 1·3 | 0·4191 ± 2·8 | 0·48 | 0·0166 ± 3·9 | 0·0539 ± 2·6 | 355 ± 20 | 353 ± 9 | 334 | 368 |
| T24 | A13 | 1824 | 424 | 24·6 | 0·46 | 0·0572 ± 1·6 | 0·4165 ± 2·7 | 0·59 | 0·0262 ± 4·1 | 0·0528 ± 2·2 | 354 ± 19 | 359 ± 11 | 425 | 320 |
| T11 | A5 | 2018 | 423 | 24·4 | 0·41 | 0·0571 ± 1·3 | 0·3988 ± 3·6 | 0·36 | 0·0172 ± 5·0 | 0·0506 ± 3·3 | 341 ± 24 | 358 ± 9 | 345 | 224 |
| T12 | A8 | 4285 | 669 | 36·9 | 0·21 | 0·0585 ± 1·3 | 0·4246 ± 2·5 | 0·50 | 0·0168 ± 4·7 | 0·0526 ± 2·2 | 359 ± 18 | 367 ± 9 | 337 | 312 |
| T22 | A9 | 1155 | 191 | 12·1 | 0·56 | 0·0591 ± 1·4 | 0·4317 ± 3·8 | 0·36 | 0·0177 ± 4·2 | 0·0530 ± 3·5 | 364 ± 28 | 370 ± 10 | 354 | 328 |
| T20 | A12 | 2011 | 311 | 19·5 | 0·49 | 0·0584 ± 1·6 | 0·4121 ± 3·0 | 0·52 | 0·0167 ± 3·6 | 0·0512 ± 2·6 | 350 ± 21 | 366 ± 11 | 335 | 248 |
| T8 | A16 | 2918 | 602 | 33·4 | 0·20 | 0·0572 ± 1·4 | 0·4186 ± 2·0 | 0·69 | 0·0176 ± 4·3 | 0·0530 ± 1·4 | 355 ± 14 | 359 ± 10 | 353 | 330 |
| T29 | A17 | 1357 | 175 | 10·8 | 0·60 | 0·0573 ± 1·7 | 0·4052 ± 3·8 | 0·45 | 0·0157 ± 4·7 | 0·0512 ± 3·4 | 345 ± 26 | 359 ± 12 | 316 | 252 |
| T34 | A18 | 1491 | 278 | 16·3 | 0·38 | 0·0572 ± 1·3 | 0·4244 ± 2·4 | 0·56 | 0·0167 ± 5·0 | 0·0538 ± 2·0 | 359 ± 17 | 359 ± 10 | 334 | 362 |
| T30 | A22 | 1581 | 259 | 15·7 | 0·36 | 0·0576 ± 1·4 | 0·4169 ± 3·4 | 0·41 | 0·0164 ± 4·3 | 0·0525 ± 3·1 | 354 ± 24 | 361 ± 10 | 329 | 306 |
| T31 | A23 | 1421 | 277 | 16·9 | 0·50 | 0·0570 ± 1·5 | 0·3992 ± 2·7 | 0·55 | 0·0169 ± 4·4 | 0·0508 ± 2·2 | 341 ± 18 | 357 ± 11 | 338 | 233 |
| T3 | A24 | 1821 | 324 | 19·9 | 0·48 | 0·0571 ± 1·7 | 0·4193 ± 3·5 | 0·49 | 0·0172 ± 4·3 | 0·0533 ± 3·0 | 356 ± 25 | 358 ± 12 | 346 | 341 |
| T39 | A25 | 2699 | 308 | 18·7 | 0·36 | 0·0592 ± 1·5 | 0·4353 ± 3·4 | 0·44 | 0·0161 ± 5·3 | 0·0533 ± 3·0 | 367 ± 25 | 371 ± 11 | 322 | 343 |
| GJ-1[g] | $n = 10$ | 2694 | 240 | 20·4 | 0·03 | 0·0965 ± 1·1 | 0·8116 ± 1·3 | 0·89 | 0·0380 ± 3·2 | 0·0607 ± 0·6 | 603 ± 16 | 594 ± 14 | 754 | 630 |

[a]Within-run background-corrected mean $^{207}Pb$ signal in counts per second.
[b]Concentration calculated relative to GJ-1 signal intensity, assuming a homogeneous concentration of 240 ppm U for the GJ-1 (mean of six ID-TIMS analyses).
[c]Corrected for background, common Pb and within-run U–Pb fractionation and normalized to reference zircon; $^{207}Pb/^{235}U$ calculated using $^{207}Pb/^{206}Pb/(^{238}U/^{206}Pb \times 1/137{\cdot}88)$.
[d]Quotient of the propagated errors of the $^{206}Pb/^{238}U$ and the $^{207}Pb/^{235}U$ ratio.
[e]Quadratic addition of within-run errors (1 SE) and daily reproducibility of GJ-1 (1 SD; see the last row in the table).
[f]Corrected for mass bias and common Pb by normalizing to reference zircon (~0·6% per a.m.u.) and using Stacey & Kramers (1975) model Pb composition, respectively.
[g]Measured ratios corrected for background and within-run inter-element fractionation; errors are 1 SD; ages (±2 SD) are measured and not true ages.

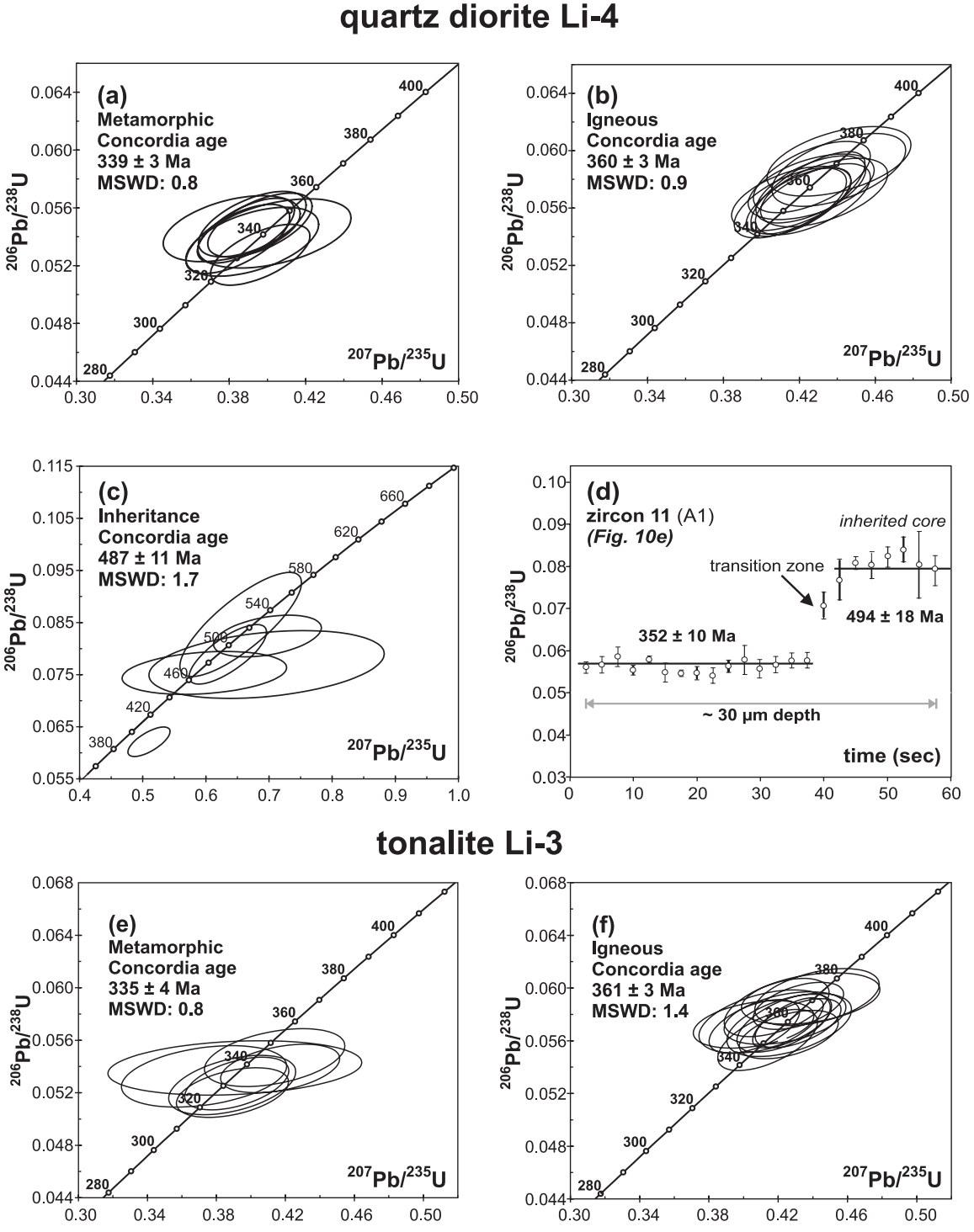


**Fig. 11.** Concordia diagrams (a–c) and a time-resolved plot of $^{206}Pb/^{238}U$ ages for the zircon with an inherited core (d; see Fig. 10e, left spot); quartz dioritic granulite Li-4. (e, f) Concordia diagrams for metamorphic and igneous zircons from the tonalitic granulite Li-3.

during analysis A1 (Table 6) the laser beam drilled into a region providing a $^{206}Pb/^{238}U$ age of 429 ± 10 Ma (likely to be a minimum constraint), apparently representing an older core.

The remaining 21 analyses of Li-4 zircon grains gave $^{206}Pb/^{238}U$ ages ranging from 327 ± 10 to 371 ± 11 Ma (2σ). Based on the CL images, some of which are shown in Fig. 12, well-preserved original domains (Fig. 12a and c),

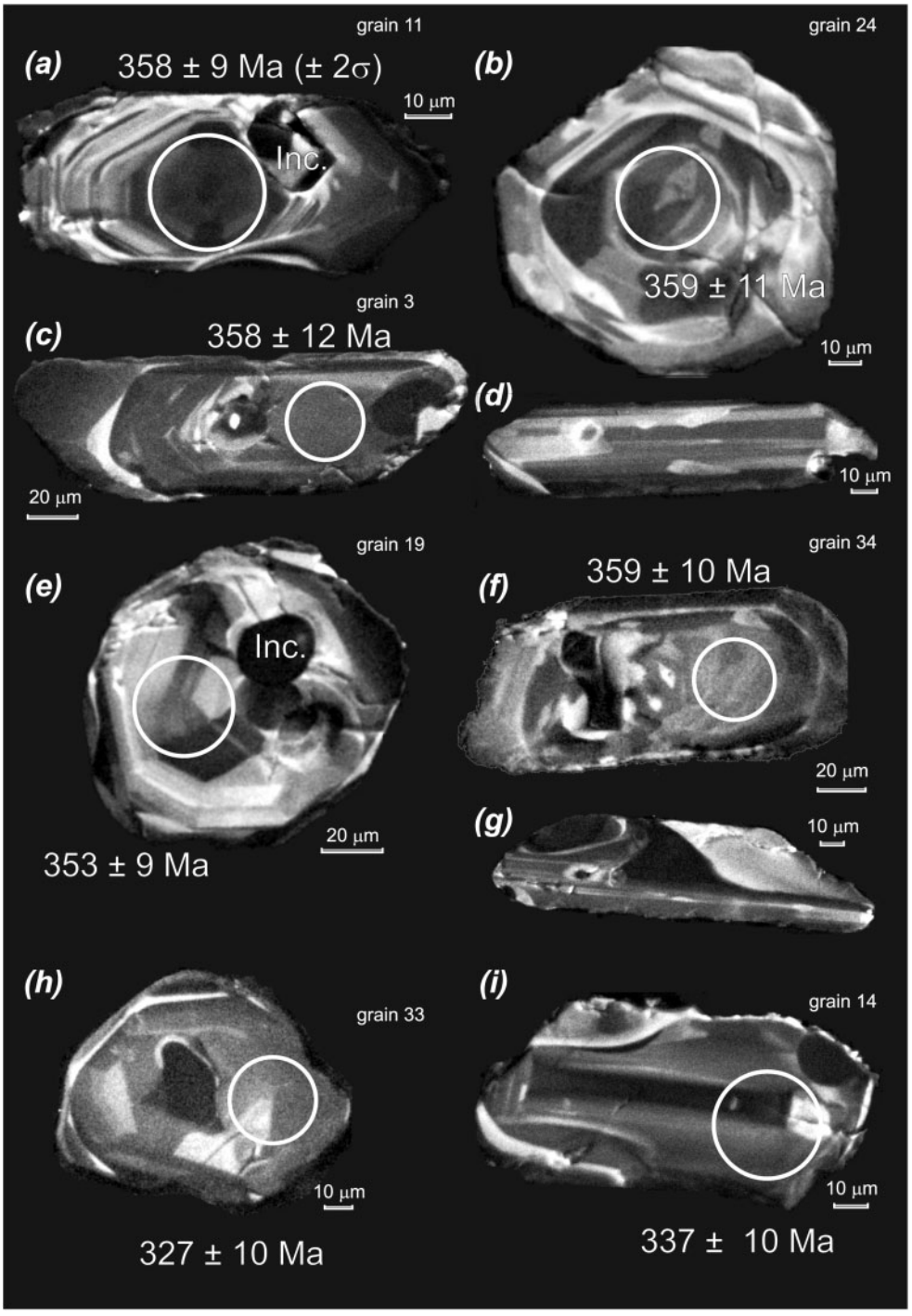


**Fig. 12.** Representative CL images of zircons from the granulite Li-3 with approximate locations of the laser-ablation pits and corresponding $^{206}Pb/^{238}U$ ages; their numbers refer to Table 6.

zones of questionable origin (Fig. 12b and e) and almost completely recrystallized zones (Fig. 12h and i) can be differentiated. The first group ($n = 11$) yielded a concordia age of 362 ± 4 Ma (2σ; MSWD = 1·4) and the last ($n = 5$) an age of 333 ± 5 Ma (MSWD = 0·75).

The remaining analyses, A10, A11 and A13, were obtained from domains in which the original oscillatory zoning is at least partially preserved (e.g. Fig. 12b and e). A concordia age of 354 ± 6 Ma (2σ) obtained for them is slightly younger than, but within error of, the age for

the older group. Analyses A15 and A26 yielded $^{206}Pb/^{238}U$ ages resembling those for the younger group, suggesting that the domains analysed were either completely recrystallized or affected by Pb loss, or both. Grouping these with the younger samples (Fig. 11e) and A10, A11 and A13 with the older age group (Fig. 11f) would result in concordia ages that differ by only 1–2 Ma from those calculated without them.

The $^{207}Pb/^{206}Pb$ and $^{208}Pb/^{232}Th$ ages support Late Devonian–Carboniferous crystallization for the zircons but cannot be used to differentiate age domains. As indicated, the LA–ICP–MS method is only able to resolve a simple scenario assuming two events, the first magmatic, the second metamorphic. Any partial resetting, mixing of components or multistage overprint would stay hidden within the analytical uncertainty. The conclusion is that the protolith formed at *c.* 360 Ma, or perhaps slightly earlier, and was strongly overprinted during granulite-facies metamorphism at about 330–340 Ma, a history similar to that of the quartz diorite sample.

## Sr–Nd isotope geochemistry

New whole-rock Sr–Nd isotopic ratios (Table 7) were supplemented by data from the literature [samples of Fiala *et al.* (1987*a*) that were analysed by Valbracht *et al.* (1994)]. One of them was quartz diorite (F105) and two were leucogranites (F98 and F102). Except for Fig. 13b, all of the Sr–Nd isotopic data were age-corrected to 360 Ma, the assumed minimum age of the igneous crystallization of the protolith of the quartz dioritic and tonalitic granulite types.

The mafic dyke provides a Nd isotopic composition significantly different from the rest of the dataset ($\varepsilon_{Nd}^{360} = +2{\cdot}8$; $T_{Nd}^{DM} = 0{\cdot}84$ Ga) (Fig. 13a). The pyroxenite enclave has a composition similar to that of Bulk Earth at 360 Ma ($\varepsilon_{Nd}^{360} = +0{\cdot}5$; $T_{Nd}^{DM} = 1{\cdot}03$ Ga). The host *LM qtzD* granulites (Li-26, Li-4 and F105) give $\varepsilon_{Nd}^{360} = -0{\cdot}4$ to $-2{\cdot}2$ ($T_{Nd}^{DM} = 1{\cdot}10$–$1{\cdot}24$ Ga); however, the $\varepsilon_{Nd}^{360}$ values for the remaining samples are significantly more negative, falling in the range $-4{\cdot}3$ to $-5{\cdot}2$ regardless of the petrology (*LM to*, *LF ch* and *LF gr*; $T_{Nd}^{DM} \sim 1{\cdot}39$–$1{\cdot}47$ Ga).

There are pronounced differences in Sr isotopic compositions (Fig. 13b): the dyke, the pyroxenite and quartz dioritic granulites are the least radiogenic ($^{87}Sr/^{86}Sr_{360} = 0{\cdot}7059$–$0{\cdot}7066$) compositions for the group, those of *LM to* ($^{87}Sr/^{86}Sr_{360}$ is 0·7082 for Li-3 and 0·7100 for Li-7) are somewhat higher. For Li-7 the rather evolved Sr isotopic signature may reflect the effects of its considerable retrogression. The felsic granulites (*LF gr*) yield by far the highest $^{87}Sr/^{86}Sr_{360}$ ratios (~0·7270: Valbracht *et al.*, 1994). The $^{87}Sr/^{86}Sr_{360}$ ratio of the charnockite (0·7154) is intermediate between *LM to* and *LF gr*.

Overall, the Nd isotopic signature of the quartz dioritic Lišov granulites resembles that of the most basic

*Table 7: Sr–Nd isotopic data for the granulites from the Lišov Massif*[a]

| Sample | Group | Rb (ppm) | Sr (ppm) | $^{87}Rb/^{86}Sr$ | $^{87}Sr/^{86}Sr^{b}$ | $^{87}Sr/^{86}Sr_{340}$ | $^{87}Sr/^{86}Sr_{360}$ | Sm (ppm)[c] | Nd (ppm)[c] | $^{147}Sm/^{144}Nd$ | $^{143}Nd/^{144}Nd^{b}$ | $^{143}Nd/^{144}Nd_{340}$ | $\varepsilon_{Nd}^{340}$ | $\varepsilon_{Nd}^{360}$ | $T_{Nd}^{DM}$ (*Ga*) |
|---|---|---|---|---|---|---|---|---|---|---|---|---|---|---|---|
| Li-25 | dyke | *15·6* | *418·4* | 0·1079 | 0·70696 (1·8) | 0·70644 | 0·70641 | *1·9* | *7·7* | 0·14526 | 0·512661 (15) | 0·512338 | +2·7 | +2·8 | 0·84 |
| Li-22A | pyroxenite | *27·8* | *112·0* | 0·7183 | 0·70965 (1·3) | 0·70617 | 0·70597 | *2·3* | *11·2* | 0·12199 | 0·512488 (6) | 0·512216 | +0·3 | +0·5 | 1·03 |
| Li-26 | *LM qtzD* | *20·9* | *643·3* | 0·0940 | 0·70642 (1·0) | 0·70596 | 0·70593 | 3·3 | 18·3 | 0·11034 | 0·512415 (8) | 0·512169 | −0·6 | −0·4 | 1·10 |
| Li-4 | *LM qtzD* | *51·8* | *555·2* | 0·2700 | 0·70797 (2·2) | 0·70667 | 0·70659 | 6·4 | 33·4 | 0·11649 | 0·512375 (4) | 0·512116 | −1·6 | −1·4 | 1·18 |
| 1073 | *BLM qtzD* | 20·1 | 91·9 | 0·6332 | 0·71387 (6·0) | 0·71081 | 0·71062 | 5·3 | 18·1 | 0·15426 | 0·512460 (14) | 0·512117 | −1·6 | −1·5 | 1·18 |
| Li-3 | *LM to* | *167·6* | *370·6* | 1·3094 | 0·71488 (2·4) | 0·70854 | 0·70817 | 8·9 | 43·4 | 0·12408 | 0·512206 (4) | 0·511930 | −5·3 | −5·1 | 1·47 |
| Li-7 | *LM to* | *31·9* | *135·6* | 0·6810 | 0·71357 (7·6) | 0·71027 | 0·71008 | 7·9 | 37·7 | 0·12709 | 0·512219 (8) | 0·511936 | −5·2 | −5·0 | 1·46 |
| Li-5 | *LF ch* | *83·0* | *87·7* | 2·7441 | 0·72942 (0·6) | 0·71614 | 0·71536 | 5·6 | 27·3 | 0·12470 | 0·512203 (38) | 0·511925 | −5·4 | −5·1 | 1·47 |
| Li-6 | *LF gr* | — | — | — | — | — | — | 2·4 | 13·5 | 0·10897 | 0·512226 (20) | 0·511983 | −4·2 | −4·3 | 1·39 |

[a]Except for quartz dioritic granulite 1073 from the Holubov borehole, Blanský les Massif [for details, see Janoušek *et al.* (2004*b*) and references therein].
[b]Values in parentheses are errors in the last decimal place (2 SE).
[c]Concentrations in italics were determined by isotope dilution using a Thermo-Finnigan Neptune multi-collector ICP–MS system at J.W. Goethe-University, Frankfurt am Main.
Subscripts indicate age to which isotopic ratios were corrected: 340 Ma (granulite-facies metamorphism) and 360 Ma (assumed protolith age for the mafic granulites); $T_{Nd}^{DM}$ are two-stage Nd model ages calculated after Liew & Hofmann (1988).

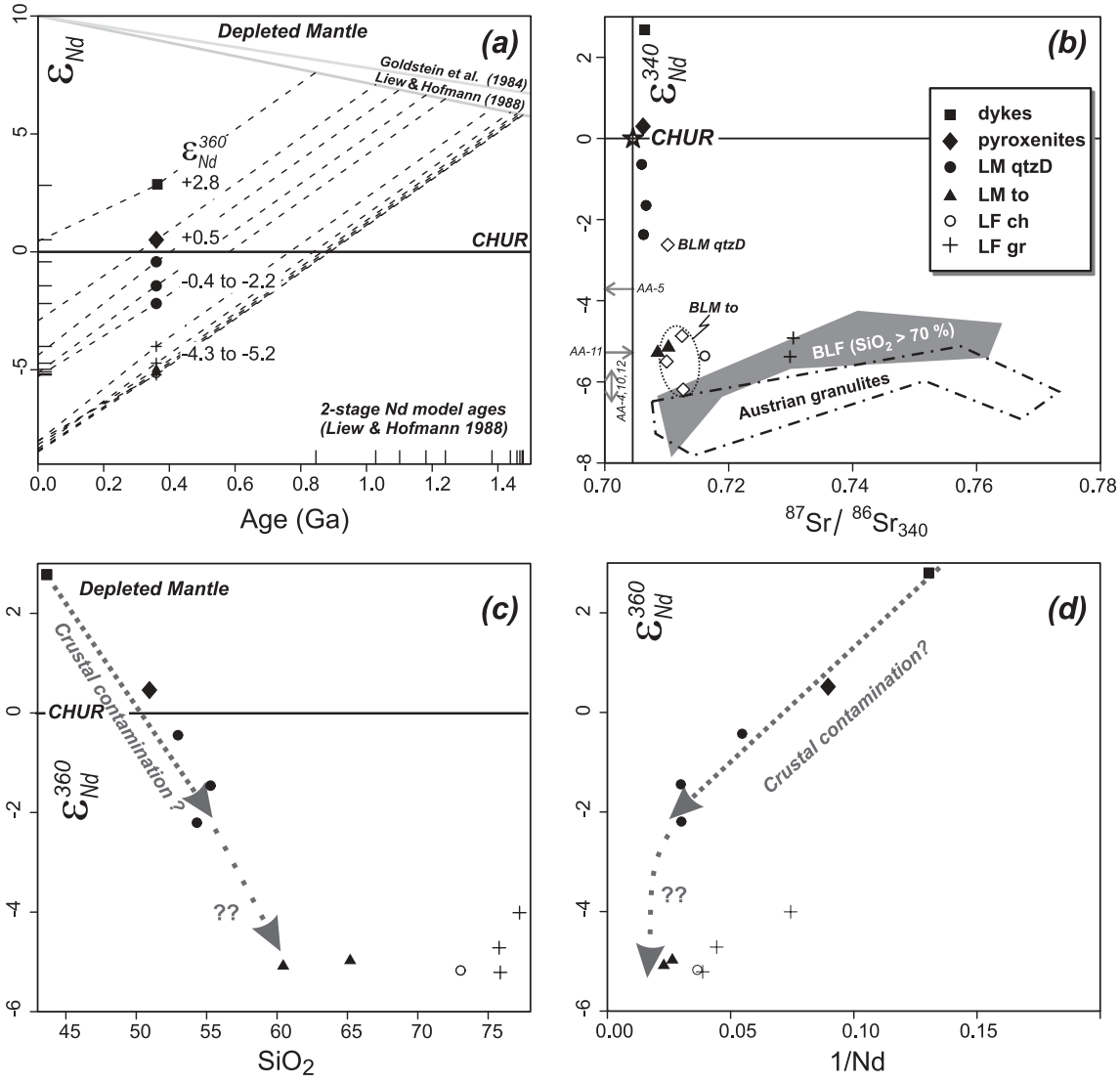


**Fig. 13.** (a) Two-stage Nd isotope evolution diagram showing ranges of $\varepsilon^{360}_{Nd}$ values for individual granulite groups from the LGM. Grey lines are Depleted Mantle evolution lines after Goldstein *et al.* (1984) and Liew & Hofmann (1988). (b) $(^{87}Sr/^{86}Sr)_{340}$ vs $\varepsilon^{340}_{Nd}$ for Moldanubian granulites. *LM* and *LF*, mafic and felsic granulites, Lišov Massif (Valbracht *et al.*, 1994, and this work). *BLM* and *BLF*, mafic and felsic granulites, Blanský les Massif (Wendt *et al.*, 1994, Nd only—samples AA denoted by arrows; Valbracht *et al.*, 1994; Janoušek *et al.*, 2004*b*). Also shown is a field for the Austrian granulite massifs (Vellmer, 1992; Becker *et al.*, 1999; Janoušek *et al.*, 2004*b*). (c) $\varepsilon^{360}_{Nd}$ vs $SiO_2$ (wt %). (d) $\varepsilon^{360}_{Nd}$ vs 1/Nd plot. The arrows in (c) and (d) show the possible development of the suite by crustal contamination. (For explanation, see the text.)

(also quartz dioritic) sample 1073 from the Holubov borehole (Kodym *et al.*, 1978) in the Blanský les Massif ($\varepsilon^{360}_{Nd} = -1{\cdot}5$: Table 7, Fig. 13b). However, the basic two-pyroxene granulite AA-5 of Wendt *et al.* (1994) had a significantly less radiogenic neodymium ($\varepsilon^{360}_{Nd} = -3{\cdot}6$). Similarly, the Nd, and to a large extent the Sr, isotopic compositions of the Lišov granulites *LM to* are similar to those of tonalitic samples from the Blanský les Massif (Valbracht *et al.*, 1994; Wendt *et al.*, 1994). The Lišov granulites *LF gr* plot in a large field defined by granodioritic–leucogranitic granulites from the Blanský les Massif (Valbracht *et al.*, 1994; Janoušek *et al.*, 2004*b*), whereas Austrian samples (Vellmer, 1992; Becker *et al.*, 1999; Janoušek *et al.*, 2004*b*) seem to have been shifted to somewhat more negative $\varepsilon^{i}_{Nd}$ values.

The spread of Sr–Nd isotopic compositions, their covariation with independent geochemical parameters (Fig. 13c and d) and the presence of inherited, mainly early Palaeozoic, xenocrystic zircon cores (Fig. 11c) indicate an important role for open-system processes such as crustal assimilation (AFC: DePaolo, 1981) or magma mixing. The significance of this inference will be addressed below.

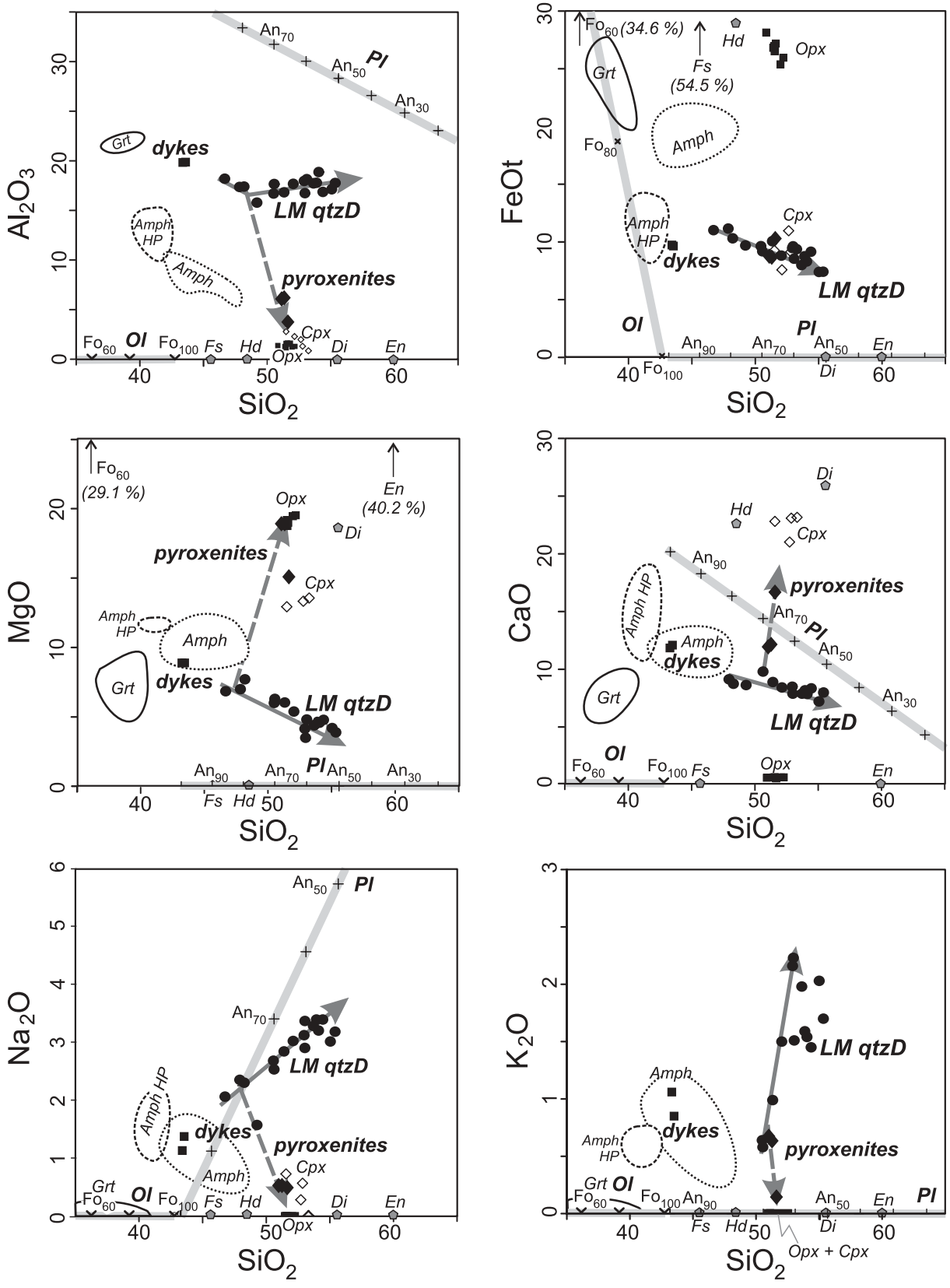

## DISCUSSION

### Devonian protoliths to some Moldanubian granulites?

The zircon population in many felsic Moldanubian granulites is characterized by the presence of crystals with oscillatory-zoned inner domains of pre-Variscan (mainly Cambrian–Ordovician) ages (Kröner *et al.*, 2000; Friedl *et al.*, 2004; see Janoušek *et al.*, 2004*b*, fig. 2, for review) and a few small, Early Proterozoic cores. However, the dated mafic-intermediate granulite samples from the LGM contain zircons that predominantly formed during the Variscan orogeny. Among these, many with well-preserved regular zoning indicate a magmatic origin. Most analyses of these zones yield consistently $^{206}Pb/^{238}U$ ages of *c.* 360 Ma interpreted as representing the minimum age of protolith crystallization. However, the absence of older Pb/U ages strongly suggests protolith formation between 360 and *c.* 370 Ma and not earlier.

In the Blanský les Massif, Wendt *et al.* (1994) recorded statistically identical Late Devonian U–Pb ages for prismatic zircons from three felsic granulite samples (365 ± 11; 366 ± 5, and 373 ± 11 Ma), although the last two reflected lower intercepts that may be open to other interpretation (Mezger & Krogstad, 1997). Very similar ages were obtained for some prismatic zircons from the granitic–granodioritic Prachatice granulites using the sensitive high-resolution ion microprobe (SHRIMP) technique (363 ± 4 Ma, weighted average for four igneous-looking grains; Kröner *et al.*, 2000).

Many original zircon crystals were recrystallized, and to a lesser extent overgrown, during the granulite-facies overprint. The U–Pb analyses of secondary domains in zircons from samples Li-3 and Li-4 gave ages of around 330–340 Ma, corresponding to the well-established timing of the high-grade metamorphism in the other Moldanubian granulite massifs (339·8 ± 2·6 Ma: Kröner *et al.*, 2000, and references therein). The CL and BSE imaging of the Lišov zircons suggest a substantial metamorphic recrystallization but little new growth. Even though crystallization of new zircon during high-grade metamorphism is by no means rare (see Wang & Griffin, 2004, and references therein), situations similar to Lišov have been described from several granulite-facies terrains worldwide (Ashwal *et al.*, 1999; Pidgeon *et al.*, 2000; Hoskin & Black, 2000).

The Lišov zircons that have preserved their original regular zoning appear to be unaffected by any Pb loss and contrast with those in which domains have been partly or completely recrystallized in response to the high-grade metamorphism during Viséan crustal stacking. Thus the results confirm the notion that the degree of preservation of igneous zoning in zircons can be used to assess the probability of Pb loss (e.g. Connelly, 2000).

### Petrogenesis of the protoliths to the Lišov granulites

The above discussion shows that several metaigneous granulite groups can be distinguished in the LGM, with largely independent petrology, geochemistry and protolith petrogenesis. The low-pressure granulites can be split into two suites, 'mafic' LM and 'felsic' LF.

#### *Mafic granulites* LM qtzD, *associated pyroxenites and dykes*

The field relationships, petrography and whole-rock geochemistry of the mafic granulites *LM qtzD* are consistent with a calc-alkaline plutonic parentage. As calc-alkaline magmatic rocks of intermediate composition cannot be produced directly by mantle melting (Wyllie, 1984), the protolith could have resulted from extensive fractionation of mantle-derived magmas or from partial melting of existing basic igneous rocks in the lower crust, a potentially fertile source for quartz dioritic and tonalitic magmas (Rapp *et al.*, 1991; Wolf & Wyllie, 1994). However, some of the dykes cutting the granulites *LM qtzD* are far too basic, have too high a positive $\varepsilon^{i}_{Nd}$ and much of their trace-element signature is too primitive for them to have been produced by partial melting of anything other than a mantle source.

In addition, the range of Sr–Nd isotopic variation in the mafic granulites and the presence of inherited pre-Devonian domains in their zircons indicate a role for crustal contamination of a mantle-derived basic magma. The exact nature of this primary magma is poorly constrained; even the dykes with the lowest $SiO_2$ are fairly differentiated, as indicated by their low Cr (~70 ppm), Ni (~26 ppm) and mg number (~62), together with a $FeO_t/MgO$ ratio slightly higher than unity (~1·1) (Tatsumi & Eggins, 1995).

**Fig. 14.** Binary plots of $SiO_2$ vs major-element oxides (wt %) for the Lišov *LM qtzD* granulites, associated dykes and pyroxenite enclaves. The tentative evolution of their igneous protolith by amphibole–Ca-rich plagioclase fractionation is shown by continuous-line arrows, evolution by accumulation of pyroxene-rich assemblages is shown by dashed arrows. The data sources are as in Fig. 2. Representative analyses of the main rock-forming minerals from Lišov are also plotted: *Opx* (filled squares), *Cpx* (open diamonds) and *Grt* (outlined field) (this work and Kotková, 1998*b*). *Amph*, magnesiohornblende from the Variscan calc-alkaline Sázava intrusion of the Central Bohemian Plutonic Complex; *Amph HP*, higher *P–T* brown pargasite and magnesiohastingsite cores of amphiboles from the Teletín quartz microdiorite that forms a part of the Sázava suite (*P* ~5 kbar and *T* >900°C: Janoušek *et al.*, 2004*a*). *Fo*, *Fa*, *Di*, *En*, *Fs* and *Hd* are theoretical compositions of the olivine and pyroxene end-members [taken in part from Le Maitre (1982)]. Theoretical ranges of plagioclase and olivine compositions are also plotted, labelled by the % of the *An* and *Fo* component, respectively.

The evolution of the most basic calc-alkaline magmas at depth is usually explained by olivine–clinopyroxene ± orthopyroxene ± Ca-plagioclase fractionation, superseded, in more siliceous and hydrous melt compositions, by amphibole–plagioclase-dominated assemblages (e.g. Wilson, 1989; Tatsumi & Eggins, 1995, and references therein). Although the pressure of crystallization and the water content of the parental magma are unconstrained at Lišov, clinopyroxene-dominated fractionation cannot account for the total variability observed within the *LM qtzD* suite. This mineral is simply too siliceous (see, e.g. $SiO_2$–$Al_2O_3$ and $SiO_2$–MgO plots; Fig. 14). On the other hand, the major-element trends are compatible with fractional crystallization of Mg- and Ca-rich amphibole and calcic plagioclase assemblages. This can be taken as indirect evidence that the original protoliths (many) of the *LM qtzD* granulites could have been amphibole-bearing and that the present-day pyroxene-dominated assemblage is, for the most part, metamorphic.

In theory, the pyroxenites forming enclaves in weakly foliated granulites *LM qtzD* could belong to a mantle-derived association of spinel peridotites that are rarely encountered in the eastern LGM (Fig. 2) (Jakeš, 1997). However, there is no structural evidence compatible with the tectonic incorporation of the pyroxenites. These rocks are devoid of high-pressure metamorphic relics and their Sr–Nd isotopic signature fits the variation in the *LM qtzD* group. Moreover, the presence of relict igneous cores in some clinopyroxene crystals in both the pyroxenites and the most basic of the granulites *LM qtzD* indicates that the pyroxenites more probably represent early mafic (Ca-clinopyroxene-bearing) cumulates crystallized from, and later disrupted and captured by, magma parental to the most basic of the *LM qtzD* granulites. Thus on the basis of Fig. 14 it can be concluded that the early development of the suite could have been by clinopyroxene (± olivine) fractional crystallization.

The field relationships of the quartz dioritic granulites, fine-grained basic dykes (Fig. 3a) and pyroxenites can be interpreted in the following sequence: (1) formation of the mafic cumulates; (2) fragmentation and inclusion of the cumulates in the intruding basic magma; (3) development of foliation in the quartz diorite; (4) intrusion of the dykes; (5) low-pressure granulite-facies metamorphic recrystallization of the whole assemblage.

### *Mafic granulites* LM to

As shown above, the protoliths of the *LM qtzD* and *LM to* granulites were coeval, opening the possibility that they might also have been cogenetic. If this were so, the Sr–Nd isotopic variation would convincingly demonstrate the importance of open-system processes (Fig. 13b to d). However, the distinctively curved trend in the diagram of $1/Nd$–$\varepsilon_{Nd}^{360}$ (Fig. 13d) joining the most mafic lithologies (dykes, pyroxenites, *LM qtzD*) with the tonalitic granulites argues against a simple binary mixing and AFC, in which $D_{Nd}$ and $r$ (rate of assimilation–fractional crystallization) were constant (Powell, 1984; Albarède, 1995; Janoušek *et al.*, 2000). If AFC was operating, the inflections at $SiO_2$ ~60 wt % in some major- and trace-element plots (Figs 6 and 7) may link to a principal change in the crystallizing assemblage (and thus $D_{Nd}$). Moreover, the more fractionated (tonalitic) magma would probably have a lower thermal energy, hindering its ability to assimilate the country rocks (lowering the $r$ parameter). Nevertheless, keeping in mind the small size of the available Sr–Nd dataset and the near absence of observable primary field relationships, the possibility that the two suites (*LM qtzD* and *LM to*) are genetically unrelated cannot be excluded.

### *Felsic granulites* LF gr

The genesis of the felsic Moldanubian granulites remains a matter of passionate debate. They have been interpreted as metamorphosed older, mostly felsic igneous (Janoušek *et al.*, 2004*b*) or volcanosedimentary rocks (Fiala *et al.*, 1987*a*, 1987*b*), possibly with a limited amount (<10–15 vol. %) of trapped high-pressure melt present (Roberts & Finger, 1997; Janoušek *et al.*, 2004*b*). However, the felsic granulites could also have originated by Variscan (~340 Ma) dry, high-pressure partial melting of metasediments (Jakeš, 1997; Kotková & Harley, 1999). This dispute remains far from resolution, and the age of the protolith of the granulites *LF gr*, and thus their genesis, is only discussed briefly here.

At Lišov, the texture and mineralogy of the massive felsic garnet-bearing hypersolvus granulites, in which unmixed ternary feldspars occur along with garnet free of reaction products, suggest preservation of their primary state after rather high-*PT* magmatic crystallization (Vrána & Jakeš, 1982). The association of Fe–Ti oxides (primary titanomagnetite + ilmenite but no graphite) argues for an oxygen fugacity higher than can be inferred from the ilmenite + graphite + pyrrhotite association of granulite rocks from the Blanský les Massif. Although the Nd isotopic composition of the felsic granulites resembles that of the *LM to* group (Fig. 13b), there are striking differences in the $^{87}Sr/^{86}Sr_{360}$ ratios. If the Sr isotopic ratios have been preserved despite the high-grade metamorphism, the increase in $^{87}Sr/^{86}Sr_{360}$ from tonalitic (~0·708) to felsic granulites (~0·727) would rule out a possible link via a Late Devonian closed-system fractional crystallization. Such retention of pre-metamorphic Sr isotopic signatures in high-grade metaigneous rocks is theoretically possible (e.g. Hradetzky & Lippolt 1993;

Kühn *et al.*, 2000; Janoušek *et al.*, 2004*b*). In any case, it is clear that a substantial body of new petrological, geochemical and geochronological data will be needed to elucidate the age and genesis of the protolith to the Lišov felsic granulites.

### *Garnet-bearing HP granulites* LGb

The rare garnet-bearing granulites *LGb* studied by Kotková (1998*b*) show a modal layering, an alternation of bands 0·05–0·2 m thick rich in pyroxene ± garnet and bands dominated by plagioclase. As a result, they form a geochemically rather heterogeneous group of metaluminous rocks (A/CNK = 0·77–0·87). Compared with the *LM qtzD* granulites they have rather flat, LREE-depleted REE patterns ($Ce_N/Yb_N$ = 2·0–2·9), with variable negative (JK 5: Eu/Eu* = 0·69) or more commonly positive (Eu/Eu* = 1·15–1·56) Eu anomalies (Fig. 9c). The Rb/Sr ratios are extremely low, mostly lower than the upper mantle limit of *c.* 0·03 (Jahn, 1990), indicating depletion in melt or fluid, or a high proportion of minerals with low Rb/Sr. The granulites *LGb* show trends of increasing MgO and mg number, accompanied by decreases in Sr, Y, $TiO_2$, $Al_2O_3$, $FeO_t$ and ΣREE with rising $SiO_2$. This, together with a change from a diminishing negative Eu anomaly to a positive one (Kotková, 1998*b*) is compatible either with a loss of melt or the progressive accumulation of mainly Mg-rich, Fe–Ca-poor pyroxene with some plagioclase. The geochemical signature of these granulites, in line with a HP metamorphic heritage, therefore corroborates a genesis largely independent of that of the other granulite types within the LGM.

### *Relationship of the Lišov mafic granulite suite to unmetamorphosed early Variscan calc-alkaline rocks*

The petrologic character, age, whole-rock geochemical and Sr–Nd isotopic compositions of the *LM qtzD* granulites resemble those of several calc-alkaline igneous complexes in the Bohemian Massif. The Late Devonian–Early Carboniferous (354·1 ± 3·5 Ma) medium-K calc-alkaline Sázava suite of the Central Bohemian Plutonic Complex (Fig. 1b; Janoušek *et al.*, 2000, 2004*a*) and the slightly older (373 ± 5 Ma and 365 ± 5 Ma) orthogneisses in its roof (Košler, 1993; Košler *et al.*, 1993) are remarkably similar. N-MORB-normalized trace-element variation diagrams (Fig. 8d) indicate that the Sázava granitoids are similar to the *LM qtzD* for most elements, with (Cs), U and Th as the main exceptions. These mobile elements are believed to have been removed by a small-scale melt or fluid loss during the prograde development of the granulites (Fiala *et al.*, 1987*a*; Vellmer, 1992; Janoušek *et al.*, 2004*b*). There is also a difference in the phosphorus content that is apparently lower in the Sázava suite. This may be an analytical artefact because, although data in the literature for the *LM qtzD* range between 0·35 and 0·65 % $P_2O_5$, none of our new determinations exceed 0·3 wt % $P_2O_5$. The Nd isotopic ratios for the Sázava suite fall within the range observed in the mafic Lišov granulites ($\varepsilon_{Nd}^{360} > -1{\cdot}4$, mainly slightly positive: Janoušek *et al.*, 1995, and unpublished data; Sokol *et al.*, 2000) and orthogneisses (Staré Sedlo: $\varepsilon_{Nd}^{360} = +3{\cdot}0$, Mirotice: $\varepsilon_{Nd}^{360} = +2{\cdot}6$ and $+2{\cdot}9$, Lašovice: $\varepsilon_{Nd}^{360} = -4{\cdot}0$ and $-4{\cdot}5$; Košler, 1993) (Fig. 1b).

It is difficult to reconstruct the original configuration of these plutonic rocks prior to the Viséan continental collision. There is no *a priori* reason to consider that the protoliths of the mafic granulites were related to the Sázava suite simply because the granulites currently occur in the vicinity of the Central Bohemian Plutonic Complex. Petrologically and geochemically similar, broadly contemporaneous, pre-collisional subduction-related calc-alkaline granitoid suites form a roughly west–east-trending belt across the whole European Variscan orogen (French Massif Central, northern Vosges, Odenwald, Schwarzwald, Central Bohemian and Nasavrky plutonic complexes, eastern Bohemia: Finger *et al.*, 1997; Janoušek *et al.*, 2004*a*, and references therein). Moreover, some of the metabasic rocks of Góry Sowie, Poland, are also characterized by largely similar major- and trace-element concentrations and Nd isotopic compositions (Kröner & Hegner, 1998; Kryza & Pin, 2002) although their age is uncertain.

## *P–T* conditions of metamorphism

### *Thermobarometry in the Lišov Massif*

Thermobarometric data obtained from two-pyroxene granulites and charnockites give estimates of $T$ = 710–720°C and $T$ = 625–745°C at $P$ = 3·5–5·0 kbar, respectively (Brey & Köhler, 1990; Lal, 1993; Reche & Martinez, 1996). The minerals used in the thermobarometry show minimal compositional variation from core to rim and this, in agreement with the textural relationships of the phases, points to a prolonged annealing and equilibration of mineral assemblages. The temperatures obtained correspond to the low-temperature part of the granulite-facies field, next to the boundary with amphibolite facies. These data are in sharp contrast to pressure and temperature estimates for other granulite bodies in the Bohemian Massif.

The unmixed ternary feldspars in felsic garnet granulites (*LF gr*) indicate peak temperatures above 900°C. The information available so far does not allow us to resolve the discrepancy between the temperature data for orthopyroxene-bearing rock types and *LF gr* granulites, even though the low grossular contents in *LF gr* garnets (1–3 mol %) agree well with the low-pressure estimates for the orthopyroxene-bearing rocks.

*Table 8: Examples of contrasting* P–T–t *history of several Variscan granulite bodies in the Bohemian Massif*

| Granulite massif | High-*P* stage | Mid- to low-*P* stage[a] | Type[b] | References |
|---|---|---|---|---|
| **Moldanubian Zone** | | | | |
| *Southern Bohemia* | | | | |
| Lišov (without LV-1) | Not present | $P = 4–5$ kbar[c], $T = 670–900$°C[c] | 2 | this study |
| Lišov—LV-1 borehole | $P \sim 13$ kbar (min.), $T = 910$°C | $P \sim 7–9$ kbar, $T \sim 680–800$°C | 1 | Kotková (1998*a*, 1998*b*) |
| Blanský les | $P = 14$ kbar, $T = 900–1000$°C | $P \sim 2–3$ kbar | 1 | Pin & Vielzeuf (1988), Owen & Dostal (1996) |
| | $P \sim 11–13$ (15) kbar, $T \sim 850–950$°C | | 1 | Vrána (1989) |
| | $P > 15$ kbar, $T > 900$°C | $P \sim 6–8$ kbar, $T \sim 700–800$°C | 1 | Kröner *et al*. (2000) |
| *Lower Austria* | | | | |
| St. Leonhard, Dunkelsteiner Wald | $P \sim 16$ kbar, $T = 1000$°C | $P \sim 6·5$ kbar, $T = 730$°C | 1 | Carswell & O'Brien (1993) |
| St. Leonhard | $P = 15–19$ kbar, $T = 950–1050$°C | $P = 8–12$ kbar, $T = 800–900$°C | 1 | Cooke (2000) |
| | | Post-decompression cooling 800–500°C at ~5–8 kbar | 1 | Cooke (2000) |
| **Saxothuringian Zone** | | | | |
| *Saxony* | | | | |
| Granulitgebirge | $P = 22$ kbar, $T = 970$°C | $P = 9$ kbar, $T = 890–940$°C | 1 | Rötzler & Romer (2001) |
| *NW Bohemia* | | | | |
| Ohře Crystalline Complex | $P = 15–17$ kbar, $T = 750–800$°C | lower amphibolite facies (+ Ms, no Sil) | 3 | Kotková (1993) |
| **Rhenohercynian Zone** | | | | |
| *Silesia* | | | | |
| Rychlebské Mts. | $P = 20–28$ kbar (up to 35 kbar), $T = 800–1000$°C | amphibolite and greenschist facies | 3 | Pouba *et al*. (1985), Pin & Vielzeuf (1988), Kryza *et al*. (1996), Klemd & Bröcker (1999) |
| **Viséan molasse** | | | | |
| *Drahany Uplands, Central Moravia* | | | | |
| Luleč conglomerate | $P \sim 12$ kbar (min.), $T \sim 820$°C (min.) | $P \sim 7$ kbar, $T \sim 800$°C | 1 + 2[d] | Kotková *et al*. (2001), Vrána & Novák (2000) |

[a]Several examples of amphibolite-facies retrogression, following HT–MP decompression, are documented in the literature.
[b]Typology denotes main trends of *P–T–t* evolution: Type 1: HT–HP → HT–MP, Type 2: HT–L(M)P, Type 3: HT–HP → amphibolite (greenschist) facies.
[c]Calculated metamorphic conditions (this work).
[d]Luleč conglomerate contains both Type 1 and Type 2 granulite populations.

### *Comparison with other granulites in the Moldanubian Zone*

The LGM displays important differences in metamorphic and structural development from other granulite bodies in the Moldanubian Zone of the Bohemian Massif. Apart from the fact that it is associated exclusively with spinel peridotites and there are no eclogites (Vrána & Jakeš, 1982; Vrána & Šrámek, 1999), the only unequivocal evidence for peak HP–HT metamorphism comes from scarce garnet-bearing mafic granulites (*LGb*, minimum P–T conditions of 13 kbar and 910°C: Kotková, 1998*b*). The relationship of these to the rest of the LGM is far from clear and they are interpreted here as an extraneous component in terms of both their protolith and metamorphic development.

Other granulite bodies in the Moldanubian Zone show a history starting with a high-pressure stage, followed by a medium- to low-pressure overprint. Detailed studies of granulite bodies in the Bohemian Massif, the Dunkelsteiner Wald and St. Leonhard complexes in Lower Austria, the Blanský les Massif in southern Bohemia and the Saxonian granulite Massif in the Saxothuringian Zone, have yielded peak pressures up to 22 kbar (Saxony) and temperatures mainly in the range 900–1000°C [see Table 8 and O'Brien & Rötzler (2003) for review].

An important feature of the nearly isothermal decompression assemblages in most of the Moldanubian granulites is the profusion of relics of high-pressure minerals or mineral assemblages. Mafic–intermediate granulites, except for those from Lišov, typically show abundant garnet overgrown by coronas or symplectite decompression assemblages of plagioclase + orthopyroxene ± clinopyroxene and hornblende. Felsic granulites commonly contain kyanite, Ca-rich garnet ($X_{Ca}$ up to 0·11–0·25) and oligoclase (andesine). Decompression products include low-Ca garnet overgrowths on early high-pressure garnet, neoformed low-Ca garnet in kyanite sites, the transformation of kyanite to sillimanite, and enhanced production of plagioclase, biotite and orthopyroxene. These assemblages have yielded pressure estimates of 6·5 kbar at 730°C in Lower Austria (Carswell & O'Brien, 1993; Cooke, 2000) and 9 kbar at 890–940°C in Saxony (Rötzler & Romer, 2001).

### *Why are the high-pressure mineral relics so scarce in the Lišov Massif?*

There is a surprising lack of high-pressure mineral relics in the main rock types of the LGM. Garnet is practically absent from the mafic granulites, and kyanite with high-Ca garnet are missing from the felsic granulites; there are even no replacement symplectites to indicate their former presence. Although the absence of aluminosilicates might be due to the low peraluminosity of the felsic Lišov granulites (Vrána & Jakeš, 1982), the lack of high-Ca garnet and corona–symplectites merits further discussion.

Decompression mineral reactions are commonly limited to, and regulated by, the short-range diffusion of ionic species (Loomis, 1979; Messiga & Bettini, 1990; Ashworth *et al.*, 1998). With reactions governed by diffusion coefficients and activity gradients, there is a strong tendency to conserve microstructural patterns such as corona–symplectites, provided that the fluid activity is low. If a *P–T* path analogous to that inferred for the garnet-bearing granulites *LGb* is to be envisaged for other Lišov rocks, then a protracted low-pressure overprint with a high fluid activity would be required to wipe out the HP metamorphic relics. The abundance of orthopyroxene, a mineral prone to hydration reactions at an increased $aH_2O$, argues strongly against the presence of $H_2O$-rich fluids, however.

Several of our samples (*LM qtzD*) preserve large plagioclase (Fig. 4c and d) and poikilitic clinopyroxene (Fig. 3d) cores that are interpreted as having survived from the original magmatic protolith. This fact, together with the absence of high-pressure metamorphic relics, supports the contention that the overwhelming majority of the Lišov granulites have never suffered HP metamorphism, having equilibrated or crystallized at mid-crustal levels.

The HP–HT Lišov granulites *LGb* also experienced a relatively long-term MP/LP–HT overprint ($T > 680$–800°C, $P \sim 7$–9 kbar: Vrána, 1990; Kotková, 1998*a*) after a nearly isothermal decompression phase. The protracted MP granulite-facies annealing and the role of garnet-consuming reactions is indicated by the presence of orthopyroxene + plagioclase ± spinel symplectites, which sometimes preserve relict garnets in their centres (Vrána & Jakeš, 1982; Kotková, 1998*b*).

## Mafic Lišov granulites—a vestige of an igneous arc crust?

The evidence from the low-pressure Lišov granulites adds to our understanding of the heterogeneity of the Variscan granulite bodies in the Moldanubian Zone of the Bohemian Massif. The presence of several granulite lithologies with contrasting petrology, geochemistry, and Sr–Nd isotope characteristics, together with the occurrence of clearly foreign slices of garnet-bearing granulites *LGb* and spinel peridotite, points to the derivation and final assembly of individual rock units in a dynamically evolving structural setting. The principal role in bringing these contrasting rock types together might have been played by a transcurrent shear zone, corresponding to the $D_3$ regional refoliation (Vrána & Šrámek, 1999), or by earlier deformation with a significant displacement intersecting upper mantle to mid-crustal levels. As a result of the superimposed deformation and imperfect exposure, knowledge of this early structural setting is limited.

If a Late Devonian age and igneous-arc affinity are accepted for the protolith to the mafic Lišov granulites, two genetic scenarios can be envisaged. The first assumes a Viséan (~340 Ma) burial and metamorphic reworking of a fragment from the higher-level Late Devonian (~360 Ma) magmatic arc. An analogous, albeit deeper (>50–60 km), subduction model was invoked by O'Brien (2000) to explain the HP–HT metamorphism in the ubiquitous felsic Moldanubian granulites.

The alternative scenario suggests that the mafic Lišov granulites represent a mid-crustal segment of a Late Devonian (Famennian) magmatic arc, a situation resembling that in the Cretaceous Sierra Nevada (Ducea, 2001; Saleeby *et al.*, 2003; Ducea *et al.*, 2003; Zandt *et al.*, 2004). The high-Al basaltic magmas generated from the mantle wedge above a subduction zone would rise to higher levels of the arc lithosphere, attempting to reach a neutral buoyancy level. Ponding in the middle crust, the hot magmas would have a large capacity for assimilation of the surrounding metasedimentary rocks, with crustal contamination triggering extensive fractional crystallization and crystal accumulation (DePaolo, 1981; Hildreth & Moorbath, 1988). The fractionated calc-alkaline tonalitic and quartz dioritic magmas would

be in equilibrium with modally layered, (garnet)–pyroxene–amphibole–plagioclase bearing mafic cumulates and residua from crustal melting (Ducea & Saleeby, 1998; Ducea, 2001), perhaps resembling the Lišov granulites *LGb*.

The key role played by plagioclase + garnet in the unmelted residue of the high-level Devonian calc-alkaline magmatic rocks is documented by the relatively LREE-enriched REE patterns, commonly characterized by negative Eu anomalies (e.g. Sázava suite of the Central Bohemian Plutonic Complex: Janoušek *et al.*, 2000). The semi-quantitative Al–Ti thermobarometry (Ernst & Liu, 1998) for relict cores of brown amphibole from the hybrid quartz microdiorite of the Sázava suite yielded $P \sim 5$ kbar and $T > 900$°C. They could therefore have crystallized, together with the bytownite centres of plagioclase crystals, from a basic magma at depth ($P \sim 5$ kbar), prior to injection or mixing into a considerably shallower, acidic magma chamber ($P \sim 3$ kbar, Janoušek *et al.*, 2004*a*). This may be understood as evidence for the existence of deeper magmatic reservoirs beneath the Late Devonian magmatic arc.

## CONCLUSIONS

(1) The Lišov Granulite Massif is distinctly different from neighbouring granulite bodies. Contrasts include low-pressure and dominantly moderate-temperature equilibration of several orthopyroxene-bearing granulites, the greater proportion of intermediate–mafic granulites, an abundance of orthopyroxene-bearing types (mafic granulites to relatively felsic charnockites), an association with spinel peridotites and pyroxenites devoid of garnet, and an absence of eclogites.

(2) Several metaigneous granulite groups can be distinguished in the LGM, with largely independent petrology, geochemistry and protolith petrogenesis.

(3) The overwhelming majority of the Lišov granulites lack any trace of high-pressure mineral relics. The peak metamorphic conditions recorded by equilibrium assemblages did not exceed 4–5 kbar and 670–800°C. The Grt–Opx–Pl–Qtz thermobarometry of charnockite equilibrium assemblages at present provides the most reliable *P–T* estimates in the granulite complex of southern Bohemia. This is because in other granulite massifs with prominent early high-pressure history thermobarometric estimates face problems with disequilibria resulting from superimposed decompression recrystallization.

(4) Some quartz-dioritic granulites *LM qtzD* preserve relict igneous textures (layering and cumulate pyroxenite enclaves) and are characterized by a remarkably primitive Sr–Nd isotopic signature ($^{87}Sr/^{86}Sr_{360} \sim 0{\cdot}706$; $\varepsilon_{Nd}^{360} = -0{\cdot}4$ to $-2{\cdot}2$). The magmatic protolith was probably emplaced during the Late Devonian, as indicated by the LA–ICP–MS U–Pb ages of ~360 Ma. Strongly recrystallized zircons and metamorphic overgrowths yield an age of 330–340 Ma for the metamorphic overprint.

(5) The isotopic signatures of the tonalitic granulites (*LM to*) for both neodymium ($\varepsilon_{Nd}^{360} \sim -5{\cdot}2$) and strontium ($^{87}Sr/^{86}Sr_{360} = 0{\cdot}70817$ and $0{\cdot}71008$) are significantly more crustal in character. The LA–ICP–MS U–Pb zircon dating implies ages for the magmatic protolith and the granulite-facies overprint that are, within error, identical to those of the quartz diorite.

(6) Garnet–orthopyroxene charnockite (*LF ch*) has a strontium isotopic composition ($^{87}Sr/^{86}Sr_{360} = 0{\cdot}71536$) intermediate between those of the groups *LM to* and *LF gr*, but its Nd isotopic signature ($\varepsilon_{Nd}^{360} = -5{\cdot}4$) is practically indistinguishable.

(7) For felsic garnet granulites (*LF gr*), the unmixed ternary feldspars indicate peak temperatures >900°C. The *LF gr* granulites could have crystallized at high temperatures and moderate pressures (*c.* 4–5 kbar?; see the low *Grs* contents of the garnet) as a hypersolvus assemblage of quartz and two ternary feldspars (mesoperthite and antiperthite) with minor garnet, plagioclase and Fe–Ti oxide. The information available so far does not allow us to resolve the discrepancy between the data for orthopyroxene-bearing rock types and *LF gr* granulites, even though the low *Grs* contents in *LF gr* garnets agree well with the low-pressure estimates for the orthopyroxene-bearing rocks.

(8) The granulites *LF gr* are characterized by a highly radiogenic strontium ($^{87}Sr/^{86}Sr_{360} \sim 0{\cdot}727$) and unradiogenic neodymium ($\varepsilon_{Nd}^{360} = -4{\cdot}3$ to $-5{\cdot}2$), the isotopic composition of which overlaps with the groups *LM to* and *LF ch*.

(9) Rare spinel peridotites and garnet-bearing *LGb* granulites with a HP record (minimum $P \sim 13$ kbar) that are restricted to a single area, are interpreted as foreign elements in an otherwise exclusively LP Lišov granulite Massif.

(10) The mafic–intermediate Lišov granulites are thought to have originated during a Viséan metamorphic overprint of metaluminous, medium-K calc-alkaline plutonic rocks formed in a Late Devonian magmatic arc. Their petrography and geochemical variation can be explained by extensive amphibole–plagioclase fractionation and crustal contamination of depleted-mantle melts (similar to, or more primitive than, the picritic dykes with $^{87}Sr/^{86}Sr_{360} \sim 0{\cdot}706$; $\varepsilon_{Nd}^{360} = +2{\cdot}8$). The age, petrology and geochemistry of the protolith are closely similar to those of the contemporaneous granitoids of the Sázava suite in the Central Bohemian Plutonic Complex and other higher-level calc-alkaline intrusions in the Variscan Belt.

(11) Combined CL and BSE imaging, and LA–ICP–MS dating of zircons is a powerful tool for deciphering

the genesis of high-grade metamorphic rocks, even in cases where the ages of igneous crystallization and metamorphic reworking were separated by intervals of only a few tens of millions of years.

## ACKNOWLEDGEMENTS

We are indebted to J. Trnková, V. Kopecký and J. Zeman for technical assistance in the isotope laboratory in Prague, V. Sixta (Czech Geological Survey Prague–Barrandov) for major-element and REE chemical analyses, and P. Sulovský and R. Čopjaková (both from Masaryk University, Brno) for electron microprobe work. In Salzburg, E. Krenn helped with the BSE imaging of zircon, B. Humer performed some of the XRF analyses, and E. Knop with F. Mayringer helped with polishing the zircon samples. We are grateful to L. Franz, F. Corfu and R. Oberhänsli for their critical reviews, as well as to M. Wilson for editorial handling. We also thank F. V. Holub and J. Žák for discussions and comments. This work originated during the research stay of V.J. at the Institute of Mineralogy, University of Salzburg, in the framework of the FWF Project 15133–GEO (F.F.). Some of the analyses were supported by the Czech Grant Agency project 205/03/0040. A.G. and the analytical work in Frankfurt were financed through DFG grant GE 1152/2-1.

## SUPPLEMENTARY DATA

Supplementary data for this paper are available at *Journal of Petrology* online.

## REFERENCES

Albarède, F. (1995). *Introduction to Geochemical Modeling*. Cambridge: Cambridge University Press.

Arculus, R. J. & Ruff, L. J. (1990). Genesis of continental crust: evidence from island arcs, granulites, and exospheric processes. In: Vielzeuf, D. & Vidal, P. (eds) *Granulites and Crustal Evolution*. Dordrecht: Kluwer Academic, pp. 7–23.

Ashwal, L. D., Tucker, R. D. & Zinner, E. K. (1999). Slow cooling of deep crustal granulites and Pb-loss in zircon. *Geochimica et Cosmochimica Acta* **63**, 2839–2851.

Ashworth, J. R., Reverdatto, V. V., Kolobov, V. Y., Sheplev, V. S. & Bryxina, N. A. (1998). Textures of diffusion-controlled reaction in contact-metamorphosed Mg-rich granulite, Kokchetav area, Kazakhstan. *Mineralogical Magazine* **62**, 213–224.

Becker, H., Wenzel, T. & Volker, F. (1999). Geochemistry of glimmerite veins in peridotites from Lower Austria—implications for the origin of K-rich magmas in collision zones. *Journal of Petrology* **40**, 315–338.

Boynton, W. V. (1984). Cosmochemistry of the rare earth elements: meteorite studies. In: Henderson, P. (ed.) *Rare Earth Element Geochemistry*. Amsterdam: Elsevier, pp. 63–114.

Brey, G. P. & Köhler, T. (1990). Geothermobarometry in four-phase lherzolites II. New thermobarometers, and practical assessment of existing thermobarometers. *Journal of Petrology* **31**, 1353–1378.

Carswell, D. A. & O'Brien, P. J. (1993). Thermobarometry and geotectonic significance of high-pressure granulites: examples from the Moldanubian zone of the Bohemian Massif in Lower Austria. *Journal of Petrology* **34**, 427–459.

Clemens, J. D. (1990). The granulite–granite connexion. In: Vielzeuf, D. & Vidal, P. (eds) *Granulites and Crustal Evolution*. Dordrecht: Kluwer Academic, pp. 25–36.

Connelly, J. N. (2000). Degree of preservation of igneous zonation in zircon as a signpost for concordancy in U/Pb geochronology. *Chemical Geology* **172**, 25–39.

Cooke, R. A. (2000). High-pressure/temperature metamorphism in the St. Leonhard Granulite Massif, Austria: evidence from intermediate pyroxene-bearing granulites. *International Journal of Earth Sciences* **89**, 631–651.

Corfu, F., Hanchar, J. M., Hoskin, P. W. O. & Kinny, P. D. (2003). Atlas of zircon textures. In: Hanchar, J. M. & Hoskin, P. W. O. (eds) *Zircon. Mineralogical Society of America and Geochemical Society Reviews in Mineralogy and Geochemistry* **53**, 469–503.

Čopjaková, R., Sulovský, P. & Paterson, B. A. (2005). Major and trace elements in pyrope–almandine garnets as sediment provenance indicators of the Lower Carboniferous Culm sediments, Drahany Uplands, Bohemian Massif. *Lithos* **82**, 51–70.

Dallmeyer, R. D., Franke, W. & Weber, K. (eds) (1995). *Pre-Permian Geology of Central and Eastern Europe*. Berlin: Springer.

Debon, F. & Le Fort, P. (1983). A chemical–mineralogical classification of common plutonic rocks and associations. *Transactions of the Royal Society of Edinburgh, Earth Sciences* **73**, 135–149.

DePaolo, D. J. (1981). Trace element and isotopic effects of combined wallrock assimilation and fractional crystallization. *Earth and Planetary Science Letters* **53**, 189–202.

Droop, G. T. R. (1987). A general equation for estimating $Fe^{3+}$ concentrations in ferromagnesian silicates using stoichiometric criteria. *Mineralogical Magazine* **51**, 431–435.

Ducea, M. (2001). The California Arc: thick granitic batholiths, eclogitic residues, lithospheric-scale thrusting, and magmatic flare-ups. *GSA Today* **11**, 4–10.

Ducea, M. N. & Saleeby, J. B. (1998). The age and origin of a thick mafic–ultramafic keel from beneath the Sierra Nevada batholith. *Contributions to Mineralogy and Petrology* **133**, 169–185.

Ducea, M. N., Kidder, S. & Zandt, G. (2003). Arc composition at mid-crustal depths: insights from the Coast Ridge Belt, Santa Lucia Mountains, California. *Geophysical Research Letters* **30**, 36-1–36-4.

Ernst, W. G. & Liu, J. (1998). Experimental phase-equilibrium study of Al- and Ti-contents of calcic amphibole in MORB—a semiquantitative thermobarometer. *American Mineralogist* **83**, 952–969.

Fiala, J., Matějovská, O. & Vaňková, V. (1987*a*). Moldanubian granulites and related rocks: petrology, geochemistry, and radioactivity. *Rozpravy Československé akademie věd, řada matematických a přírodních věd* **97**, 1–102.

Fiala, J., Matějovská, O. & Vaňková, V. (1987*b*). Moldanubian granulites: source material and petrogenetic considerations. *Neues Jahrbuch für Mineralogie, Abhandlungen* **157**, 133–165.

Fiala, J., Fuchs, G. & Wendt, J. I. (1995). Moldanubian Zone—stratigraphy. In: Dallmeyer, R. D., Franke, W. & Weber, K. (eds) *Pre-Permian Geology of Central and Eastern Europe*. Berlin: Springer, pp. 417–428.

Finger, F., Roberts, M. P., Haunschmid, B., Schermaier, A. & Steyrer, H. P. (1997). Variscan granitoids of Central Europe: their typology, potential sources and tectonothermal relations. *Mineralogy and Petrology* **61**, 67–96.

Franke, W. (2000). The mid-European segment of the Variscides: tectonostratigraphic units, terrane boundaries and plate tectonic evolution. In: Franke, W., Haak, V., Oncken, O. & Tanner, D. (eds)

*Orogenic Processes: Quantification and Modelling in the Variscan Belt. Geological Society, London, Special Publications* **179**, 35–61.

Friedl, G., Finger, F., Paquette, J. L., von Quadt, A., McNaughton, N. J. & Fletcher, I. R. (2004). Pre-Variscan geological events in the Austrian part of the Bohemian Massif deduced from U/Pb zircon ages. *International Journal of Earth Sciences* **93**, 802–823.

Fuchs, G. & Matura, A. (1976). Zur Geologie des Kristallins der südlichen Böhmischen Masse. *Jahrbuch der Geologischen Bundesanstalt* **119**, 1–43.

Fuhrman, M. L. & Lindsley, D. H. (1988). Ternary-feldspar modeling and thermometry. *American Mineralogist* **73**, 201–215.

Gerdes, A. (2005). Laser ablation ICP–MS U–Th–Pb dating of zircon: application and limits. In: European Winter Conference on Plasma Spectrochemistry, 30.1.–2.2.2005, Budapest.

Goldstein, S. L., O'Nions, R. K. & Hamilton, P. J. (1984). A Sm–Nd isotopic study of atmospheric dusts and particulates from major river systems. *Earth and Planetary Science Letters* **70**, 221–236.

Griffin, W. L., Wang, X., Jackson, S. E., Pearson, N. J., O'Reilly, S. Y., Xu, X. & Zhou, X. (2002). Zircon chemistry and magma mixing, SE China: in-situ analysis of Hf isotopes, Tonglu and Pingtan igneous complexes. *Lithos* **61**, 237–269.

Harvey, P. K. & Atkin, B. P. (1981). The rapid determination of Rb, Sr and their ratios in geological materials by X-ray fluorescence spectrometry using a rhodium X-ray tube. *Chemical Geology* **32**, 155–165.

Hildreth, W. & Moorbath, S. (1988). Crustal contributions to arc magmatism in the Andes of Central Chile. *Contributions to Mineralogy and Petrology* **98**, 455–489.

Horstwood, M. S. A., Foster, G. L., Parrish, R. R., Noble, S. R. & Nowell, G. M. (2003). Common-Pb corrected *in situ* U–Pb accessory mineral geochronology by LA–MC–ICP–MS. *Journal of Analytical Atomic Spectrometry* **18**, 837–846.

Hoskin, P. W. O. & Black, L. P. (2000). Metamorphic zircon formation by solid-state recrystallization of protolith igneous zircon. *Journal of Metamorphic Geology* **18**, 423–439.

Hoskin, P. W. O. & Schaltegger, U. (2003). The composition of zircon and igneous and metamorphic petrogenesis. In: Hanchar, J. M. & Hoskin, P. W. O. (eds) *Zircon. Mineralogical Society of America and Geochemical Society Reviews in Mineralogy and Geochemistry* **53**, 27–62.

Hoskin, P. W. O., Kinny, P. D., Wyborn, D. & Chappell, B. W. (2000). Identifying accessory mineral saturation during differentiation in granitoid magmas: an integral approach. *Journal of Petrology* **41**, 1365–1396.

Hradetzky, H. & Lippolt, H. J. (1993). Generation and distortion of Rb–Sr whole-rock isochrons—effects of metamorphism and alteration. *European Journal of Mineralogy* **5**, 1175–1193.

Irvine, T. N. & Baragar, W. R. A. (1971). A guide to the chemical classification of the common volcanic rocks. *Canadian Journal of Earth Sciences* **8**, 523–548.

Jacobsen, S. B. & Wasserburg, G. J. (1980). Sm–Nd evolution of chondrites. *Earth and Planetary Science Letters* **50**, 139–155.

Jahn, B. M. (1990). Origin of granulites: geochemical constraints from Archean granulite facies rocks of the Sino-Korean Craton, China. In: Vielzeuf, D. & Vidal, P. (eds) *Granulites and Crustal Evolution*. Dordrecht: Kluwer Academic, pp. 471–492.

Jakeš, P. (1967). Retrogression of pyroxene granulites from Lišov. Prague: Geological Institute, Czech Academy of Sciences, unpublished manuscript (in Czech).

Jakeš, P. (1997). Melting in high-*P* region—case of Bohemian granulites. *Acta Universitatis Carolinae, Geologica* **41**, 113–125.

Janoušek, V., Rogers, G. & Bowes, D. R. (1995). Sr–Nd isotopic constraints on the petrogenesis of the Central Bohemian Pluton, Czech Republic. *Geologische Rundschau* **84**, 520–534.

Janoušek, V., Bowes, D. R., Rogers, G., Farrow, C. M. & Jelínek, E. (2000). Modelling diverse processes in the petrogenesis of a composite batholith: the Central Bohemian Pluton, Central European Hercynides. *Journal of Petrology* **41**, 511–543.

Janoušek, V., Farrow, C. M. & Erban, V. (2003). GCDkit: new PC software for interpretation of whole-rock geochemical data from igneous rocks. *Geochimica et Cosmochimica Acta* **A67**, 186.

Janoušek, V., Braithwaite, C. J. R., Bowes, D. R. & Gerdes, A. (2004*a*). Magma-mixing in the genesis of Hercynian calc-alkaline granitoids: an integrated petrographic and geochemical study of the Sázava intrusion, Central Bohemian Pluton, Czech Republic. *Lithos* **78**, 67–99.

Janoušek, V., Finger, F., Roberts, M. P., Frýda, J., Pin, C. & Dolejš, D. (2004*b*). Deciphering petrogenesis of deeply buried granites: whole-rock geochemical constraints on the origin of largely undepleted felsic granulites from the Moldanubian Zone of the Bohemian Massif. *Transactions of the Royal Society of Edinburgh, Earth Sciences*, **95**, 141–159.

Klemd, R. & Bröcker, M. (1999). Fluid influence on mineral reactions in ultrahigh-pressure granites; a case study in the Snieznik Mts. (West Sudetes, Poland). *Contributions to Mineralogy and Petrology* **136**, 358–373.

Kodym, O., Jakeš, P. & Schovánek, P. (1978). Granulite und ultramafische Gesteine aus der Strukturbohrung Holubov. *Sborník geologických věd, Geologie* **32**, 7–47.

Košler, J. (1993). Age and geochemistry of the Staré Sedlo and Mirotice complexes, Bohemian Massif, Czech Republic. Ph.D. thesis, University of Glasgow.

Košler, J., Aftalion, M. & Bowes, D. R. (1993). Mid–late Devonian plutonic activity in the Bohemian Massif: U–Pb zircon isotopic evidence from the Staré Sedlo and Mirotice gneiss complexes, Czech Republic. *Neues Jahrbuch für Mineralogie, Monatshefte*, 417–431.

Kotková, J. (1993). *Tectonometamorphic History of Lower Crust in the Bohemian Massif—Example of North Bohemian Granulites. Czech Geological Survey Special Paper* **2**.

Kotková, J. (1998*a*). Garnet-bearing mafic granulites from the Lišov granulite massif. *Geolines* **6**, 37.

Kotková, J. (1998*b*). Pyroxene granulites with garnet from the Lišov granulite massif. Prague: Czech Geological Survey, unpublished grant report (in Czech).

Kotková, J. & Harley, S. L. (1999). Formation and evolution of high-pressure leucogranulites: experimental constraints and unresolved issues. *Physics and Chemistry of the Earth, Part A: Solid Earth and Geodesy* **24**, 299–304.

Kotková, J., Novák, M., Leichmann, J. & Houzar, S. (2001). Nature and provenance of exotic rock types from Lower Carboniferous conglomerates (eastern Bohemian Massif). *Geolines* **13**, 81–82.

Kretz, R. (1983). Symbols for rock-forming minerals. *American Mineralogist* **68**, 277–279.

Kröner, A. & Hegner, E. (1998). Geochemistry, single zircon ages and Sm–Nd systematics of granitoid rocks from the Góry Sowie (Owl Mts), Polish West Sudetes: evidence for early Palaeozoic arc-related plutonism. *Journal of the Geological Society, London* **155**, 711–724.

Kröner, A., O'Brien, P. J., Nemchin, A. A. & Pidgeon, R. T. (2000). Zircon ages for high pressure granulites from South Bohemia, Czech Republic, and their connection to Carboniferous high temperature processes. *Contributions to Mineralogy and Petrology* **138**, 127–142.

Kryza, R. & Pin, C. (2002). Mafic rocks in a deep-crustal segment of the Variscides (the Góry Sowie, SW Poland); evidence for crustal contamination in an extensional setting. *International Journal of Earth Sciences* **91**, 1017–1029.

Kryza, R., Pin, C. & Vielzeuf, D. (1996). High-pressure granulites from the Sudetes (south-west Poland): evidence of crustal subduction and

collisional thickening in the Variscan Belt. *Journal of Metamorphic Geology* **14**, 531–546.

Kühn, A., Glodny, J., Iden, K. & Austrheim, H. (2000). Retention of Precambrian Rb/Sr phlogopite ages through Caledonian eclogite facies metamorphism, Bergen Arc Complex, W Norway. *Lithos* **51**, 305–30.

Lal, R. K. (1993). Internally consistent recalibrations of mineral equilibria for geothermobarometry involving garnet–orthopyroxene–plagioclase–quartz assemblages and their application to the South Indian granulites. *Journal of Metamorphic Geology* **11**, 855–866.

Leake, B. E., Woolley, A. R., Arps, C. E. S., Birch, W. D., Gilbert, M. C., Grice, J. D., *et al.* (1997). Nomenclature of amphiboles: report of the Subcommittee on Amphiboles of the International Mineralogical Association Commission on New Minerals and Mineral Names. *Mineralogical Magazine* **61**, 295–321.

Le Maitre, R. W. (1982). *Numerical Petrology*. Amsterdam: Elsevier.

Liew, T. C. & Hofmann, A. W. (1988). Precambrian crustal components, plutonic associations, plate environment of the Hercynian Fold Belt of Central Europe: indications from a Nd and Sr isotopic study. *Contributions to Mineralogy and Petrology* **98**, 129–138.

Loomis, T. P. (1979). A natural example of metastable reactions involving garnet and sillimanite. *Journal of Petrology* **20**, 271–292.

Ludwig, K. R. (2001). Isoplot/Ex version 2.49, a geochronological toolkit for Microsoft Excel. Berkeley: Berkeley Geochronology Center.

Lugmair, G. W. & Marti, K. (1978). Lunar initial $^{143}Nd/^{144}Nd$: differential evolution line of the lunar crust and mantle. *Earth and Planetary Science Letters* **39**, 349–357.

Marshall, D. J. (1988). *Cathodoluminescence of Geological Materials*. Boston, MA: Unwin Hyman.

Melín, M. & Kunst, M. (1992). *MINCALC Development Kit 2.1*. Prague: Geological Institute of the Czech Academy of Sciences (in Czech).

Messiga, B. & Bettini, E. (1990). Reactions behaviour during kelyphite and symplectite formation: a case study of mafic granulites and eclogites from the Bohemian Massif. *European Journal of Mineralogy* **2**, 125–144.

Mezger, K. & Krogstad, E. J. (1997). Interpretation of discordant U–Pb zircon ages: an evaluation. *Journal of Metamorphic Geology* **15**, 127–140.

Morimoto, N. (1988). Nomenclature of pyroxenes. *Mineralogical Magazine* **52**, 535–550.

O'Brien, P. J. (2000). The fundamental Variscan problem: high-temperature metamorphism at different depths and high-pressure metamorphism at different temperatures. In: Franke, W., Haak, V., Oncken, O. & Tanner, D. (eds) *Orogenic Processes: Quantification and Modelling in the Variscan Belt. Geological Society, London, Special Publications* **179**, 369–386.

O'Brien, P. J. (2006). Type-locality granulites: high-pressure rocks formed at eclogite-facies conditions. *Mineralogy and Petrology* (in press).

O'Brien, P. J. & Carswell, D. A. (1993). Tectonometamorphic evolution of the Bohemian Massif: evidence from high pressure metamorphic rocks. *Geologische Rundschau* **82**, 531–555.

O'Brien, P. J. & Rötzler, J. (2003). High-pressure granulites: formation, recovery of peak conditions and implications for tectonics. *Journal of Metamorphic Geology* **21**, 3–20.

Owen, J. V. & Dostal, J. (1996). Contrasting corona structures in mafic granulite from the Blanský Les complex, Bohemian Massif, Czech Republic. *Canadian Mineralogist* **34**, 959–966.

Pagel, M., Barbin, V., Blanc, P. & Ohnenstetter, D. (eds) (2000). *Cathodoluminescence in Geosciences*. Berlin: Springer.

Pearce, J. A. & Parkinson, I. J. (1993). Trace element models of mantle melting: application to volcanic arc petrogenesis. In: Prichard, H. M., Alabaster, T., Harris, N. B. W. & Neary, C. R. (eds) *Magmatic Processes and Plate Tectonics. Geological Society, London, Special Publications* **76**, 373–403.

Peccerillo, R. & Taylor, S. R. (1976). Geochemistry of Eocene calc-alkaline volcanic rocks from the Kastamonu area, Northern Turkey. *Contributions to Mineralogy and Petrology* **58**, 63–81.

Petrakakis, K. (1997). Evolution of Moldanubian rocks in Austria: review and synthesis. *Journal of Metamorphic Geology* **15**, 203–222.

Pidgeon, R. T. (1992). Recrystallization of oscillatory zoned zircon: some geochronological and petrological implications. *Contributions to Mineralogy and Petrology* **110**, 463–472.

Pidgeon, R. T., Nemchin, A. A. & Hitchen, G. J. (1998). Internal structures of zircons from Archaean granites from the Darling Range batholith: implications for zircon stability and the interpretation of zircon U–Pb ages. *Contributions to Mineralogy and Petrology* **132**, 288–299.

Pidgeon, R. T., Macambira, M. J. B. & Lafon, J. M. (2000). Th–U–Pb isotopic systems and internal structures of complex zircons from an enderbite from the Pium Complex, Carajas Province, Brazil; evidence for the ages of granulite facies metamorphism and the protolith of the enderbite. *Chemical Geology* **166**, 159–171.

Pin, C. & Vielzeuf, D. (1983). Granulites and related rocks in Variscan Median Europe: a dualistic interpretation. *Tectonophysics* **93**, 47–74.

Pin, C. & Vielzeuf, D. (1988). Les granulites de haute-pression d'Europe moyenne temoins d'une subduction eo-hercynienne; implications sur l'origine des groupes leptyno-amphiboliques. *Bulletin de la Société Géologique de France* **4**, 13–20.

Pouba, Z., Paděra, K. & Fiala, J. (1985). Omphacite granulite from the NE marginal area of the Bohemian Massif (Rychleby Mts). *Neues Jahrbuch für Mineralogie, Abhandlungen* **151**, 29–52.

Powell, R. (1984). Inversion of the assimilation and fractional crystallization (AFC) equations; characterization of contaminants from isotope and trace element relationships in volcanic suites. *Journal of the Geological Society, London* **141**, 447–452.

Rapp, R. P., Watson, E. B. & Miller, C. F. (1991). Partial melting of amphibolite/eclogite and the origin of Archean trondhjemites and tonalites. *Precambrian Research* **51**, 1–25.

Reche, J. & Martinez, F. J. (1996). GPT: an Excel spreadsheet for thermobarometric calculations in metapelitic rocks. *Computers and Geosciences* **22**, 775–784.

Richard, P., Shimizu, N. & Allègre, C. J. (1976). $^{143}Nd/^{146}Nd$, a natural tracer: an application to oceanic basalts. *Earth and Planetary Science Letters* **31**, 269–278.

Roberts, M. P. & Finger, F. (1997). Do U–Pb zircon ages from granulites reflect peak metamorphic conditions? *Geology* **25**, 319–322.

Rötzler, J. & Romer, R. L. (2001). *P–T–t* evolution of ultrahigh-temperature granulites from the Saxon Granulite Massif, Germany. Part I: Petrology. *Journal of Petrology* **42**, 1995–2013.

Saleeby, J., Ducea, M. & Clemens-Knott, D. (2003). Production and loss of high-density batholithic root, southern Sierra Nevada, California. *Tectonics* **22**, 3-1–3-24.

Saunders, A. D., Norry, M. J. & Tarney, J. (1991). Fluid influence on the trace element compositions of subduction zone magmas. In: Tarney, J., Pickering, K. T., Knipe, R. J. & Dewey, J. F. (eds) *The Behaviour and Influence of Fluids in Subduction Zones*. London: The Royal Society, pp. 151–166.

Slabý, J. (1983). Modal composition and petrochemistry of granulites of the Lišov and Blanský les Mts. massifs, southern Bohemia. *Časopis pro mineralogii a geologii* **28**, 41–60 (in Czech with English abstract).

Sokol, A., Domečka, K., Breiter, K. & Janoušek, V. (2000). The underground storage near Příbram—a source of new information about granitoids of the Central Bohemian Pluton. *Bulletin of the Czech Geological Survey* **75**, 89–104.

Stacey, J. & Kramers, J. (1975). Approximation of terrestrial lead isotope evaluation by a two-stage model. *Earth and Planetary Science Letters* **26**, 207–221.

Steiger, R. H. & Jäger, E. (1977). Subcommission on Geochronology; convention on the use of decay constants in geo- and cosmochronology. *Earth and Planetary Science Letters* **36**, 359–362.

Suk, M. (1982). *Geological map of Czechoslovakia 1:25 000, sheet 32-222 Lišov*. Prague: Czech Geological Survey (in Czech).

Suk, M., Dornič, J., Hokr, Z., Holásek, O., Holub, V., Líbalová, J., Odehnal, L., Sattran, V., Šalanský, K., Zima, K. & Žebera, K. (1978). *Explanations to the geological map of Czechoslovakia 1:25 000, sheet 22-444 Ševětín*. Prague: Czech Geological Survey (in Czech).

Suk, M., Holub, V., Knobloch, E., Krásný, J., Líbalová, J., Holásek, O., Lomoz, M., Malecha, A., Mrňa, F., Pokorný, J., Sattran, V., Střída, M., Šalanský, K. & Žebera, K. (1981). *Explanations to the geological map of Czechoslovakia 1:25 000, sheet 32-222 Lišov*. Prague: Czech Geological Survey (in Czech).

Sun, S. S. & McDonough, W. F. (1989). Chemical and isotopic systematics of oceanic basalts: implications for mantle composition and processes. In: Saunders, A. D. & Norry, M. (eds) *Magmatism in the Ocean Basins. Geological Society, London, Special Publications* **42**, 313–345.

Tatsumi, Y. & Eggins, S. (1995). *Subduction Zone Magmatism*. Cambridge, MA: Blackwell.

Vajner, V. (1964). Die geologisch–petrographische Verhältnisse des Granulits von Lišov. *Sborník geologických věd, Geologie* **6**, 65–87 (in Czech with German summary).

Valbracht, P. J., Vrána, S., Beetsma, J. J., Fiala, J. & Matějka, D. (1994). Sr and Nd isotopic determinations in three Moldanubian granulite massifs in southern Bohemia. *Journal of the Czech Geological Society* **39**, 114.

van Breemen, O., Aftalion, M., Bowes, D. R., Dudek, A., Mísař, Z., Povondra, P. & Vrána, S. (1982). Geochronological studies of the Bohemian Massif, Czechoslovakia, and their significance in the evolution of Central Europe. *Transactions of the Royal Society of Edinburgh, Earth Sciences* **73**, 89–108.

Vellmer, C. (1992). Stoffbestand und Petrogenese von Granuliten und granitischen Gesteinen der südlichen Böhmischen Masse in Niederösterreich. Ph.D. thesis, Georg-August-Universität Göttingen.

von Justi, J. H. G. (1754). Nachricht von einer neuen Art eines neues Halbedelgesteines so kürzlich in Mähren entdeckt worden. *Neue Wahrheiten zum Vorteil der Naturkunde und des gesellschaftlichen Lebens der Menschen* **1**.

Vrána, S. (1989). Perpotassic granulites from southern Bohemia: a new rock-type derived from partial melting of crustal rocks under upper mantle conditions. *Contributions to Mineralogy and Petrology* **103**, 510–522.

Vrána, S. (1990). Contrasting *P–T* evolution of granulite and charnockite masses in the Bohemian Massif. In: *Terranes in the Circum-Atlantic Paleozoic Orogens. Abstracts of the International Conference on Paleozoic Orogens in Central Europe*. Göttingen–Giessen.

Vrána, S. & Jakeš, P. (1982). Orthopyroxene and two-pyroxene granulites from a segment of charnockitic crust in southern Bohemia. *Bulletin of the Czech Geological Survey* **57**, 129–143.

Vrána, S. & Novák, M. (2000). Petrology and geochemistry of granulite clasts in the Viséan Luleč conglomerate, Kulm in Central Moravia, Czech Republic. *Bulletin of the Czech Geological Survey* **75**, 405–413.

Vrána, S. & Šrámek, J. (1999). Geological interpretation of detailed gravity survey of the granulite complex in southern Bohemia and its structure. *Bulletin of the Czech Geological Survey* **74**, 261–277.

Vrána, S., Blümel, P. & Petrakakis, K. (1995). Moldanubian Zone—metamorphic evolution. In: Dallmeyer, R. D., Franke, W. & Weber, K. (eds) *Pre-Permian Geology of Central and Eastern Europe*. Berlin: Springer, pp. 453–468.

Wang, X. & Griffin, W. L. (2004). Unusual Hf contents in metamorphic zircon from coesite-bearing eclogites of the Dabie Mountains, east–central China: implications for the dating of ultrahigh-pressure metamorphism. *Journal of Metamorphic Geology* **22**, 629–637.

Watson, E. B. & Harrison, T. M. (1983). Zircon saturation revisited: temperature and composition effects in a variety of crustal magma types. *Earth and Planetary Science Letters* **64**, 295–304.

Wendt, J. I., Kröner, A., Fiala, J. & Todt, W. (1994). U–Pb zircon and Sm–Nd dating of Moldanubian HP/HT granulites from south Bohemia, Czech Republic. *Journal of the Geological Society, London* **151**, 83–90.

Wilson, M. (1989). *Igneous Petrogenesis*. London: Unwin Hyman.

Winchester, J. A. & Floyd, P. A. (1977). Geochemical discrimination of different magma series and their differentiation products using immobile elements. *Chemical Geology* **20**, 325–343.

Wolf, M. B. & Wyllie, P. J. (1994). Dehydration-melting of amphibolite at 10 kbar: the effects of temperature and time. *Contributions to Mineralogy and Petrology* **115**, 369–383.

Wyllie, P. J. (1984). Constraints imposed by experimental petrology on possible and impossible magma sources and products. *Philosophical Transactions of the Royal Society of London, Series A* **310**, 439–456.

Zandt, G., Gilbert, H., Owens, T. J., Ducea, M., Saleeby, J. & Jones, C. H. (2004). Active foundering of a continental arc root beneath the southern Sierra Nevada in California. *Nature* **431**, 41–46.